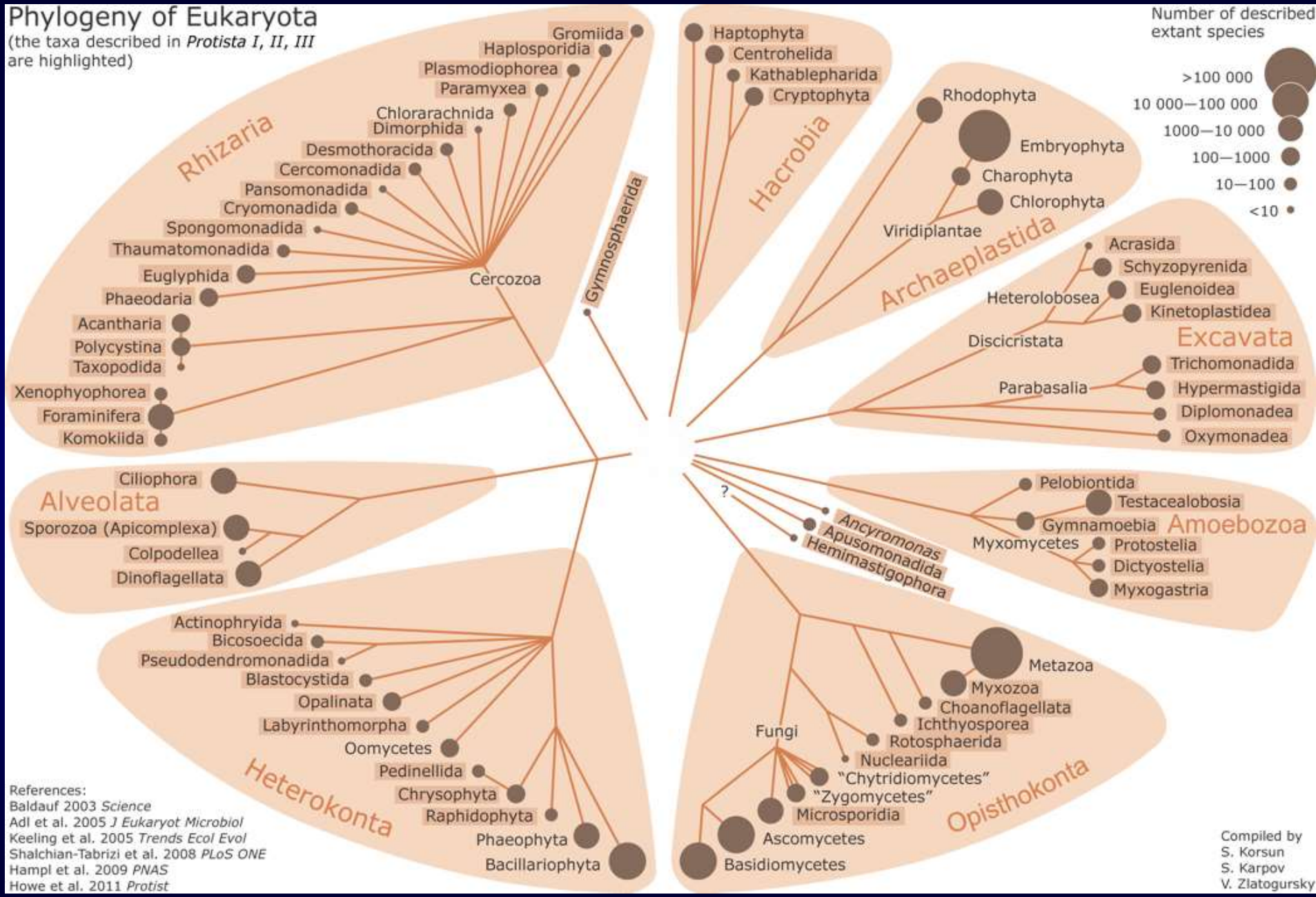

References:
Baldauf 2003 *Science*
Adl et al. 2005 *J Eukaryot Microbiol*
Keeling et al. 2005 *Trends Ecol Evol*
Shalchian-Tabrizi et al. 2008 *PLoS ONE*
Hampl et al. 2009 *PNAS*
Howe et al. 2011 *Protist*

Compiled by
S. Korsun
S. Karpov
V. Zlatogursky

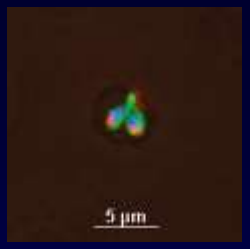

Паразиты человека:

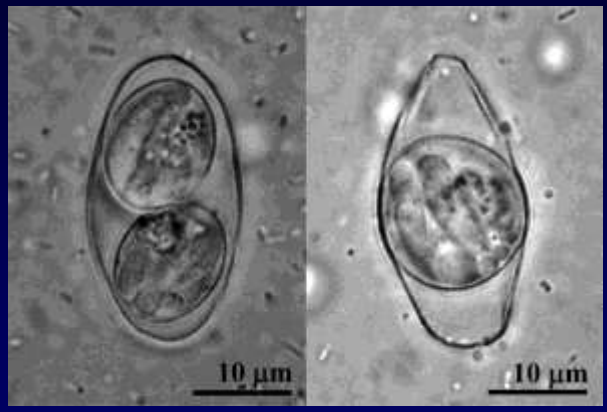

Coccidia, Сем. Eimeriidae, виды:

Isospora belli (I. hominis) Wenyon, 1923;

Cyclospora cayetenensis Ortega, Gilman, Sterling, 1994;

сем. Cryptosporidiidae; вид

Cryptosporidium parvum (*C. muris*) Tyzzer, 1912;

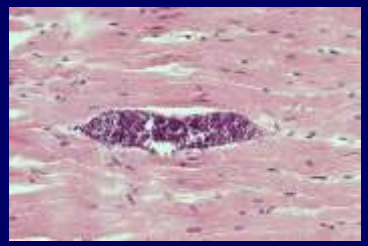

сем. Sarcocystidae, подсемейство. Sarcocystinae, виды:

Sarcocistis suihominis (Tadros, Laarman, 1976) Heydom, 1977;

S. hominis (S.bovihominis) (Railliet, Lucet, 1891) Dubey, 1976;

сем. Toxoplasmatinae, вид

Toxoplasma gondii (Nicolle, Manceaux, 1908), Nicolle, Manceaux, 1909;

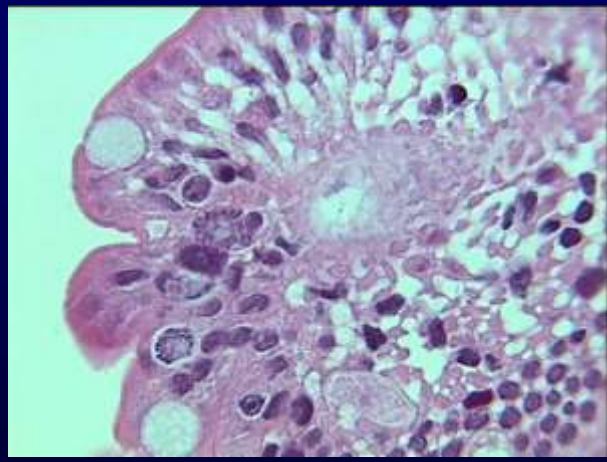

Haemospororida, сем. Plasmodiidae, виды:

Plasmodium vivax (Grassi, Feletti, 1890);

P. malariae (Grassi, Feletti, 1892);

P. (Laverania) falciparum (Welch, 1897);

P. ovalae (Stefens,1922).

Piroplasmorida, отр. Piroplasmida, сем. Babesiidae, виды:

Babesia bovis (Babes, 1888);

B. bigemina (Smith, Kilborne, 1893);

B. divergens (MacFadyean, Stokman, 1911).

B. microti (Franca, 1910) (некоторые относят к сем. Theileriidae, роду *Theileria*).

Система споровиков (Adl et al., 2018)

Apicomplexa Levine 1980, emend. Adl et al. 2005

Aconoidasida Mehlhorn et al. 1980 [= Hematozoa Vivier 1982] (P)

Haemosporорida Danilewsky 1885. *Plasmodium*.

Piroplasmorida Wenyon 1926. *Babesia*, *Theileria*.

Nephromycida Cavalier-Smith 1993, emend. Adl et al. 2019. *Nephromyces*, *Cardiosporidium*

Conoidasida Levine 1988 (P)

Coccidia Leuckart 1879 (P). *Adelina, Hepatozoon, Eimeria*.

Gregarinasina Dufour 1828 (P). *Cryptosporidium, Gregarina, Selenidium*.

Blastogregarinea Chatton and Villeneuve 1936, emend. Simdyanov et al. 2018. *Siedleckia*.

Incertae sedis Apicomplexa: Agamococcidiorida Levine 1979. *Gemmocystis, Rhytidocystis*.

Incertae sedis Apicomplexa: Protococcidiorida Kheisin 1956. *Coelothropha*, *Grellia*, *Eleutheroschizon*.

Incertae sedis Apicomplexa: *Agreggata*.

Инвазионная стадия

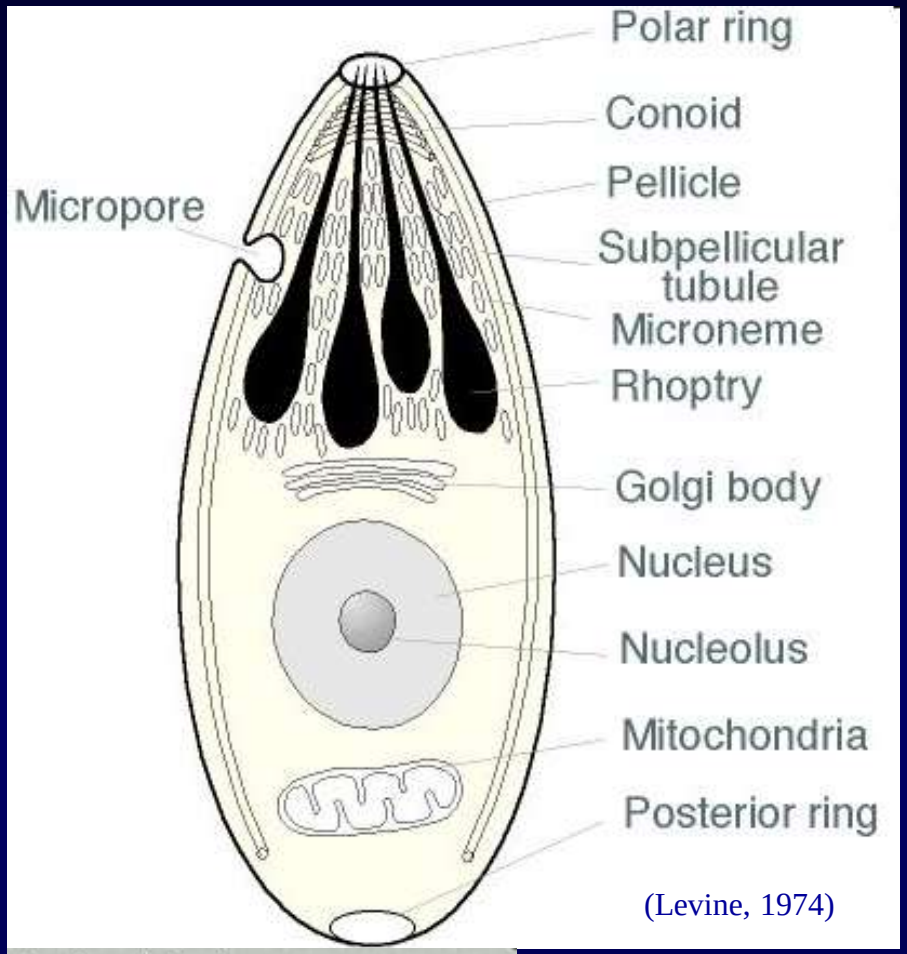

(Levine, 1974)

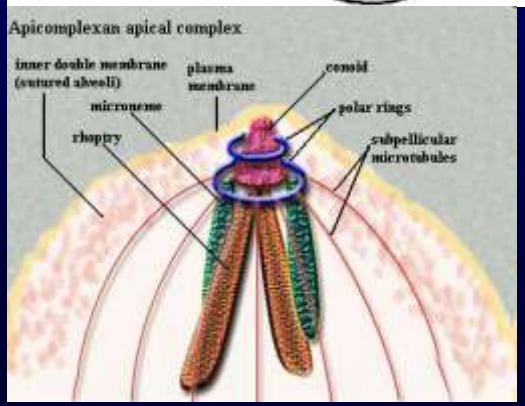

Plasmodium gallinaceum
(Haematozoa, Apicomplexa)

(По Scholtyseck, 1979)

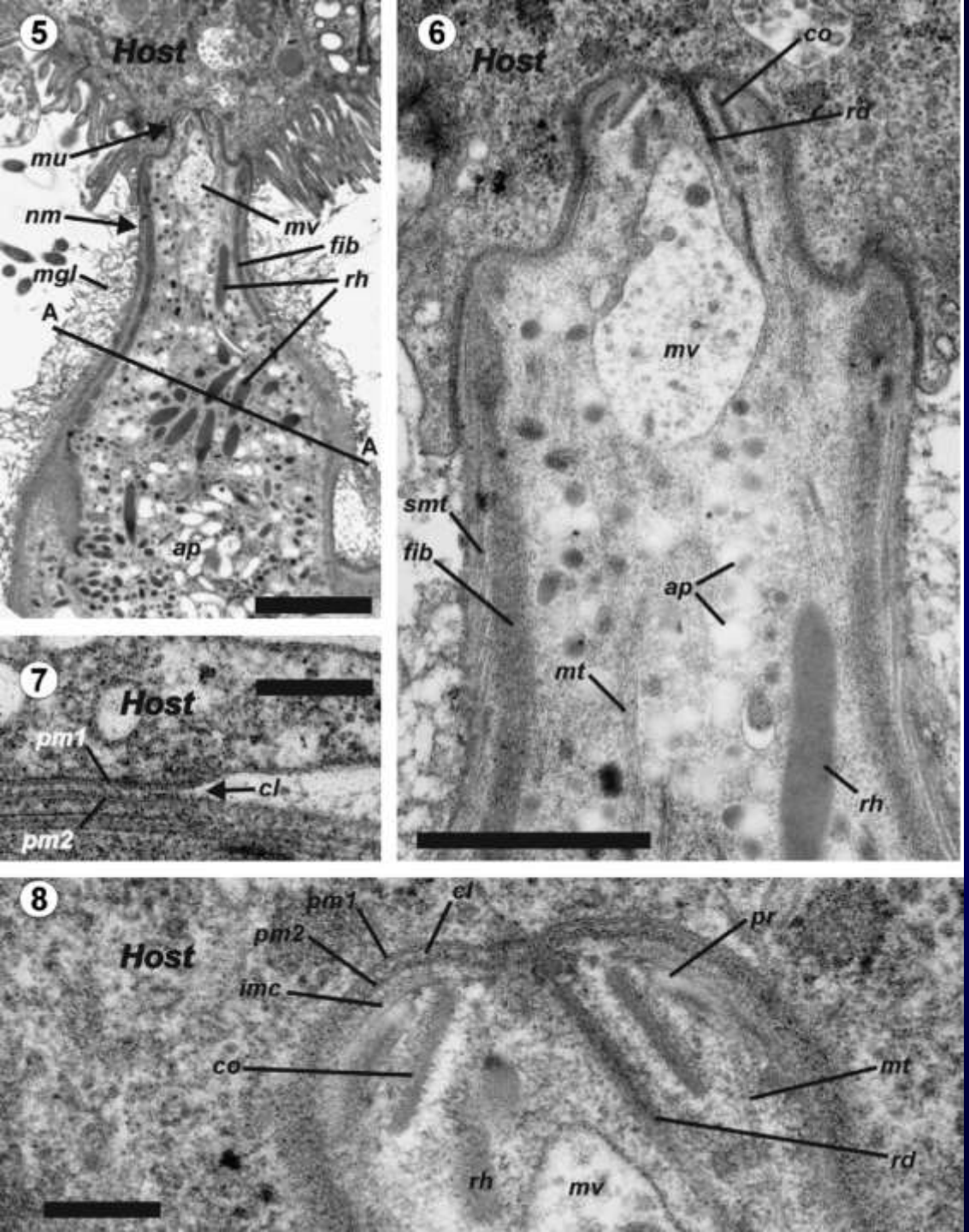

Fine structure and putative feeding mechanism of the archigregarine *Selenidium orientale* (Apicomplexa: Gregarinomorpha)

Fine structure of the forebody of *Selenidium orientale* trophozoite (TEM, longitudinal sections. 5, 6, 7, specimen No. 1; 8, specimen No. 2). 5, 6. Trophozoite forebody at different magnifications. 7. Peripheral area of a septated junction between parasite and host cell. 8. Mucron. Abbreviations: amylopectin granule (ap), modified glycocalyx of trophozoite anterior part (mgl), cortical fibrillar bundles (fib), clearance (cl) between host cell and gregarine plasma membranes (pm1 and pm2, respectively), conoid (co), host cell (Host), microtubules (mt), mucron (mu), mucronal vacuole (mv), neck of mucron (nm), polar ring (pr), rhoptry (rh), rhoptry duct (rd), inner membrane complex (imc), Line and letters A–A on 5: level of the section. Scale bars: 5 - 2 mkm, 6 - 1 mkm, 7, 8 - 0.2 mkm.

(Simdyanov & Kuvardina, 2007)

Микропоры

- Инваганация плазмалеммы, проходящая сквозь альвеолярных комплекс.
- Играет роль в пиноцитозе.
- Гомологичны парасомам инфузорий.
- Возникшие вакуоли покрыты клатрином (=пиноцитоз)

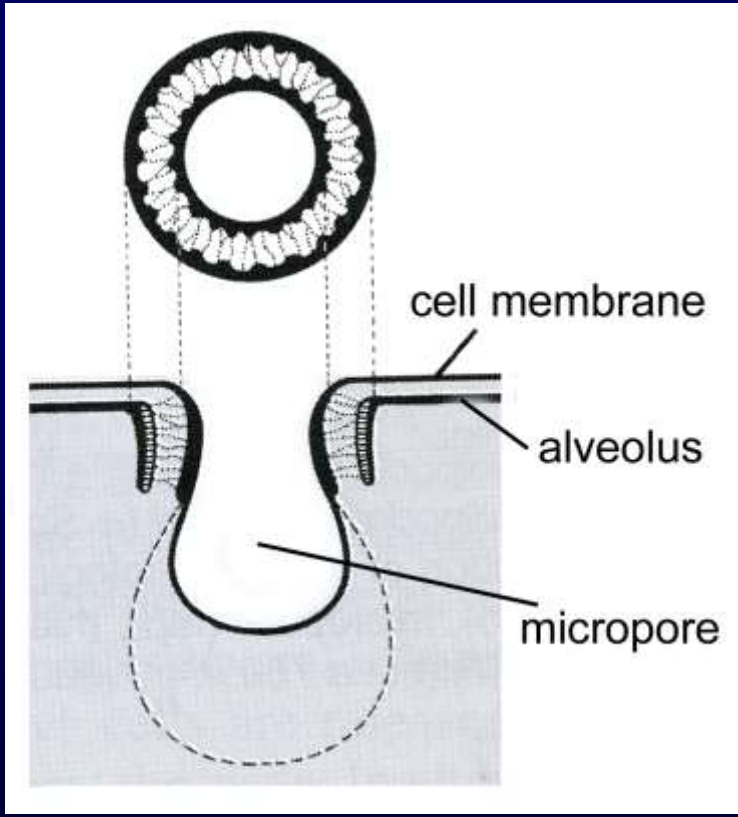

Митоз

- Ядерная мембрана открывается на полюсах.
- Тем не менее, остается интактной.

Встречаются: открытый и полузакрытый ортомитоз, полузакрытый плевромитоз.

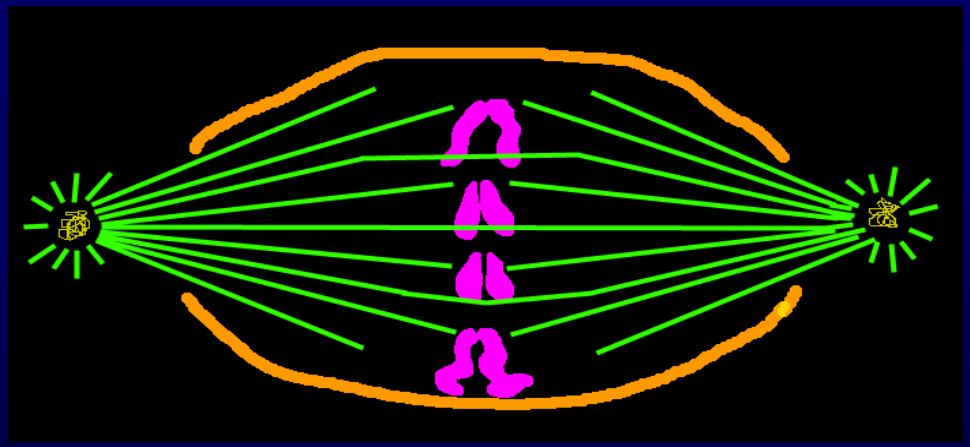

Митохондриальный геном

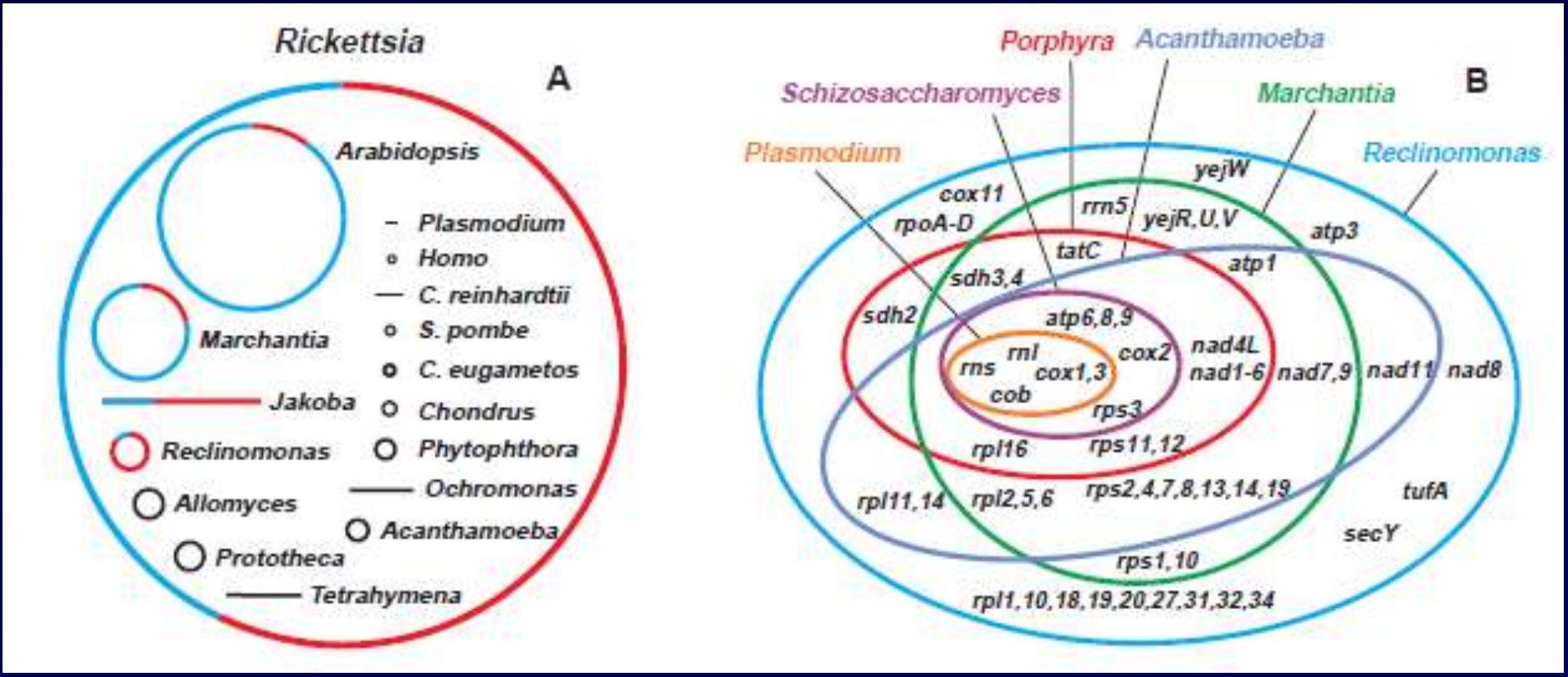

Size and gene content of mitochondrial genomes compared with an a-Proteobacterial (*Rickettsia*) genome. (**A**) Circles and lines represent circular and linear genome shapes, respectively. For genomes >60 kbp, the DNA coding for genes with known function (red) is distinguished from that coding for unidentified ORFs and intergenic sequences (blue). Species names are *C.* (*Chlamydomonas*) *reinhardtii*, *C.* (*Chlamydomonas*) *eugametos*, and *S.* (*Schizosaccharomyces*) *pombe*. (**B**) Gene complement of mitochondrial genomes. Each oval corresponds to one organism; genes included within an oval are present in the mtDNA of that organism. Only rRNA genes (*rnl, rns, rrn5*) and protein-coding genes are shown here. Full organism names, gene identities, and gene functions are listed in, except that *tatc* (*mttB*; also called *ymf16*) is newly recognized as a gene encoding a protein involved in membrane targeting and protein translocation.

(Gray et al., 1999)

Apicoplast

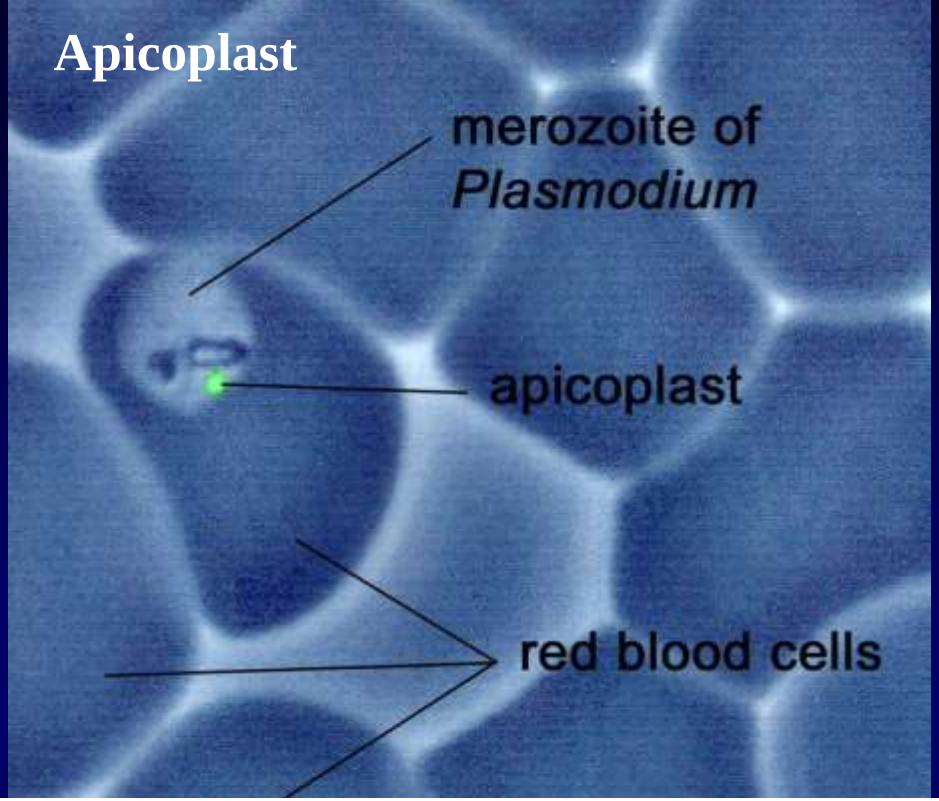

Origin, targeting, and function of the apicomplexan plastid

David S. Roos, Michael J. Crawford, Robert G.K. Donald,
Jessica C. Kissinger, Leszek J. Klimczak and Boris Striepen

The discovery of a plastid in *Plasmodium*, *Toxoplasma* and related protozoan parasites provides a satisfying resolution to several long-standing mysteries: the mechanism of action for various surprisingly effective antibiotics, the subcellular location of an enigmatic 35 kb episomal DNA, and the nature of an unusual intracellular structure containing multiple membranes. The apicomplexan plastid highlights the importance of lateral genetic transfer in evolution and provides an accessible system for the investigation of protein targeting to secondary endosymbiotic organelles. Combining molecular genetic identification of targeting signals with whole genome analysis promises to yield a complete picture of organellar metabolic pathways, and new targets for drug design.

tion of apicomplexan parasites [4-8,9**,10,11]. Cell biological studies confirm the essential eukaryotic nature of *Plasmodium* and *Toxoplasma*, however. These parasites contain a single nucleus, a single mitochondrion, and various specialized secretory organelles thought to be essential for host cell invasion and intracellular survival [12,13]. Rough endoplasmic reticulum (studded with typical eukaryotic ribosomes) is readily recognized, and parasite secretory proteins are characterized by a classical N-terminal signal sequence. The highly 'stripped-down' nature of *Plasmodium* merozoites makes the Golgi apparatus hard to identify morphologically [14,15], but a well-formed Golgi is readily apparent in *Toxoplasma* [13]. The secretory

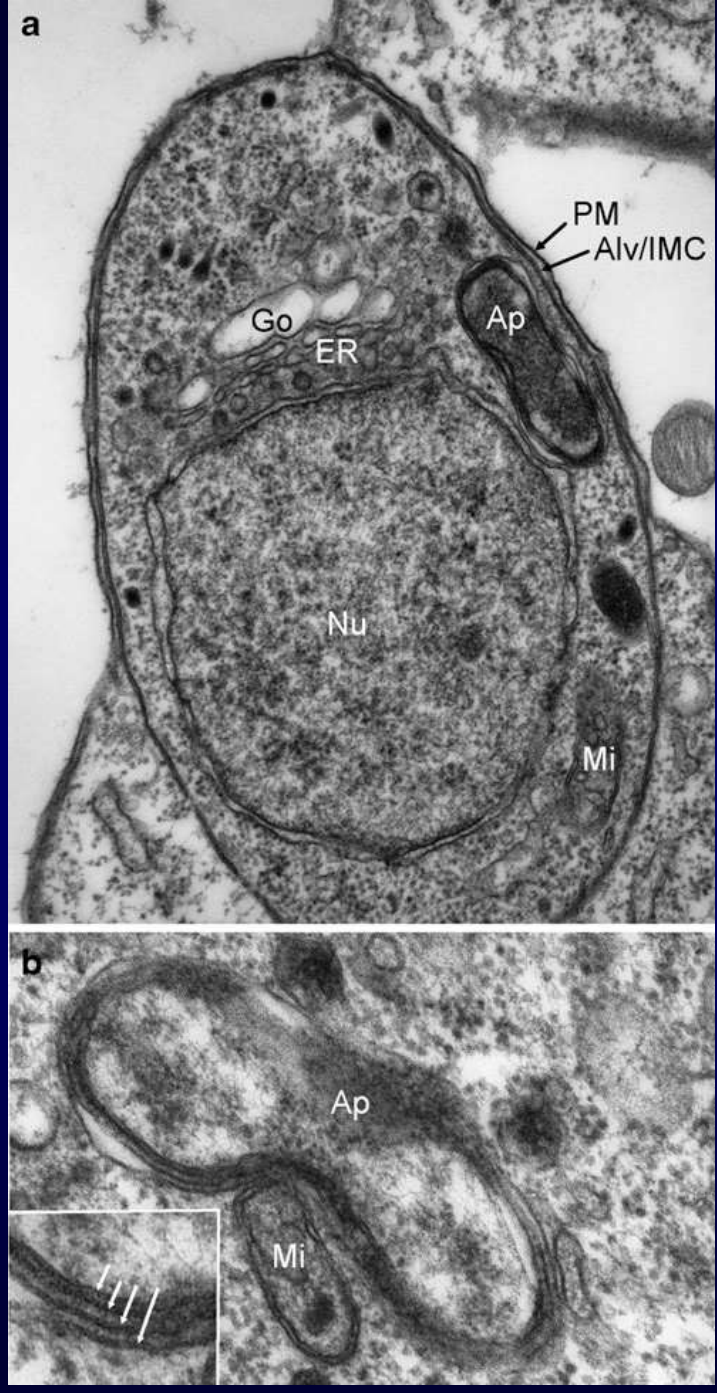

(McFadden, 2011)

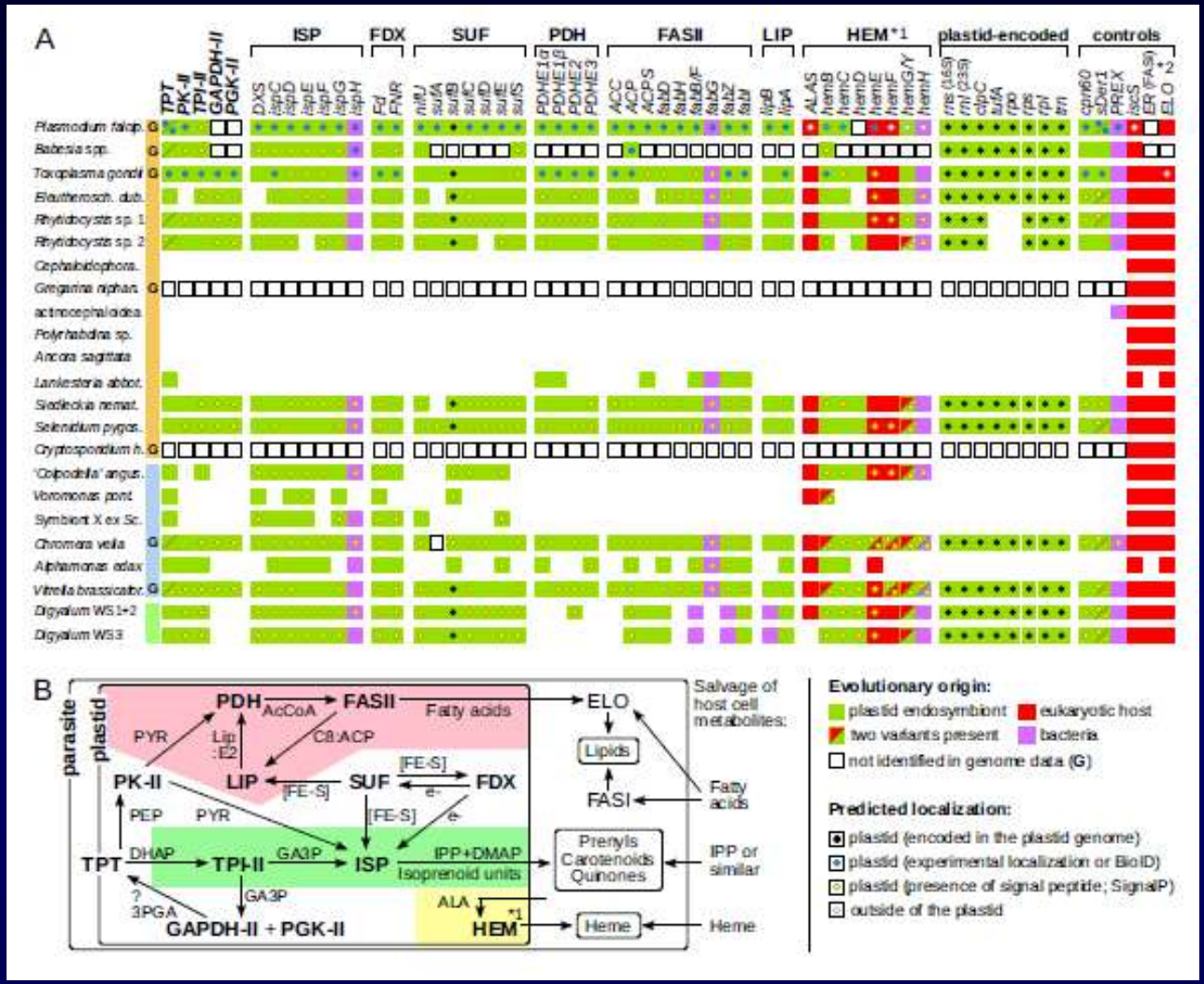

Core plastid metabolism in apicomplexans and their relatives. (A) Presence of genes and pathway modules (top; abbreviations in Supplementary file 4) in representative genomes (G) and transcriptomes (left. Each gene (box) is color-coded as to its evolutionary origin, as determined by a maximum likelihood phylogeny (plastid-encoded rps, rpl, rpo, trn genes were not analyzed). Empty boxes indicate gene absence in completed genomes and blank spaces indicate absence in transcriptomes. Intracellular localization of corresponding proteins is shown by a circle inside the box and summarizes known experimental data (Supplementary file 4) or de novo prediction in silico by SignalP v4.1 (Supplementary file 5); it is missing in proteins with incomplete N-termini. Note that only some enzymes of the heme pathway (HEM) are localized in the plastid (*1) and that signal peptides in FAS:ER and ELO were not predicted (*2). (B) Dependence network of plastid protein modules for the biosynthesis of key metabolites – isoprenoid precursors IPP and DMAP, fatty acids and heme – which underlie dependency on the plastid organelle in Apicomplexa. Colored regions contain modules specific to one pathway: fatty acid (pink), isoprenoid precursor (pale green) and heme biosynthesis (yellow). Interactions are reconstructed from the literature and substrates are shown near arrows (PYR = pyruvate; AcCoA = acetyl coenzyme A, Lip:E2 = lipoylation on PDHE2; C8:ACP = octanoyl:acyl carrier protein; [FE-S]=iron sulphur cluster; PEP = phosphoenolpyruvate; e-=electron reductive power; GA3p=glyceraldehyde-3-phosphate; 3PGA = 3 phosphoglycerate; ALA = d-aminolevulinic acid; ?=uncertainty). DOI: https://doi.org/10.7554/eLife.49662.006 (Janouskovec et al. eLife 2019;8:e49662).

Plastids in Apicomplexa

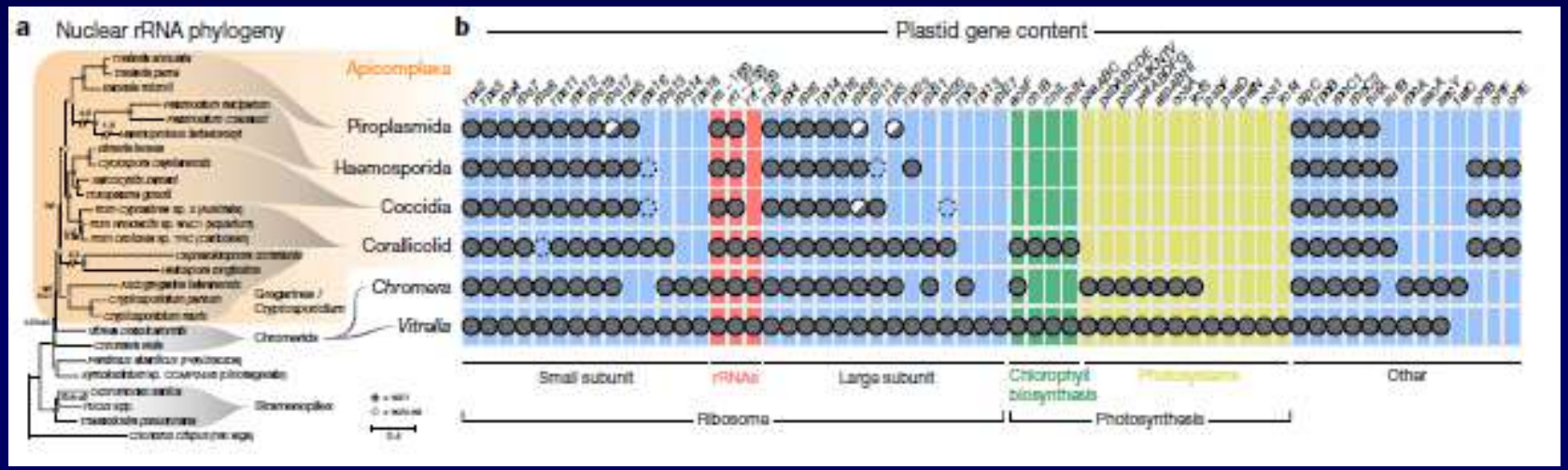

a, Maximum likelihood phylogeny based on concatenation of nucleus-encoded 18S, 5.8S and 28S rRNA genes. Corallicolids branch within the parasitic Apicomplexa, as sister to the Coccidia. Values before and after the forward slash at nodes denote the maximum likelihood bootstrap values and Bayesian posterior probabilities, respectively. **b**, Plastid gene content of the Apicomplexa and free-living relatives. Presence is denoted by filled circles; variable presence between species within a clade is denoted by half-filled circles; dotted circles represent possible gene remnants (pseudogenes or highly divergent sequences). *Chromera* lacks plastid-encoded *chlB*, *chlL* and *chlN* genes, and instead uses nuclear-encoded genes for light-dependent protochlorophyllide reduction. For photosystem genes, *psaABC* indicates *psaA*, *psaB* and *psaC*; the equivalent abbreviated notation is also used for *psbABCDE*, *psbHIJKNTV*, *petABDFG* and *atpABHI* (Kwong et al., 2019).

New comprehension of the apicoplast of *Sarcocystis* by transmission electron tomography

(Tomova et al., 2006)

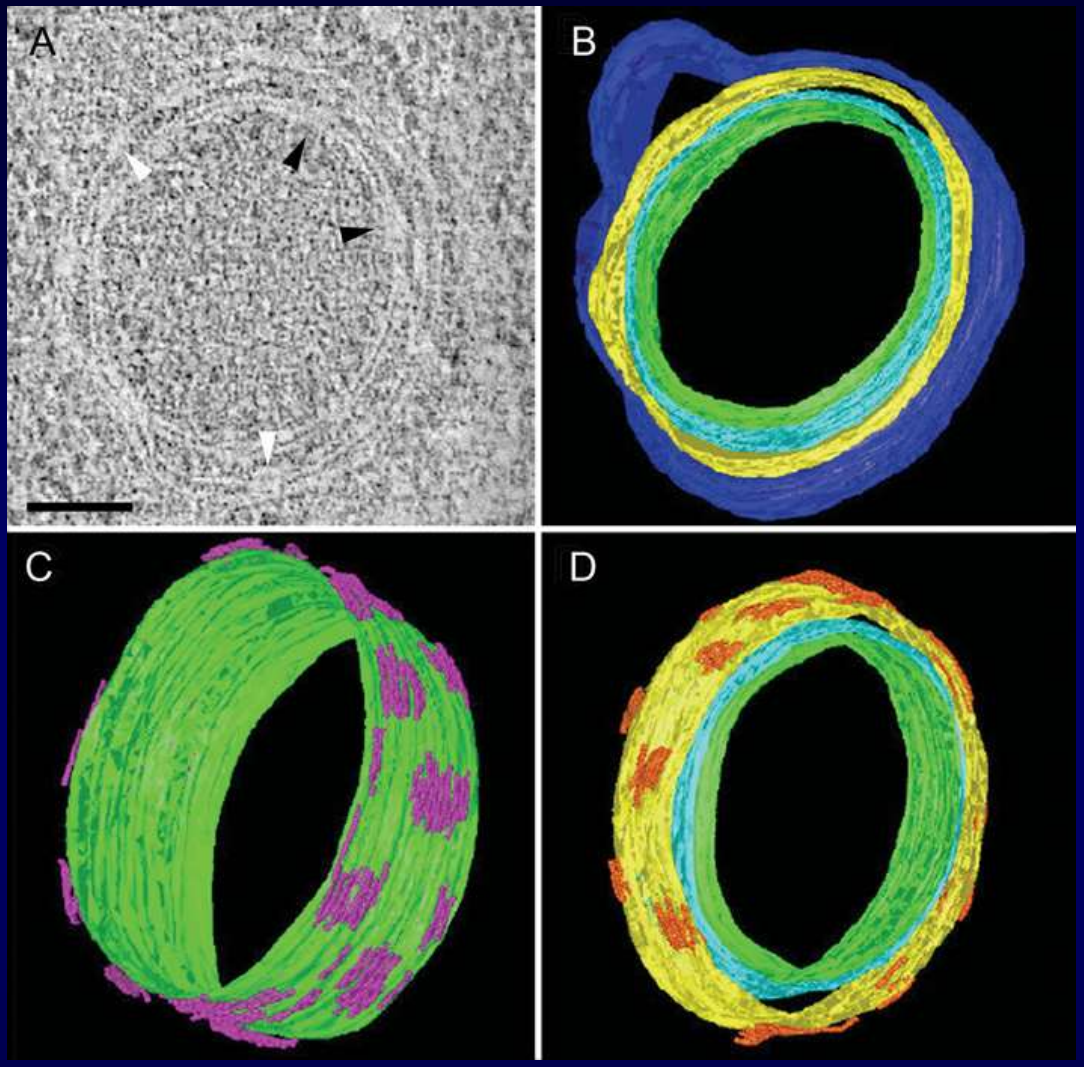

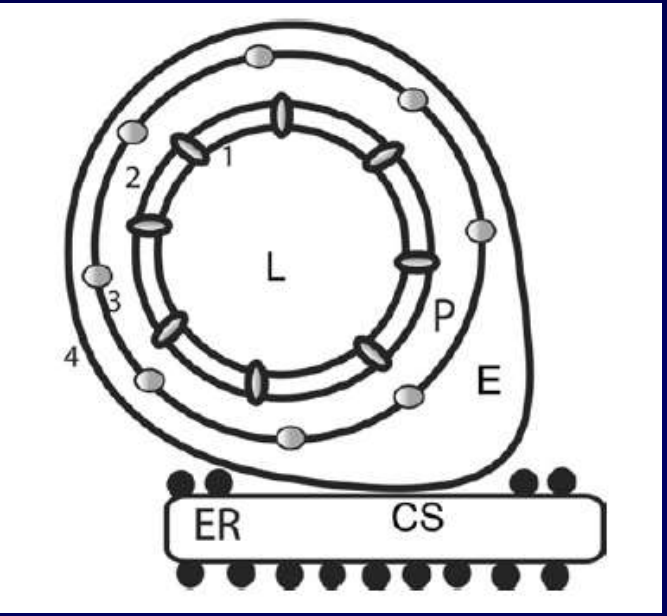

1, first inner membrane; 2, second inner membrane; 3, periplastid membrane; 4, outer membrane; L, lumen; P, periplastid space; E, exoplastid space; CS, contact site.

Three-dimensional models of the apicoplast membranes and the protein complexes in the different apicoplast membranes
(A) A median slice of the apicoplast in *Sarcocystis* generated from a double-tilt tomographic reconstruction. The image shows the four continuous membranes, the protein complexes in the inner membrane (black arrowheads), the protein complexes in the outer membrane (white arrowheads) and a protuberance of the outer membrane into the cytoplasm of the parasite (asterisk). Scale bar, 100 nm. (B) Three-dimensional model of the four membranes surrounding the apicoplast: in green the innermost membrane, in light blue the second membrane, in yellow the periplastid membrane and in dark blue the outermost membrane are shown. In the upper left part of the image, a clear protuberance of the outer membrane can be observed. (C) The model illustrates the distribution and size of the protein complexes (violet) between the two inner membranes. For clarity, only the innermost membrane (in green) is shown. Note that the model is not scaled correctly with respect to models (B, D). (D) Distribution of the protein complexes (orange) in the third periplastid membrane. A Supplementary Video to accompany this Figure can be seen at http://www.biolcell.org/boc/098/boc0980535add.htm.

Membrane Contact Sites between Apicoplast and ER in *Toxoplasma gondii* Revealed by Electron Tomography (Tomova et al., 2009)

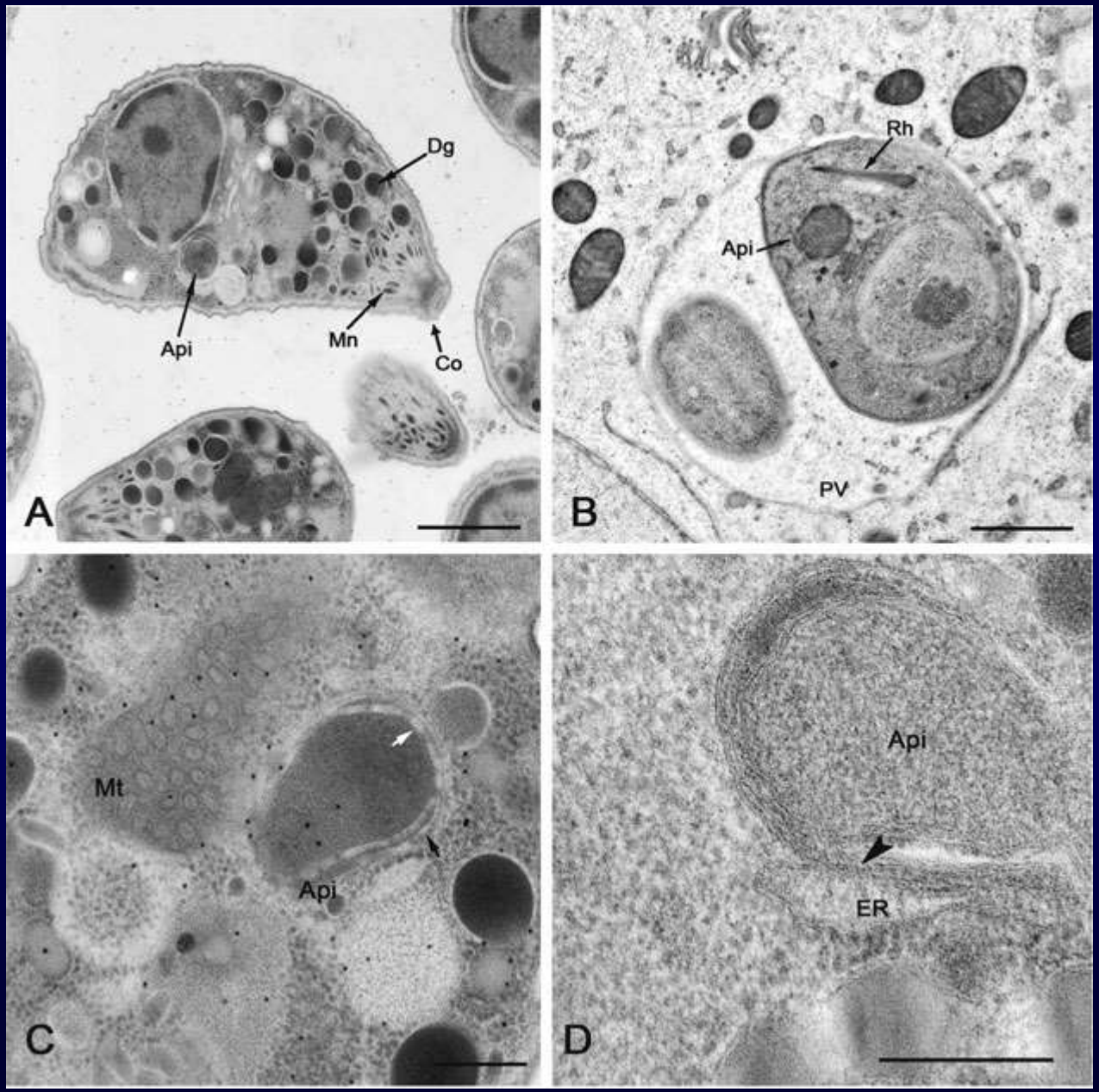

Micrographs (60–70 nm thick sections) illustrating the parasite *Toxoplasma gondii* with a focus on the apicoplast.

A) An overview of a sample of free tachyzoites substituted in 2% osmium tetroxide and embedded in Epon. The typical features for the phylum are clearly distinguishable: nucleus, conoid (Co), dense granules (Dg), micronems (Mn) and apicoplast (Api). B) An intracellular parasite substituted with 0.1% uranyl and embedded in Lowicryl HM20. Parasitophorous vacuole (PV) and rhoptry (Rh).
C) An apicoplast with its typical features: the four membranes; patches spanning the inner membranes (white arrow) and those on the periplastid (black arrow) are clearly visible. D) Another apicoplast, where the close association with the ER is indicated by an arrowhead. Note that the gold particles in images (A) and (C) are randomly applied fiducial markers used for image alignment. Epon embedded samples were post-stained with 20% uranyl acetate and lead citrate, as described. Lowicryl sections were examined without being post-stained. The scale bars in (A) and (B) are 500 nm and in (C) and (D) 100 nm. Figure 1 also illustrates the differences in contrast, structure preservation and visualization depending on the sample preparation.

Membrane Contact Sites between Apicoplast and ER in *Toxoplasma gondii* Revealed by Electron Tomography (Tomova et al., 2009)

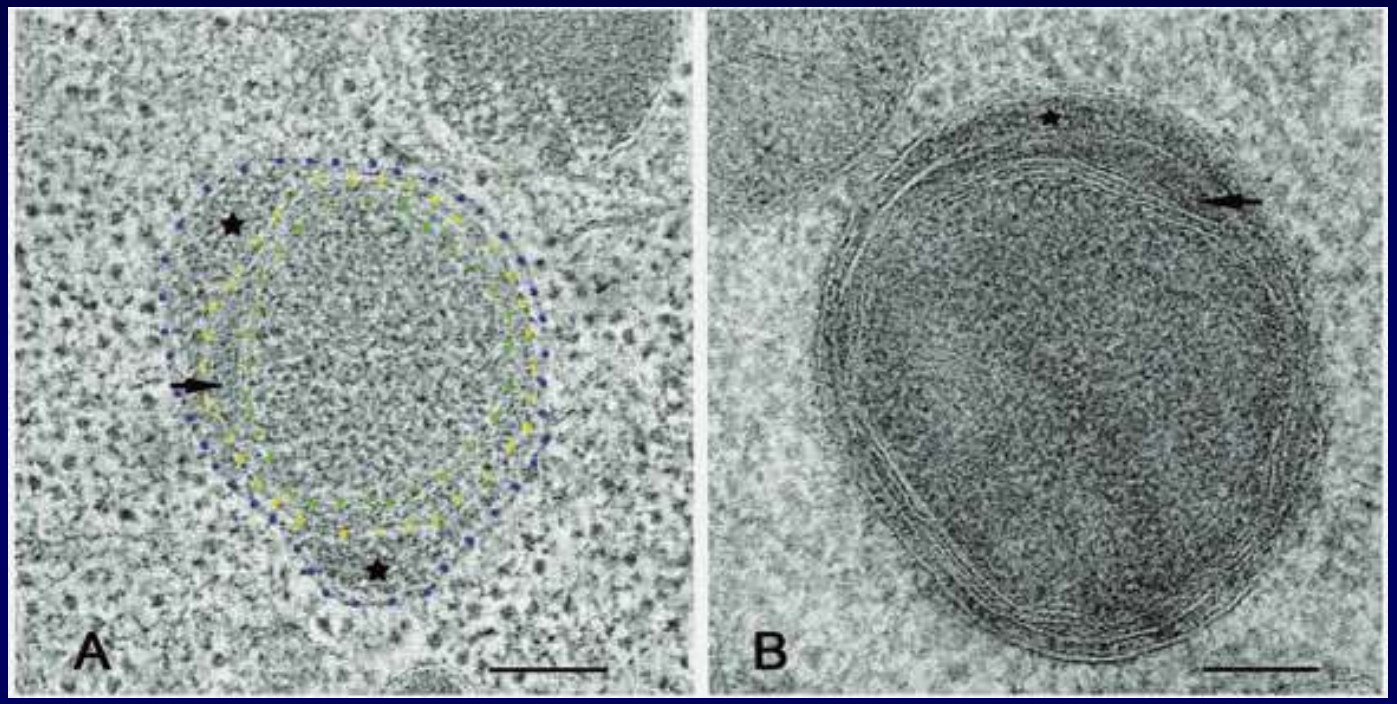

Different apicoplasts, showing the variability of the exoplastid compartment (EPC) and the periplastid compartment (PPC).
A) A tomographic slice of a reconstruction from a thick section (200 nm). The exoplastid space (asterisk) and the periplastid space (arrow) are indicated. For clarity the innermost membrane, the periplastid membrane (PPM) and the outermost membrane are indicated with colours green, yellow and blue, respectively. B) Micrograph of 60–70 nm thick section, showing the same features. Both images are from samples substituted in 0.1% uranyl acetate and embedded in Lowicryl HM20. No additional contrasting was applied. The scale bars are 50 nm.

Membrane Contact Sites between Apicoplast and ER in *Toxoplasma gondii* Revealed by Electron Tomography (Tomova et al., 2009)

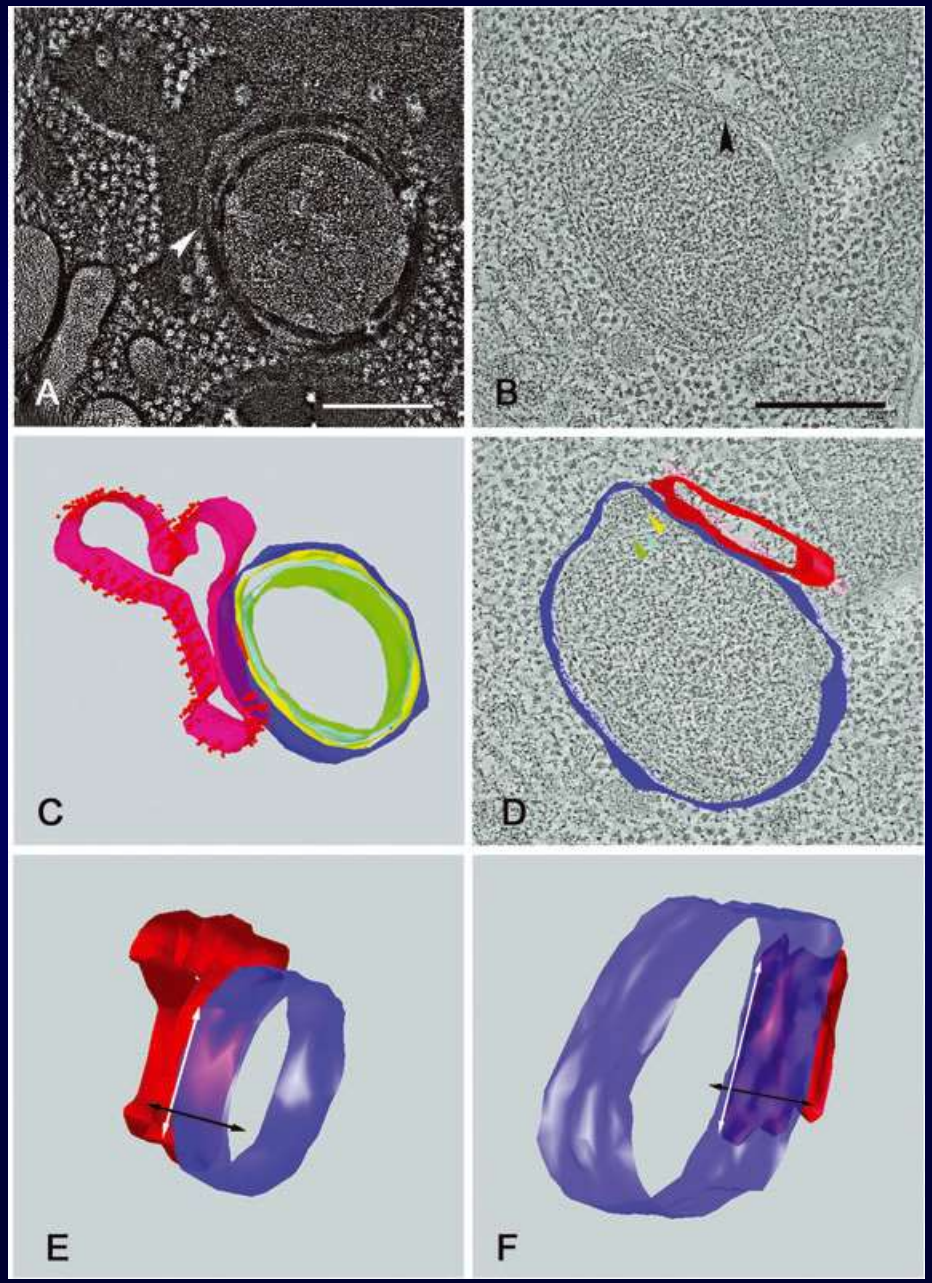

Images illustrating the relation between the ER and the apicoplast outermost membrane.
A) Image of an apicoplast (inverted contrast) from a tomographic reconstruction of a thin section (60–70 nm). The relation between the membranes of the ER and the apicoplast is pointed (white arrowhead). B) Tomographic slice of another apicoplast. This is a reconstruction of a thick section (200 nm). The lamellar structure of all the membranes is visible. No additional contrasting was applied. The close alignment of the outermost apicoplast membrane and the ER is pointed by an arrowhead. C) View of a model generated by the tomographic reconstructions of the apicoplast in (A). The ER sheet is made transparent so the outermost membrane (dark blue) is being visible as an intact, continuous membrane not fusing at any point with the membrane of the ER (red). D) View of a model generated by the tomographic reconstruction of the plastid shown in (B). Only the outermost membrane of the plastid and the closely apposed ER sheet are presented. E and F) are the models of the two reconstructions, (E) of the thin section and (F) of the thick section, respectively. They represent only the apicoplast outermost membrane (transparent, dark blue) and the ER sheet (red). The models are oriented in a way to enable the visualization of the ER sheet through the inner side of the outermost apicoplast membrane. The arrows indicate the Z direction of the sample volume (black) and the direction parallel to the membranes (white). These images illustrate the actual dimensions of the MCSs. The zones with highest intensity (very bright purple, resulting from the exact overlap of bright red – the ER membrane and the transparent blue – the outermost apicoplast membrane) represent the place of closest apposition of the two membranes. In (E) such overlap (resulting in bright purple) occupies the complete membrane in Z, which is approximately 50 nm while in (F) it is clearly just one third of it and it also corresponds to approximately 50 nm. The scale bars in (A) and (B) are 200 nm.

Жизненный цикл споровиков

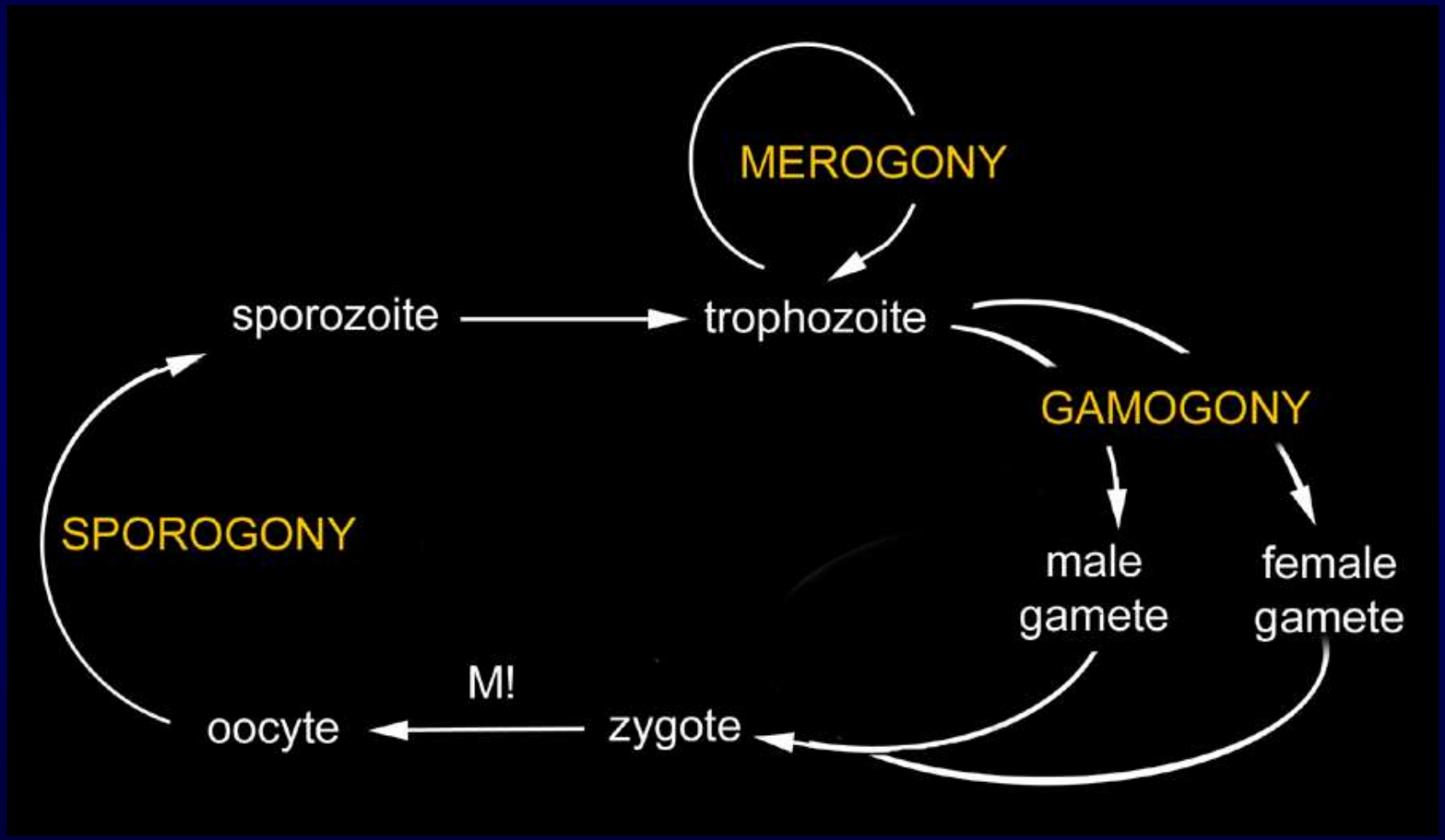

Studies on Meiotic Division in Coccidial amd Malarial Parasites (Canning, Anwar, 1968)

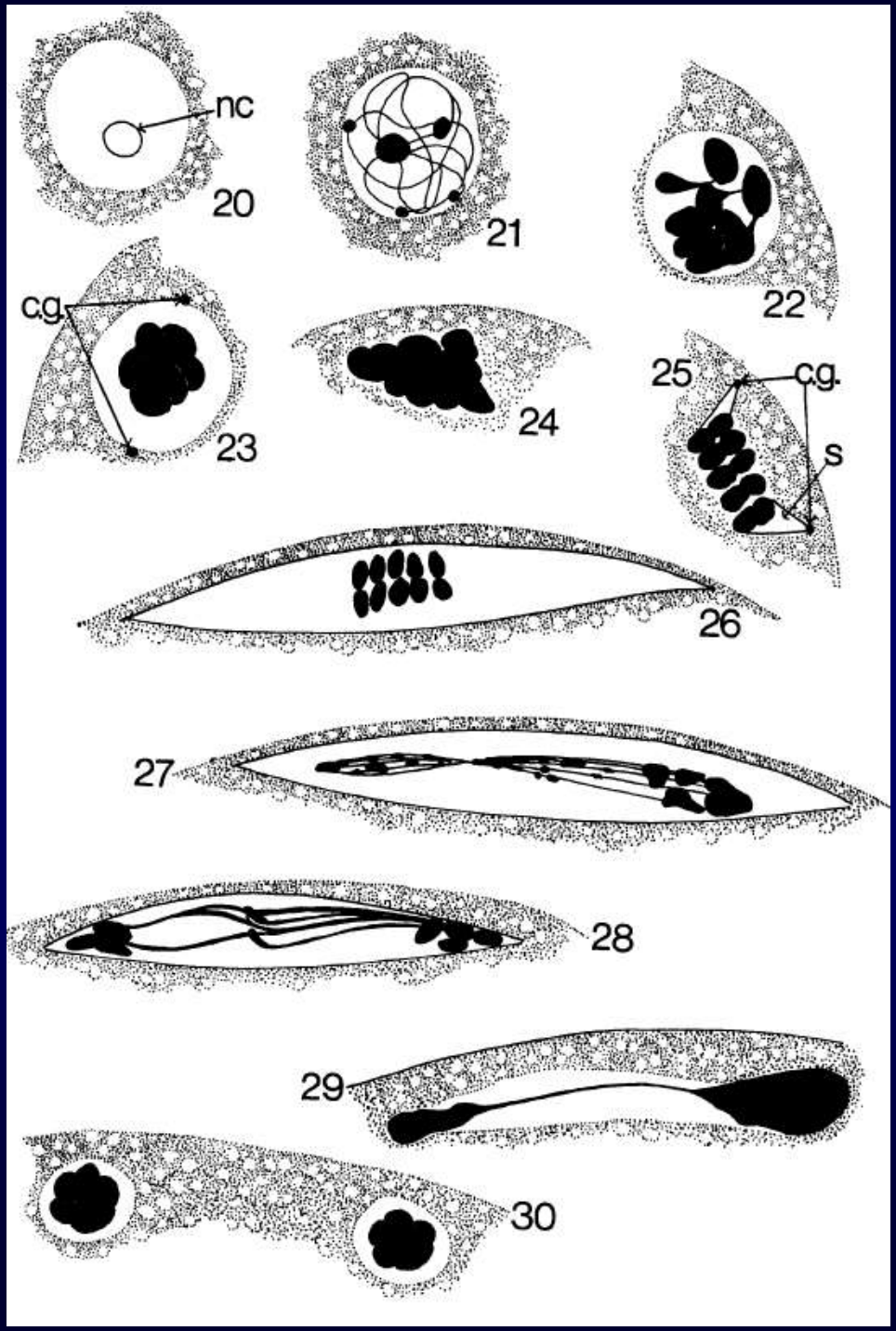

Figs.20-30. Diagrammatic representation of meiosis in *Eimeria* oocysts. 20. Resting nucleus with nucleolus (n.c.). 21. Early prophase nucleus showing filamentous chromosomes with beaded portions. 22. Condensation of filaments into 10 rod-like chromosomes with rounded ends. 23. Arrangement of chromosomes like a mulberry in the center of the nucleus and appearance of centriolar granules (c.g.) on the nuclear membrane. 24. Spreading out of chromosomes after break-down of nuclear membrane. 25. Alignment of chromosomes in 2 rows of 5 on a spindle(s) between the 2 centriolar granules (c.g.). 26. Arrangement of the 2 rows of chromosomes parallel to the long axis of the now very elongate spindle. 27. Stretching of the chromosomes as beaded filaments during migration to the spindle poles. 28. Condensation of chromosomes as short rods at spindle poles towards the end of their migration across the spindle. 29. Almost complete separation of clusters of chromosomes at spindle poles. 30. Separate daughter nuclear each with 5 chromosomes after meiosis.

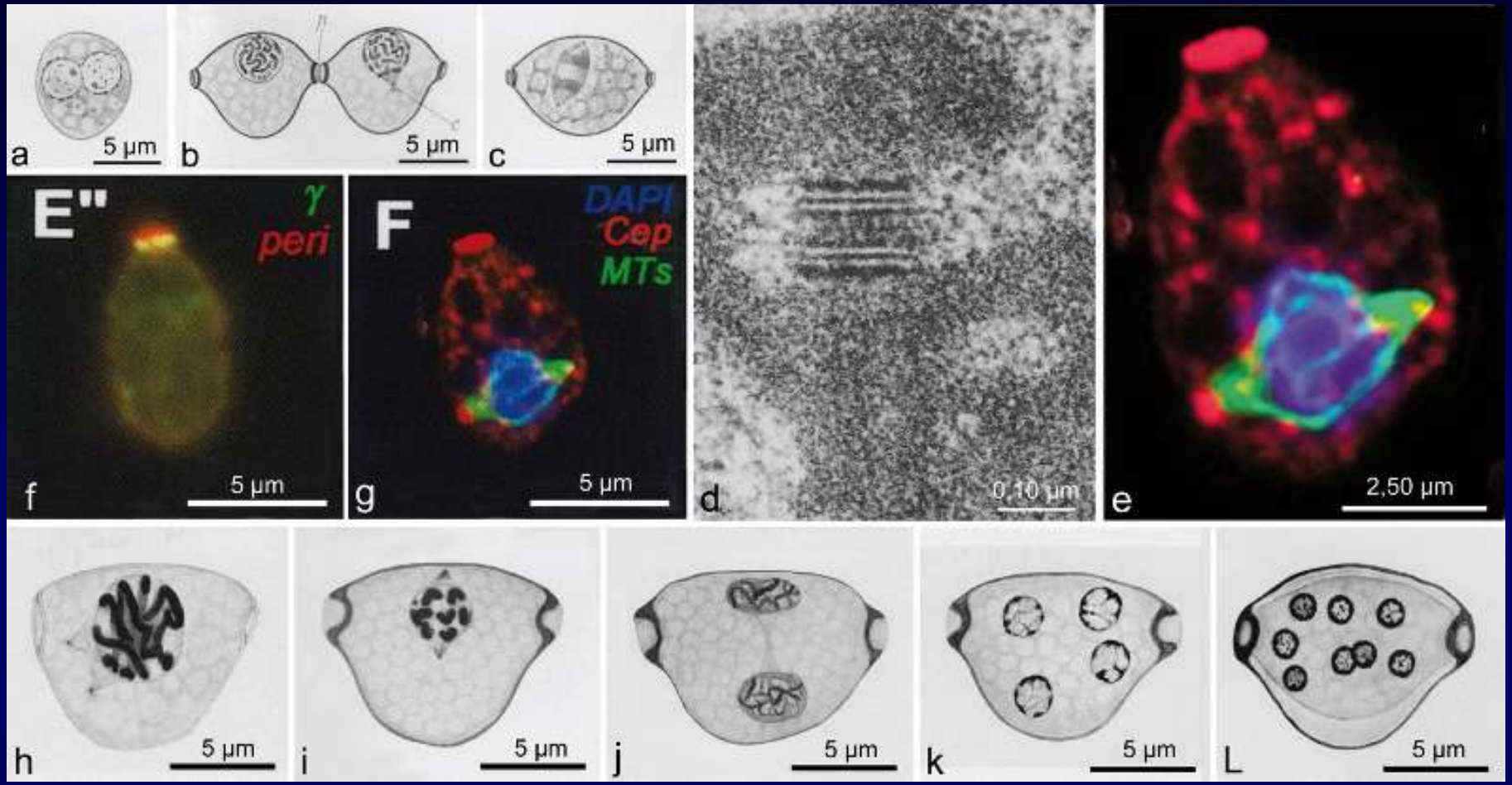

Nuclear and cell differentiation during the sporogony of *Stylocephalus*, *Grebnickiella* and *Lecudina*. **a–c.** Zygote and young *S.longicollis* sporoblast: (a) formation of the zygote with the male and female nuclei of the gametes. (b) sporoblast at the beginning of the first nuclear division. (c) first mitosis; (a–c from smears stained with Heidenhain's hematoxylin). **d.** TEM of a young *Grebnickiella* sporoblast showing a synaptonemal complex of the first nuclear division after fertilization which demonstrated the meiosis in this species. **e–g.** Indirect immunoflorescence of the first division in the *L.tuzetae* sporoblast (e and g), with the position of the spindle visualized with Antibodies against anti-α-tubulin (green), anti-cep (red) and DNA (purple) staining with DAPI. **f.** Immunostaining for γ-tubulin and the pericentriolar cep protein (The pericentriolar material contains proteins responsible for microtubule nucleation and anchoring including γ-tubulin, pericentrin and ninein.). h–l. Different stages of sporogony in *S.longicollis* prepared by histological sectioning at 5–6 µm and Heidenhain's hematoxylin staining. h. First meiotic division at the pachytene stage with two hemi-spindles, **i.** metaphase of the first meiotic division. **j.** Interphase after the formation of the first two nuclei, **k.** sporoblast with the four nuclei. **l.** Third and final mitosis producing eight nuclei in *S.longicolis*. [From (a–c) Leger, 1904; (d) Molon-Noblot & Desportes, 1977; (e–g) Kuryama et al., 2005; (h-l) Grell, 1940]

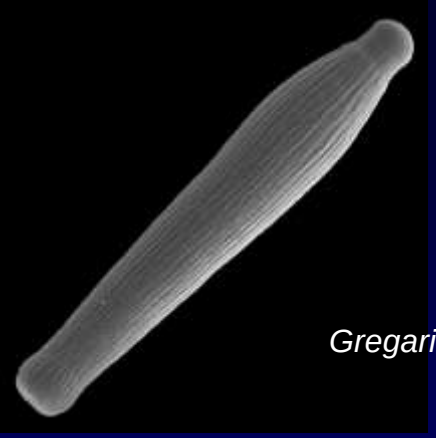

Gregarina polymorpha

Monocystis agilis

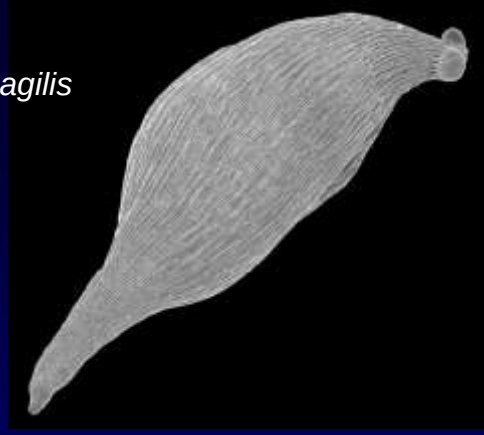

Diversity of apicomplexans

«*Some people think that such simple creatures cannot have that many morphological types, but I have calculated that there are, conservatively speaking,* ***2,654,736*** *possible morphologically different oocysts for Eimeria, to say nothing of differences in host, location in host organs and cells, etc. My calculations take into account such morphologic characters* ***as*** *oocyst and sporocyst shape and size, number of layers in the oocyst wall, color, roughness, absence or presence and type of micropyle, micropylar cap, oocyst residuum, sporocyst residuum, polar granule, Stieda body, sporozoite refractile globules, etc.-numbers mount up fast in a geometric progression.*» (Norman Levine, 1962. Protozoology Today. J.Protozool., v.9 (1), pp. 1-6.)

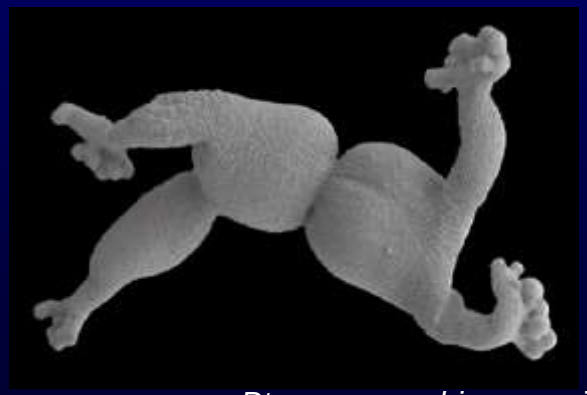

Pterospora schizosoma in syzygy

Plasmodium gallinaceum

Система споровиков (Adl et al., 2018)

Apicomplexa Levine 1980, emend. Adl et al. 2005

Aconoidasida Mehlhorn et al. 1980 [= Hematozoa Vivier 1982] (P)

Haemosporорida Danilewsky 1885. *Plasmodium*.

Piroplasmorida Wenyon 1926. *Babesia*, *Theileria*.

Nephromycida Cavalier-Smith 1993, emend. Adl et al. 2019. *Nephromyces*, *Cardiosporidium*

Conoidasida Levine 1988 (P)

Coccidia Leuckart 1879 (P). *Adelina, Hepatozoon, Eimeria*.

Gregarinasina Dufour 1828 (P). *Cryptosporidium, Gregarina, Selenidium*.

Blastogregarinea Chatton and Villeneuve 1936, emend. Simdyanov et al. 2018. *Siedleckia*.

Incertae sedis Apicomplexa: Agamococcidiorida Levine 1979. *Gemmocystis, Rhytidocystis*.

Incertae sedis Apicomplexa: Protococcidiorida Kheisin 1956. *Coelothropha*, *Grellia*, *Eleutheroschizon*.

Incertae sedis Apicomplexa: *Agreggata*.

Hypothetical tree of Apicomplexa.

Three principal parasitic groups are coloured and their life cycle indicated, as well as Cryptosporidium that likely emerged from within gregarines. Numbers on branches and thickness indicates diversity (i.e. named species).

Jan Šlapeta, 2011

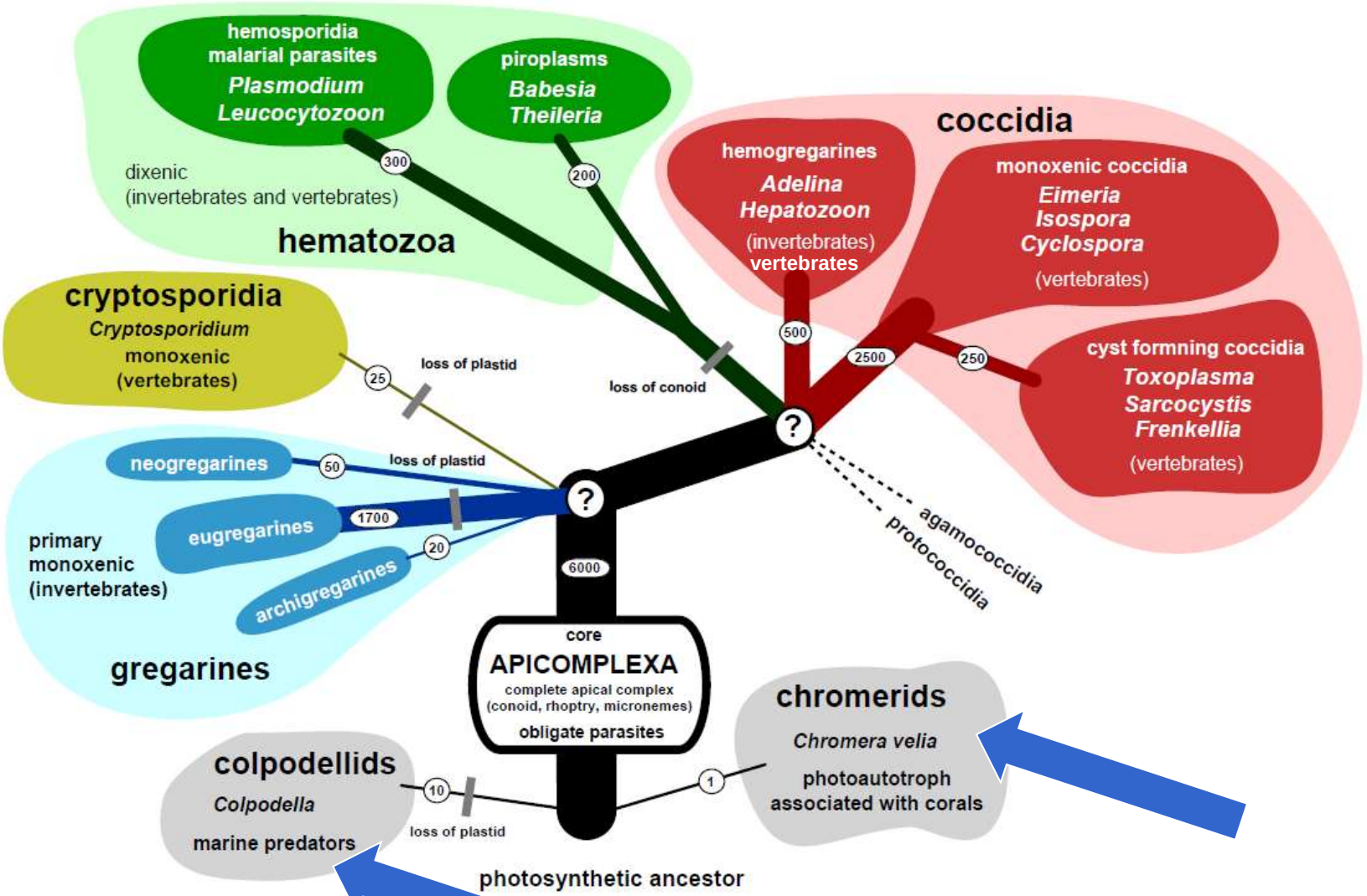

Chrompodellids (Janouškovec et al., 2015)

Diversity of apicomplexans

Структуры	Грегарины	Гемогрегарины	Эймериорины	Гемоспоридии	Пироплазмиды
полярное кольцо	есть\нет	есть	есть	есть	есть \ нет
коноид	есть	есть	есть	есть \ нет	нет
микронемы	есть \ нет	есть	есть	есть	есть \ нет
роптрии	есть	есть	есть	есть	есть
субпелликулярные микротрубочки	есть	есть	есть	есть	есть \ нет
микропоры	есть	есть	есть	есть	есть
дефинитивный хозяин	БПЗ	БПЗ	ПЗ	БПЗ (диптеры)	БПЗ (клещи)
промежуточный хозяин	обычно нет \ БПЗ	ПЗ	обычно нет	ПЗ	ПЗ
локализация в ПЗ (в БПЗ)	----- (кишечник, полости тела, ткани)	кровь, ткани (кишечник)	Кишечник, ткани (-----)	кровь, ткани (кишечник)	кровь, ткани (кишечник)
механизм передачи	ооцисты	via БПЗ: поедая или при питании кровью	ооцисты	via БПЗ	via БПЗ
типы шизогонии	мерогония есть \ нет, гаметогония, спорогония,	мерогония, гаметогония, спорогония	мерогония, гаметогония, спорогония	мерогония, гаметогония, спорогония	мерогония, спорогония
число мерозоитов в поколении	?	неограниченное	ограниченное	неограниченное	неограниченное
половая детерминация	есть	есть	есть	есть	? + есть

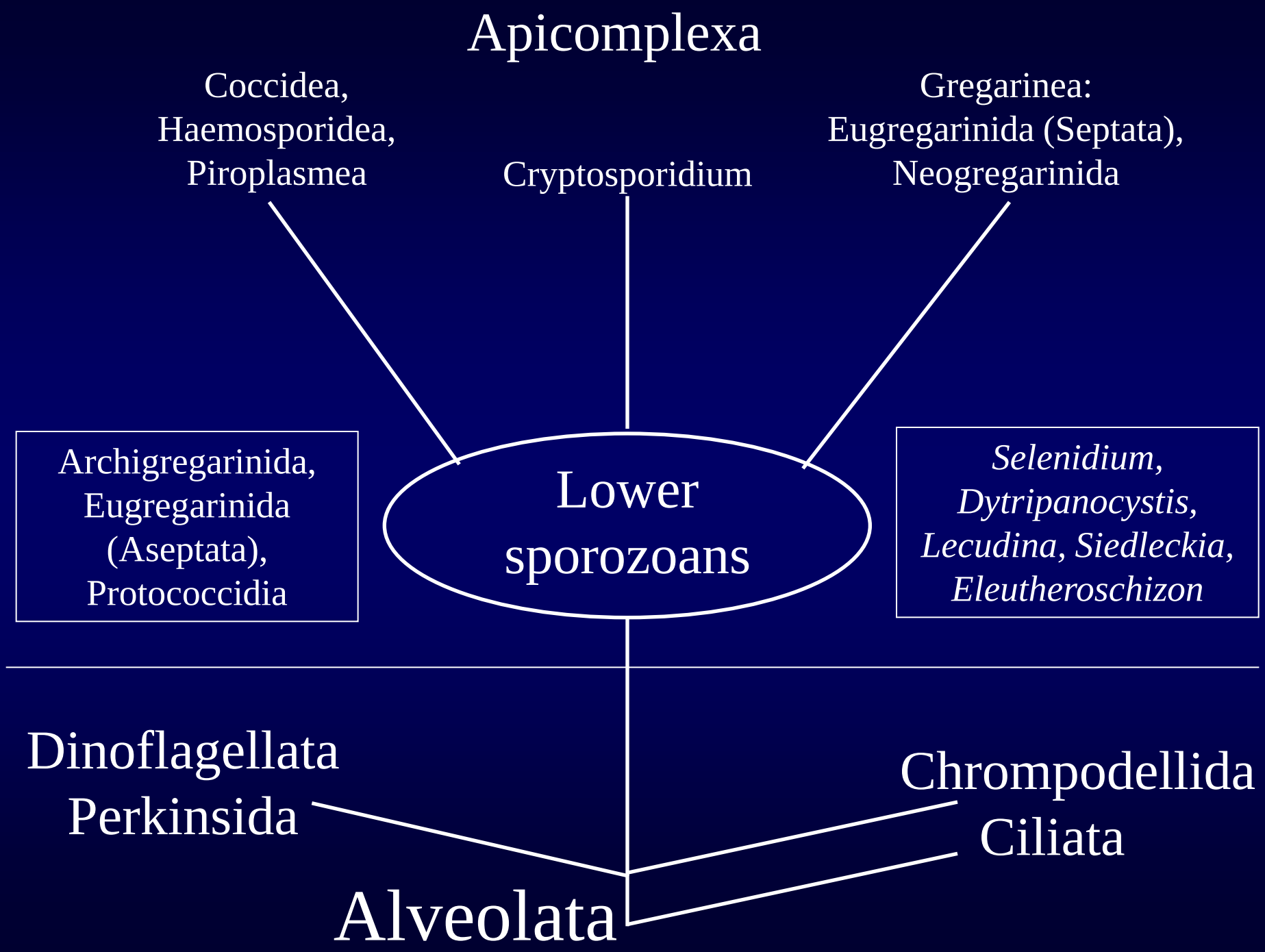
Apicomplexa
Coccidea,
Haemosporidea,
Piroplasmea
Cryptosporidium
Gregarinea:
Eugregarinida (Septata),
Neogregarinida
Archigregarinida,
Eugregarinida
(Aseptata),
Protococcidia
Lower
sporozoans
Selenidium,
Dytripanocystis,
Lecudina, *Siedleckia*,
Eleutheroschizon
Dinoflagellata
Perkinsida
Chrompodellida
Ciliata
Alveolata

Внутриклеточный паразитизм:

- утрата клеточной полярности,
- утрата клеточной подвижности,
- усложнение жизненного цикла за счет мерогонии.

Внеклеточный паразитизм:

- усовершенствование локомоторного аппарата,
- Усовершенствование прикрепительного аппарата.

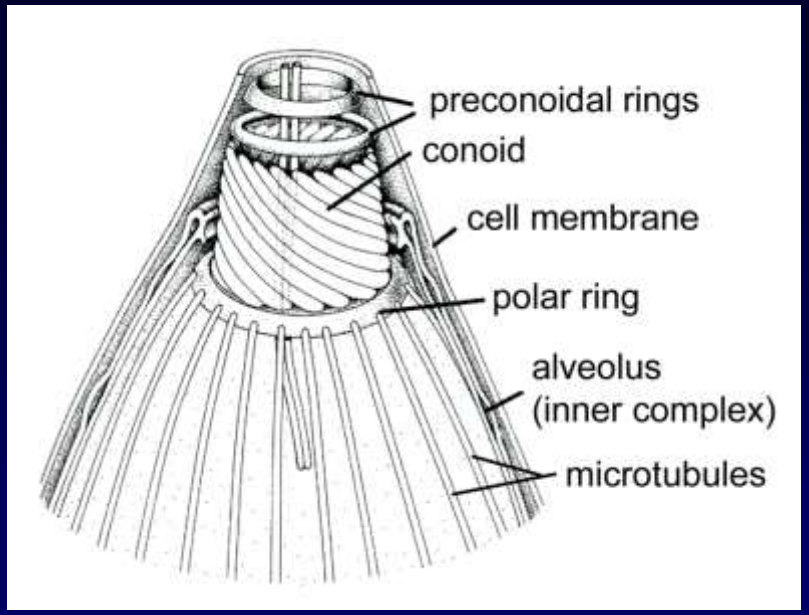

Toxoplasma gondii

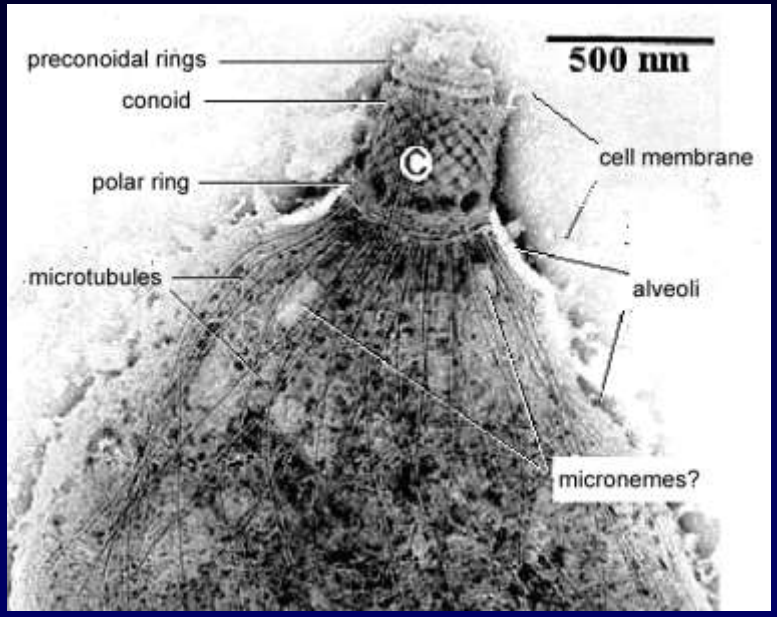

(Morrisette et al. 1997)

Коноид:

- Открытый конус
- Образован из модифицированного тубулина, организованного отлично от тубулина в микротрубочках (трубочки не полые, мелко исчерченные).
- Используется для мизоцитоза или как туннель для протоков роптрий.

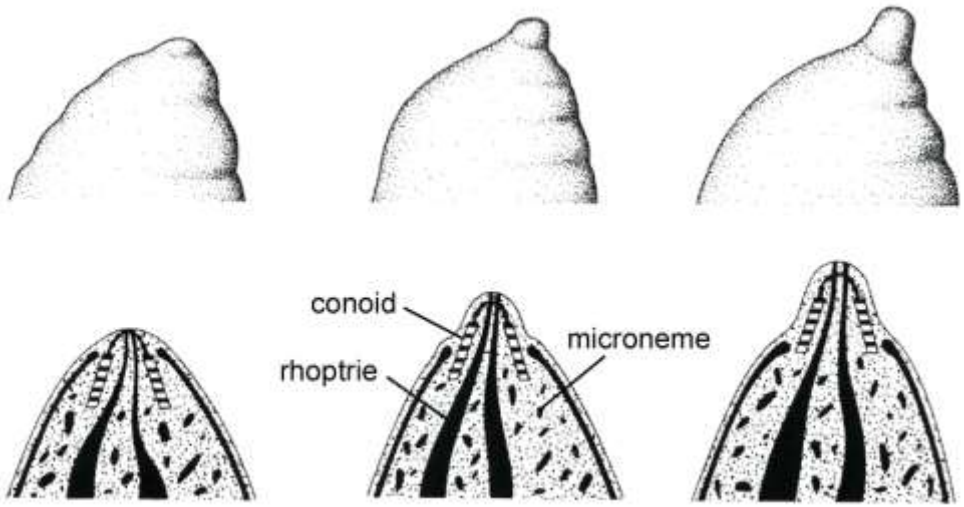

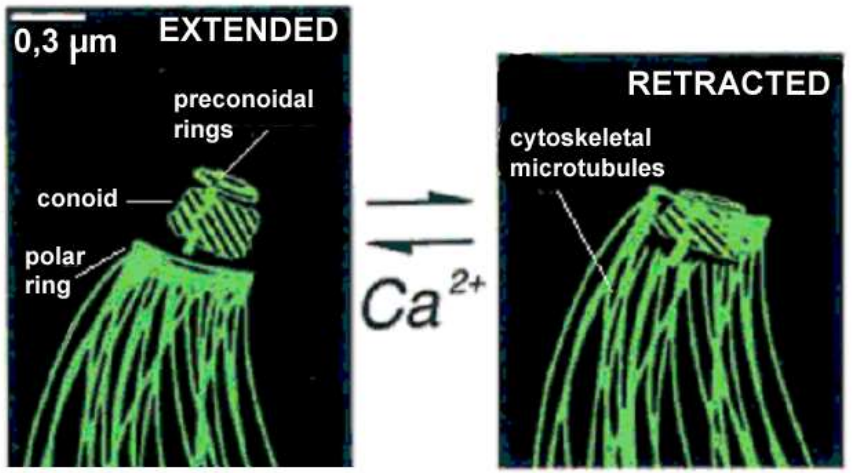

(Hu et al., 2002)

Transmission electron microscopy. Right: Control cell. The inner membranes are continuous up to the conoid (arrowheads). Rhoptries (r) and dense granules (g) are pointed out. Left: Ionophore-treated tachyzoites. The conoid is extruded (arrowheads), and the inner pellicle ends at the bottom of it. Rhoptries and dense granules are seen.

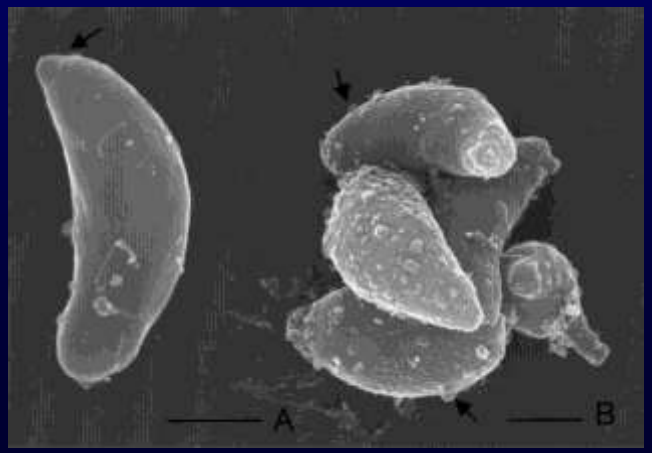

Conoid: structure and function
Toxoplasma gondii

Scanning electron microscopy. A. Control cell; a smooth surface and the conoid region (arrow) are observed. B. Ionophore-treated cells. A group of tachyzoites with blebs all over the cell surface (arrows).

(Monteiro et al., 2001)

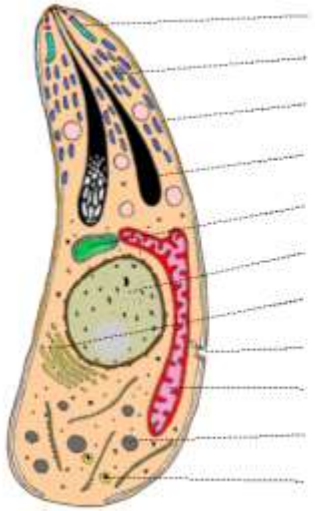

The acidocalcisome

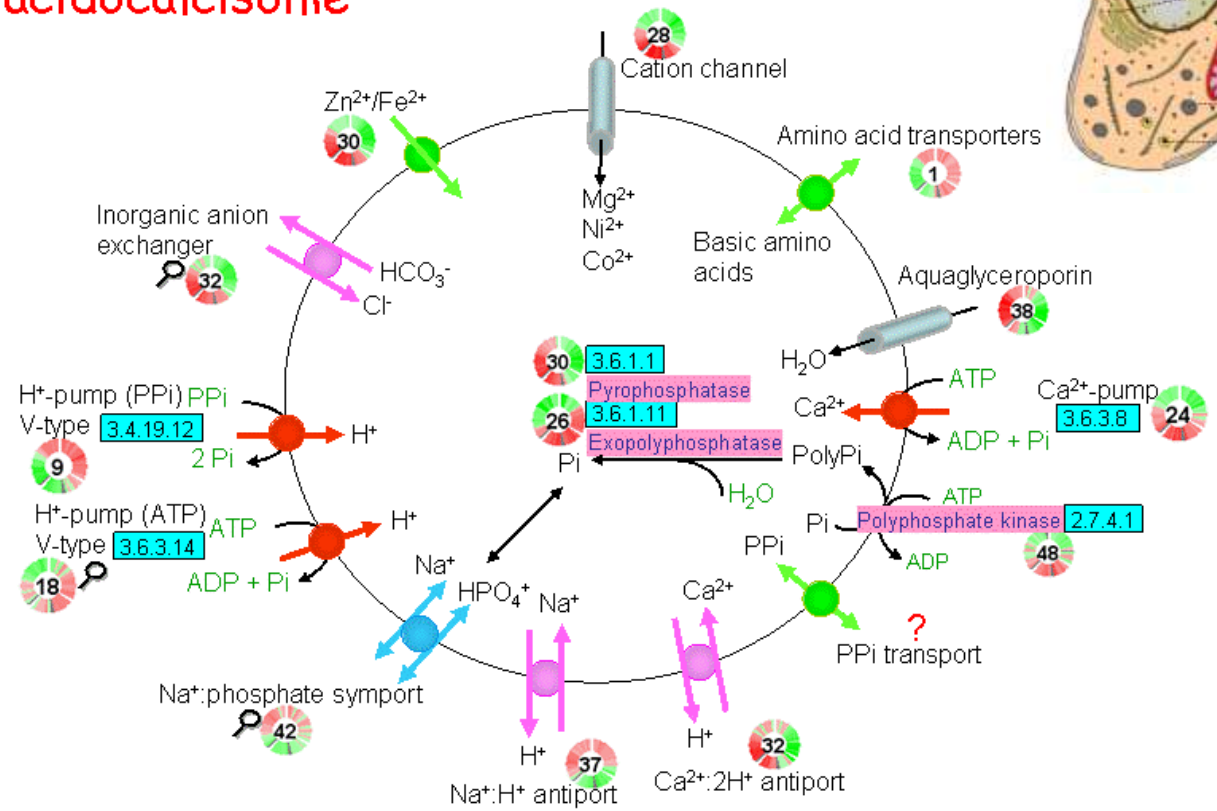

The acidocalcisome is rich in pyrophosphate, short and long-chain polyphosphate (PolyPi), magnesium, calcium, sodium and zinc. A proton (H^+) gradient is established by a vacuolar H^+-ATPase and a vacuolar H^+-pyrophosphatase. Ca^{2+} uptake occurs in exchange for H^+ by a reaction catalyzed by a vacuolar Ca^{2+}- ATPase. Ca2+ release could occur in exchange for H+ and is favored by sodium-proton exchange. An aquaporin (aquaglyceroporin) allows water transport. Other transporters (for example, for Mg, Zn,, basic amino acids) are probably present. Phosphate (Pi) is probably accumulated via the Na^+:Pi symporter as there are no genes encoding Pi and or PPi transporters in the genome. An exopolyphosphatase and a pyrophosphatase may also be present. Polyphosphate kinase could function to generate PolyPi and transport it into the acidocalcisome. A question mark indicates the lack of genetic evidence for their presence. Compilation assisted by Silvia Moreno.

Adapted from Miranda K, de Souza W, Plattner H, Hentschel J, Kawazoe U, Fang J, Moreno SN. Acidocalcisomes in Apicomplexan parasites. Exp Parasitol. 2008 118(1):2-9. PMID: 17761167

Acidocalcisomes in *Toxoplasma gondii*

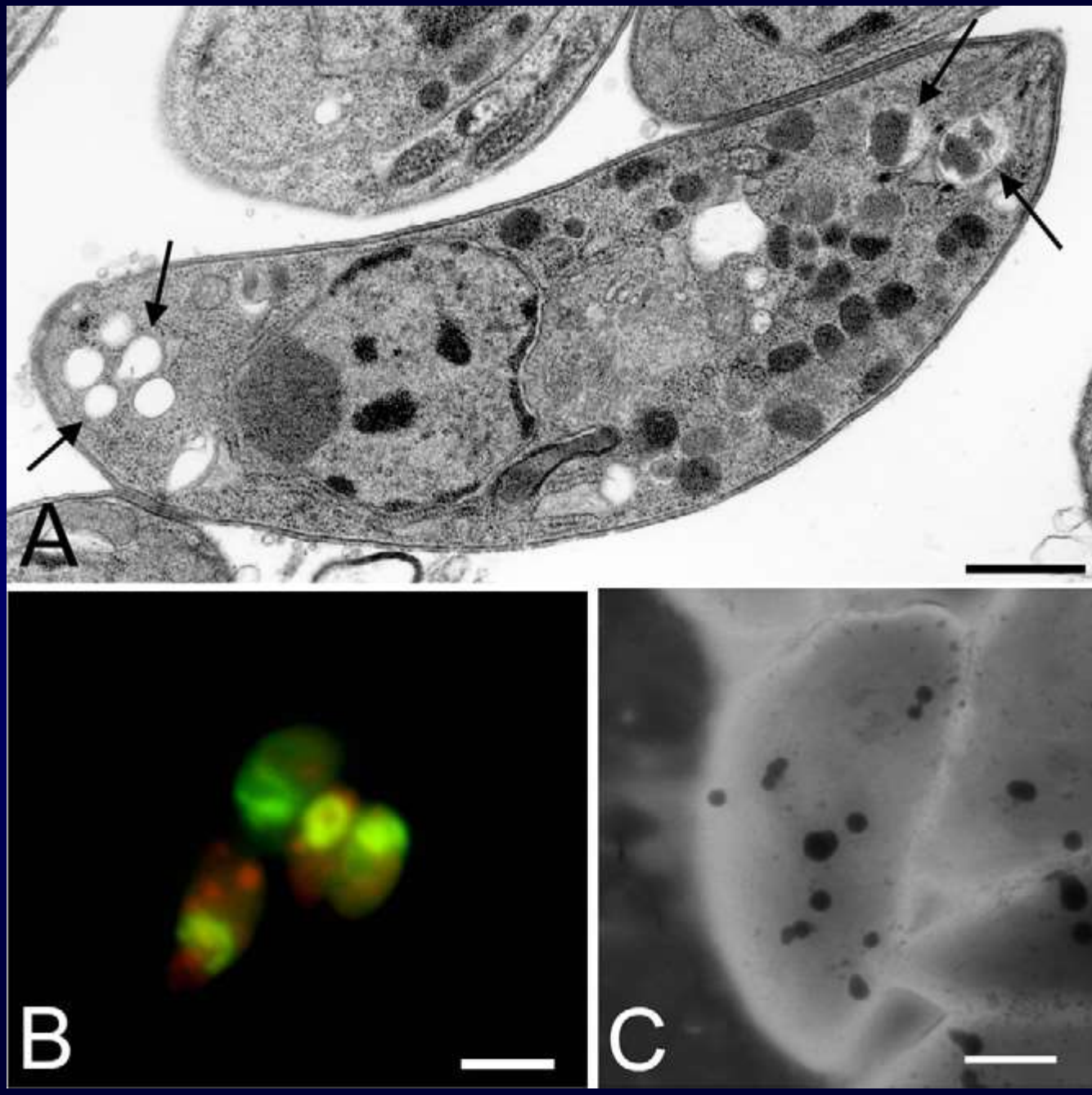

Morphology of acidocalcisomes in whole cells and sections. (A) Ultrathin sections of *Toxoplasma gondii* showing the acidocalcisomes as empty vesicles or containing electron dense material (arrows). (B) Acridine orange staining of acidocalcisomes (red vesicles) of *T. gondii* tachyzoites. (C) Visualization of acidocalcisomes in whole unfixed *Toxoplasma gondii* allowed to adhere to Formvar- and carboncoated grids and then observed by direct transmission electron microscopy (using an energy filter). Acidocalcisomes (black granules) appear disperse in the cytoplasm. Bars (A) = 500 nm; (B) = 3 m; (C) = 1 m (Docampo, Moreno, 2011).

Acidocalcisomes in *Toxoplasma gondii*

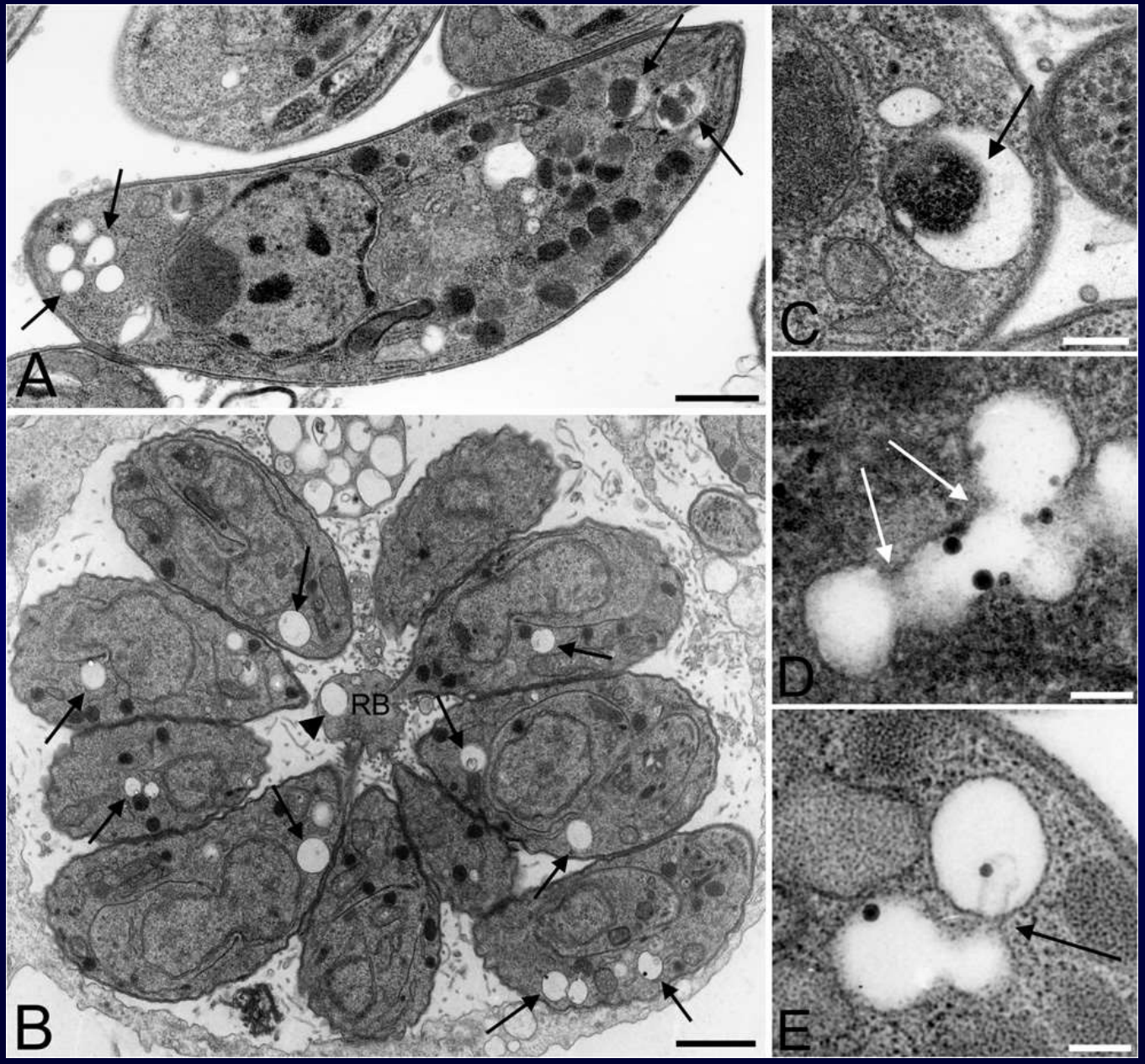

Transmission electron microscopy of *Toxoplasma gondii* acidocalcisomes in isolated tachyzoites and intracellular parasites. (A–E), thin sections of isolated *T. gondii* tachyzoites (A) and intracellular parasites (B) showing several acidocalcisomes (arrows) (C–D), high magnification of portions of tachyzoites showing several profiles of acidocalcisomes. They appear as empty vesicles containing some residual electron dense material as a result of the procedure used for routine transmission electron microscopy. Note that some organelles seem to fuse with each other or to undergo fission (D–E). Scale bars: (A) 500 nm; (B) 3 lm; (C) 200 nm; (D) 100 nm; (E) 200 nm. (A, C–E) from Moreno et al. (2007a), with permission (Miranda et al., 2008).

Acidocalcisomes in *Eimeria acervulina*

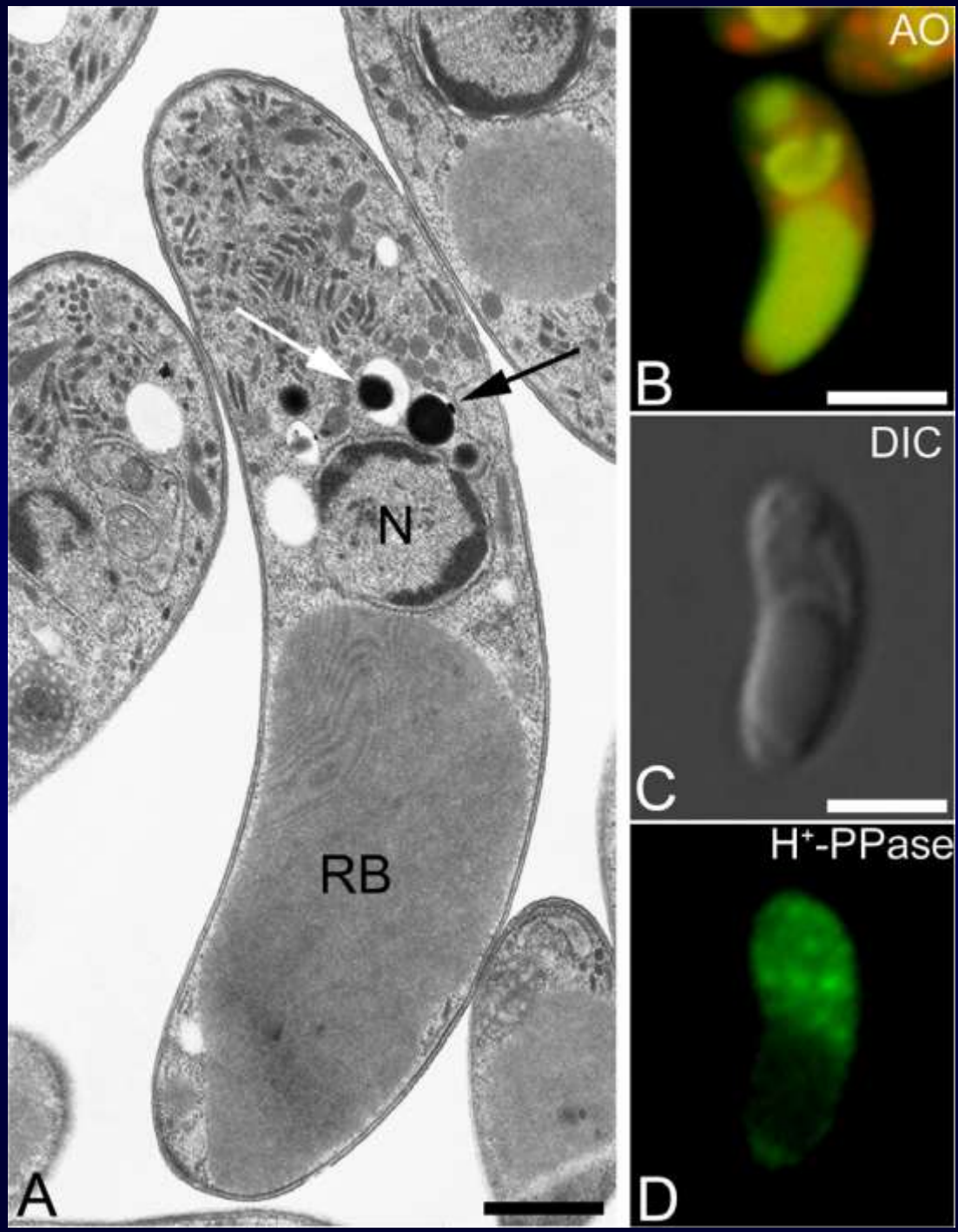

(A) Transmission electron microscopy of sporozoites of *Eimeria acervulina*, showing the fine structure of acidocalcisomes (arrows). Acidocalcisomes partially (white arrow) of totally (black arrow) filled by the electron dense content, mainly present in the form of polyphosphate-bound cations (not shown), are observed. RB, refractile body, N, Nucleus. Scale bar, 500 nm. (B) Acridine orange of a sporozoite of *E. acervulina*. Several acidic organelles (stained in orange) are observed in the cytoplasm. Note binding of acridine orange to the nucleus and the refractile body (green). Scale bar: 3 lm. (C) and (D) Immunofluorescence of *E. acervulina* using antibodies raised against a conserved sequence of Arabidopsis thaliana V-H+PPase. Staining of small intracellular structures (presumably the acidocalcisomes) can be seen in the anterior region of the parasite (D). (C) Differential interferential contrast microscopy corresponding to the fluorescence image shown in (D). Scale bar: 3 mkm (Miranda et al., 2008).

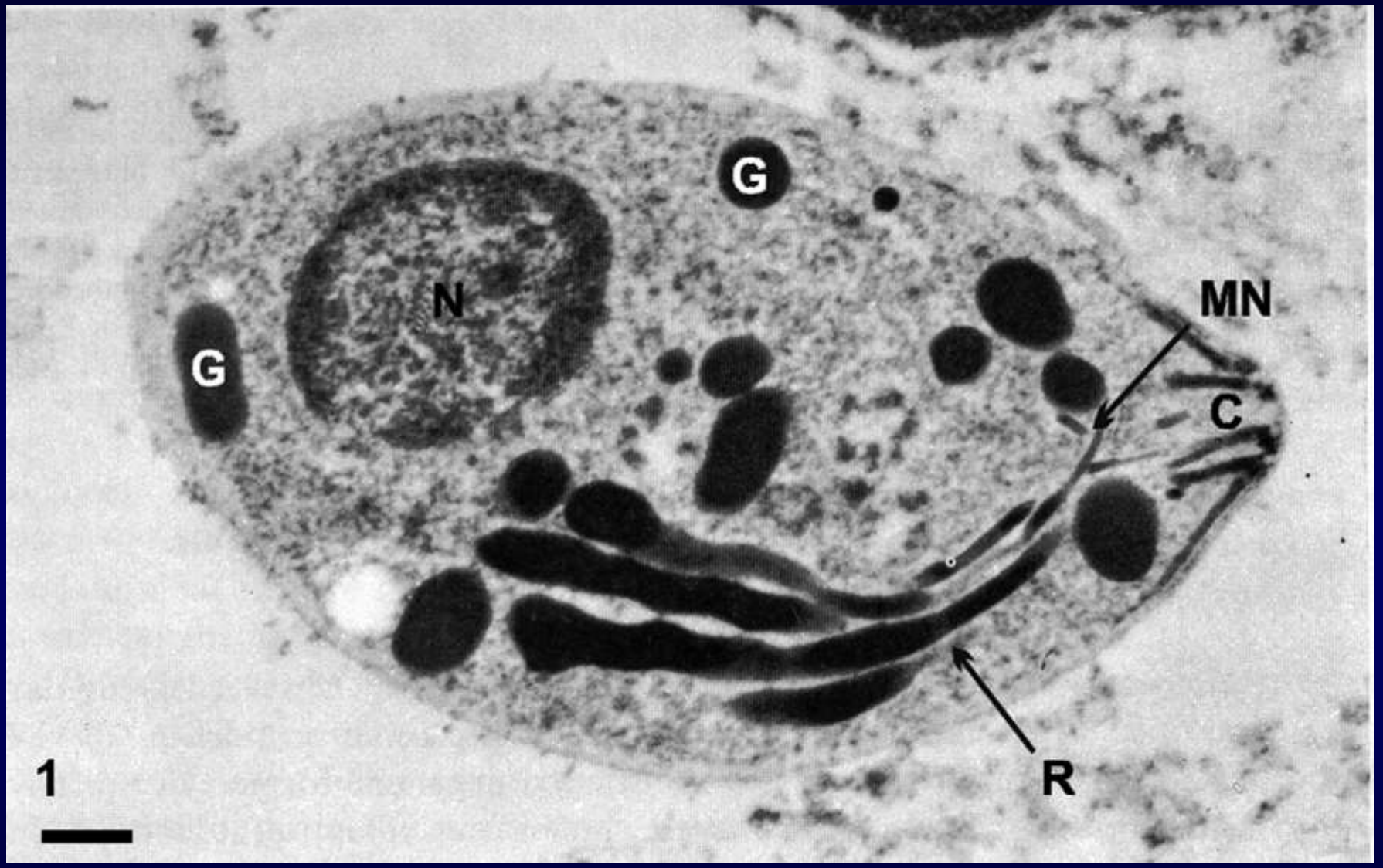

Transmission electron microscopy of a tachyzoites of *Toxoplasma gondii* submitted to the ethanolic phosphotungstic acid technique, which labels structures containing basic proteins. In addition to the nucleus (N), staining of the dense granules (G), Rhoptries (R), Micronemes (M) and the Conoid (C) is observed. Bar, 0.3µm. After De Souza and Souto-Padrón 1978.

Varied microneme abundance in Apicomplexa (Dubois, Soldati-Favre, 2019)

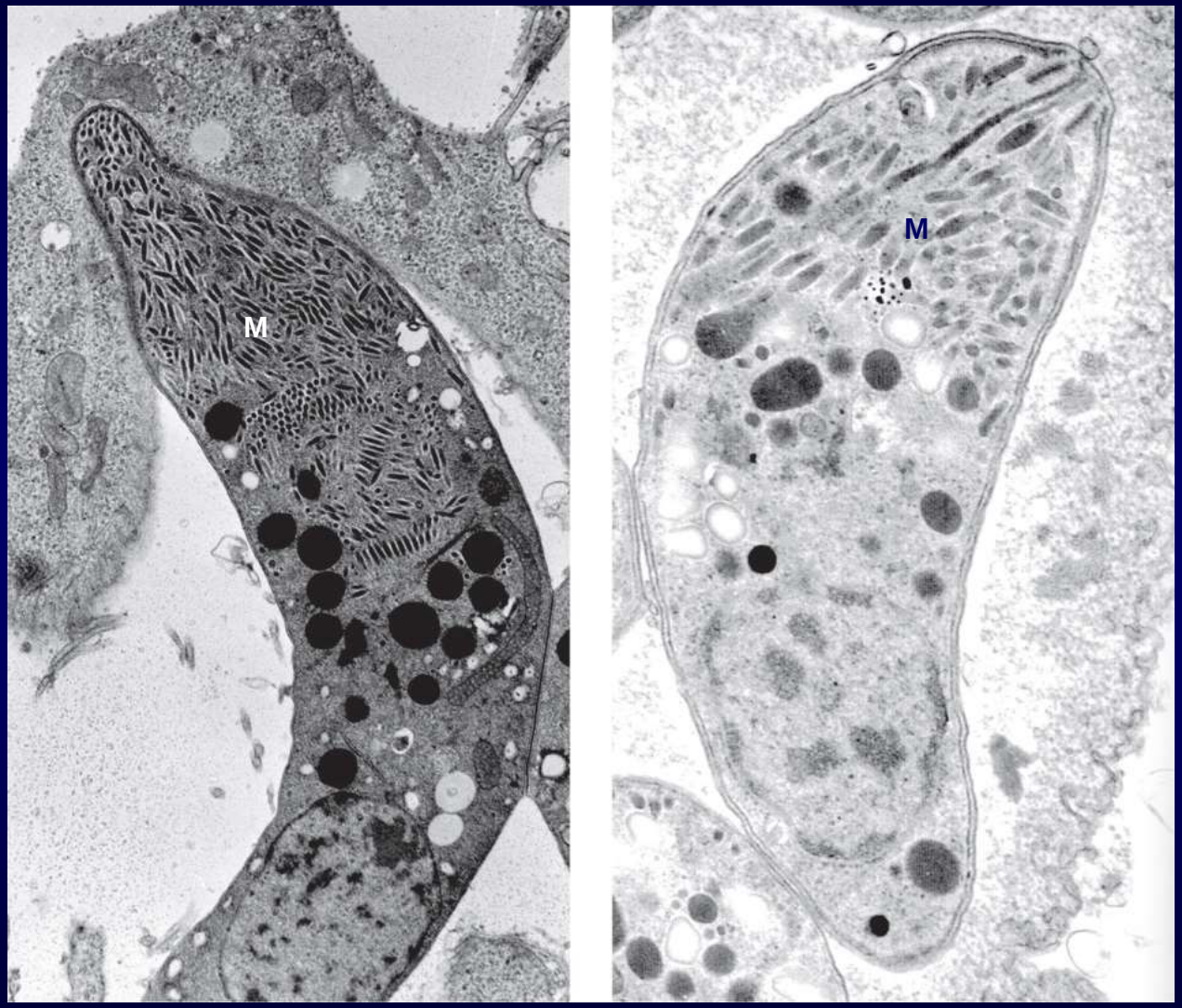

Electron microscopy images of (a) *Sarcocystis muris* cystozoite (Scale bar: 2 μm) and (b) *Toxoplasma gondii* bradyzoite (Scale bar: 500 nm). Micronemes (M) Image (a) provided by JF. Dubremetz (b) Reproduced with permission (Dubremetz & Ferguson, 2009)

Microneme Proteins in Apicomplexans (Carruthers, Tomley, 2008)

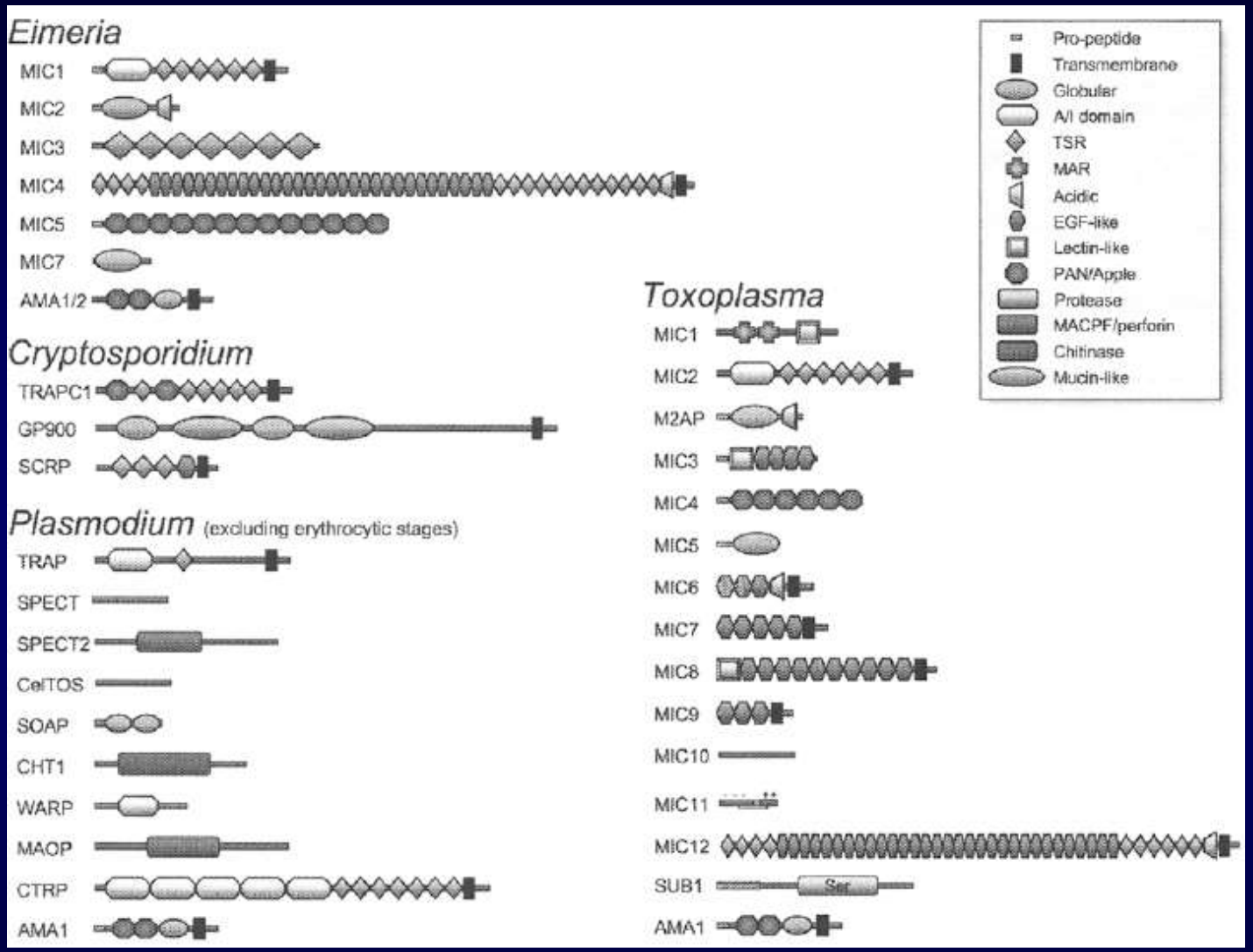

Modular MICs. Schematic representations of known micronenne proteins from four different apicomplexan genera are depicted (notto scale). Accession numbers, where available: *Bmerla tenella* MIC1, M73495; EtMIC2, Z71755; EtMIC3, AAR87667; EtMIC4, CAC34726; EtMICS, AJ245536; C/yptospor/c//(im parv^tymTRAP-C1 ,AAB92609;GP900,AAC98153;CpSCRP AF061328; *Plasmodium falciparum* TRAP, AACl 867; *Plasmodium berghei SPECT*, BAD08209; PbSPECT2, BAD83404; PbCelTOS, BAD97683; PbSOAP, AAL07530; PbCHTI, CAC40151; PbWARP, AAK83296; PbMOAP, AAV28504; PbCTRP, AAF73158; *Toxoplasma gondii* MIC1, CAA96466;TgMIC2,AAB63303;TgM2AP,AAK74070;TgMIC3,CAB56644;TgMIC4AAD33906; TgMIC5,CAA70921;TgMIC6,AAD28185;TgMIC7,AAK35070;TgMIC8,AAK19757;TgMIC9, AAK19758; TgMICIO, AAG32024; TgMICII, AAN16379; TgMIC12, AAK58479; TgAMAI, AF010264; TgSUBI, AAK94670. A color version of this figure is available online at www.eurekah.com.

Schematic model of AMA1-processing events in Plasmodium falciparum merozoites.

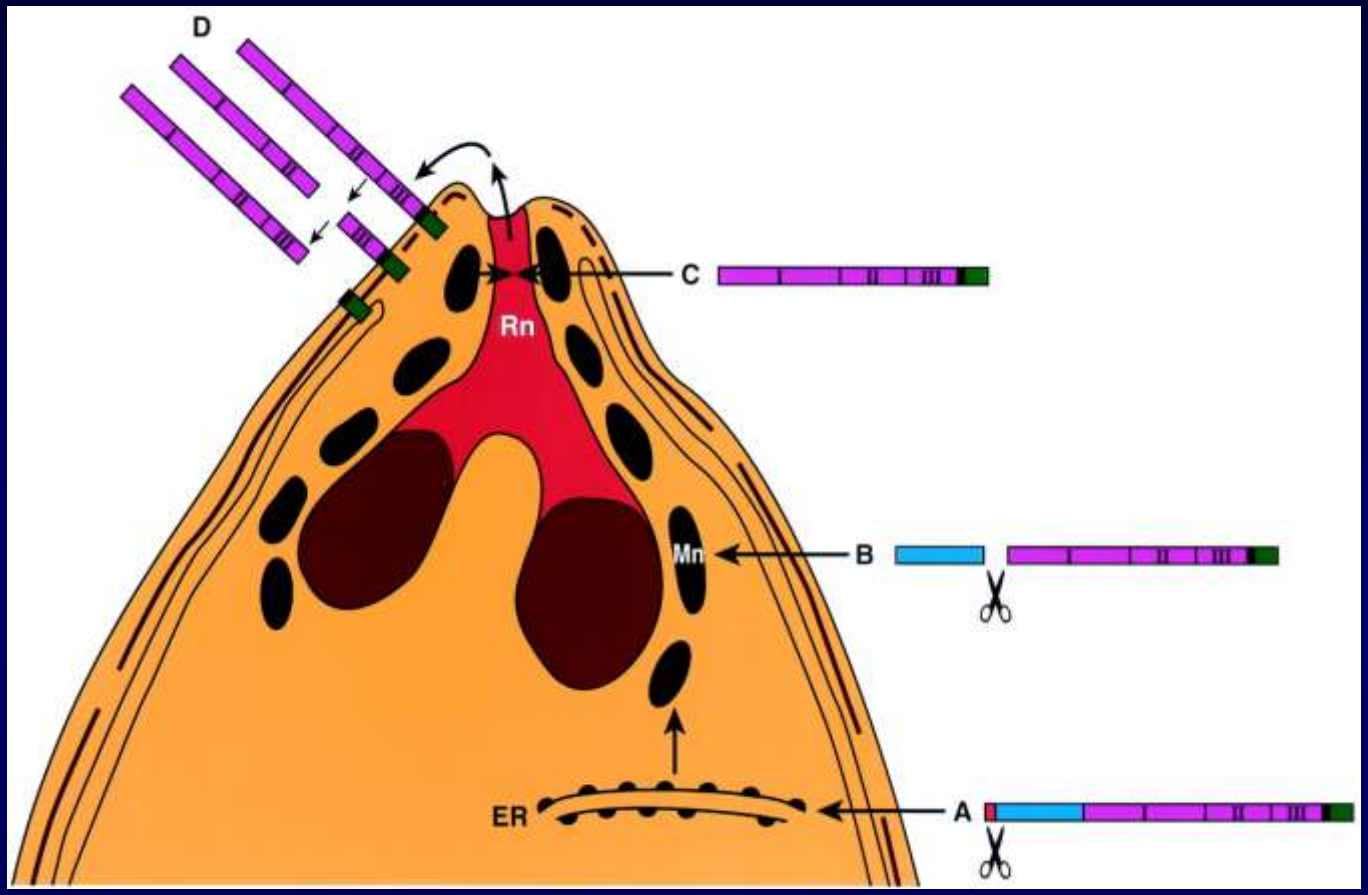

•Schematic model of AMA1-processing events in *P. falciparum* merozoites. AMA1 is synthesized as an 83-kDa precursor protein (A) with signal peptide to allow transport through the endoplasmic reticulum (ER), where removal of the signal peptide presumably occurs. From there it traffics to the micronemes (Mn). The N-terminal pro-region segment is proteolytically cleaved there (B), and the mature 62-kDa polypeptide is translocated out of the micronemes (C) via the neck of the rhoptry (Rn) to the merozoite surface, where it undergoes further C-terminal processing (D), releasing part of the ectodomain off the surface membrane. The domains of AMA1 are represented as follows: signal peptide, red; pro-domain, blue; ectodomains 1, 2, and 3, pink; transmembrane domain, black; and cytoplasmic tail, green.

Healer J. et al. Infect. Immun. 2002;70:5751-5758

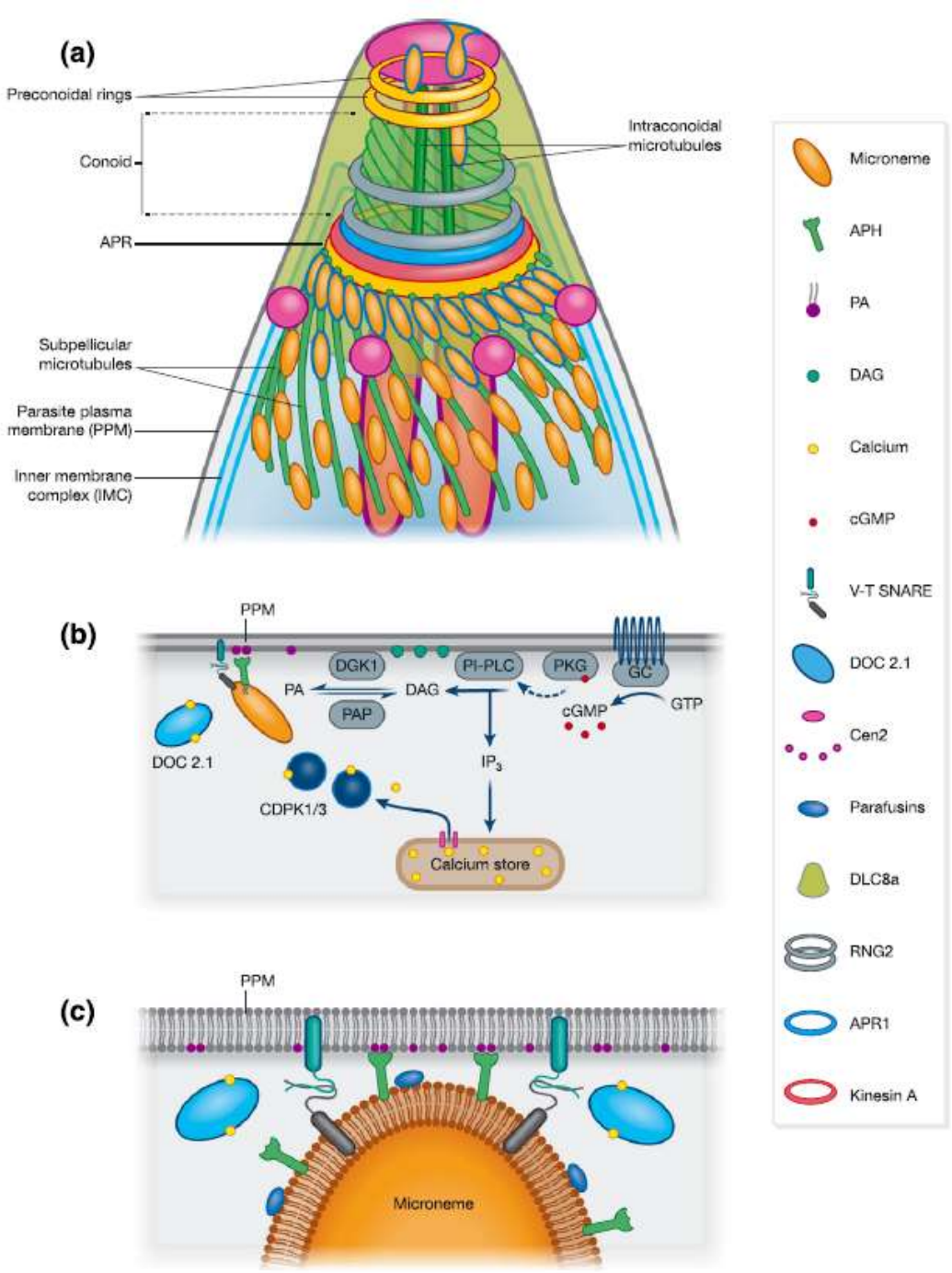

Schematic diagram of signaling and exocytosis related proteins (Dubois, Soldati-Favre, 2019)

Schematic diagram of signaling and exocytosis related proteins.(a) Schematic representation of *Toxoplasma gondii* tachyzoite, highlighting exocytosis related proteins. (b) Diagram of signalling cascade. (c) Zoom in on microneme fusion with parasite plasma membrane.
PPM: parasite plasma membrane; IMC: inner membrane complex; APR: apical polar ring; APH: acylated plekstrin homology domain containing protein; PA: phosphatidic acid; DAG: diacylglycerol; DGK: diacylglycerol kinase 1; IP3: inositol-trisphosphate; PI-PLC: phosphoinositide phospholipase C; PKG: protein kinase G; GC: guanylate cyclase; APH: acylated plekstrin homology domain containing protein; DOC2.1: double C2 containing protein; PRP1/PGM2: Parafusins; Cen2: Centrin 2; DLC8a: Dynein light chain 8a; RNG2: Ring2; APR1: Apical polar ring 1. Kinesin A and a representative V-T SNARE complex (Dubois, Soldati-Favre, 2019).

3D reconstruction showing micronemes in conoid (Dubois, Soldati-Favre, 2019)

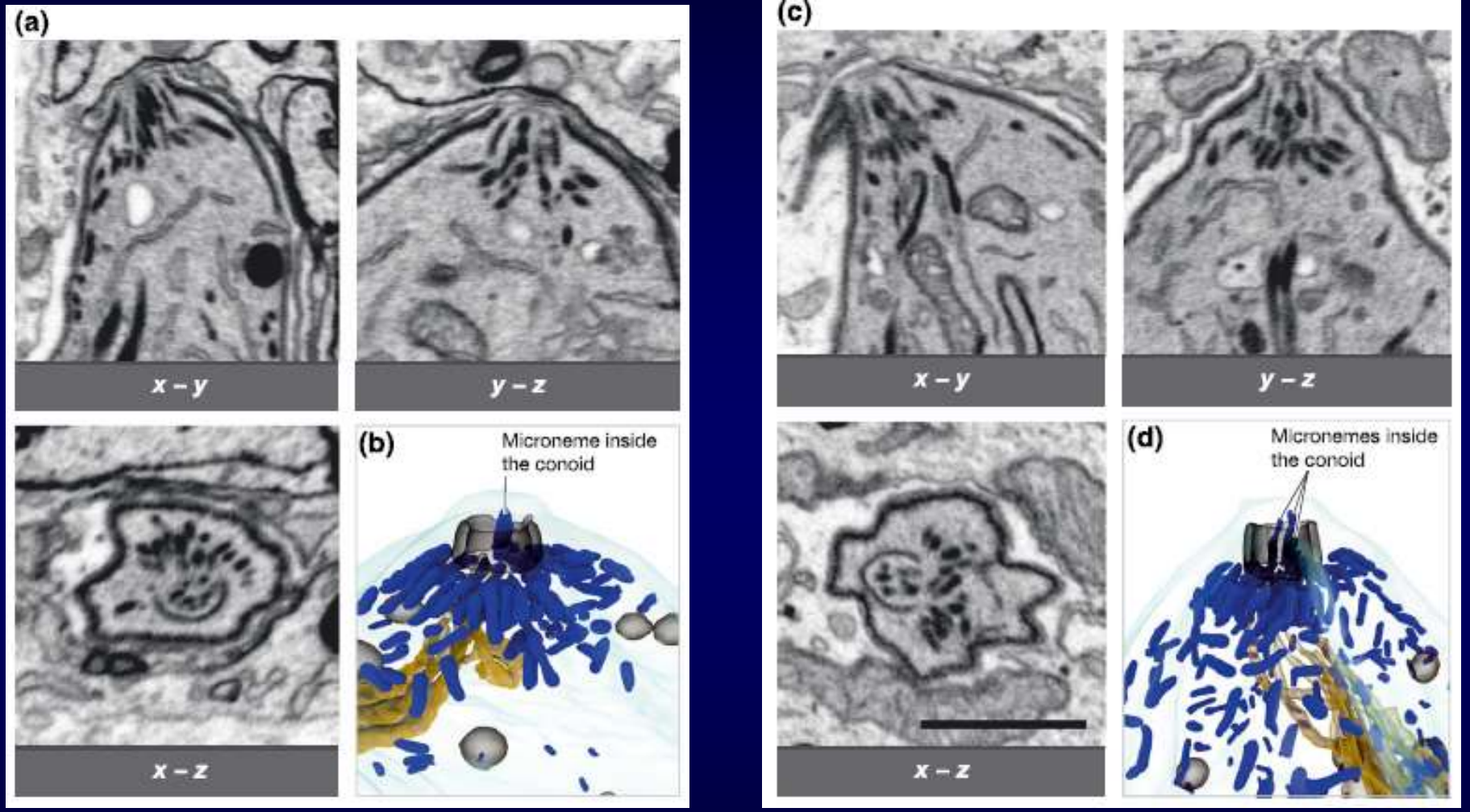

3D reconstruction showing micronemes in conoid. (a–d) Orthogonal views of apical part of the *Toxoplasma gondii* tachyzoite from imaged volume acquired with focused ion beam SEM (FIBSEM) microscope and (b,d) corresponding 3D reconstruction, highlighted the distribution of the apical micronemes (blue) around or inside the conoid (transparent black) together with rhoptry's necks (transparent yellow), dense granules (transparent brown), and tachyzoite plasma membrane (transparent cyan) for (a,b) ΔKU80 and (c,d) TFP2-KO strain (KO does not affect micronemes; Hammoudi et al., 2018). Scale bar: 1 µm

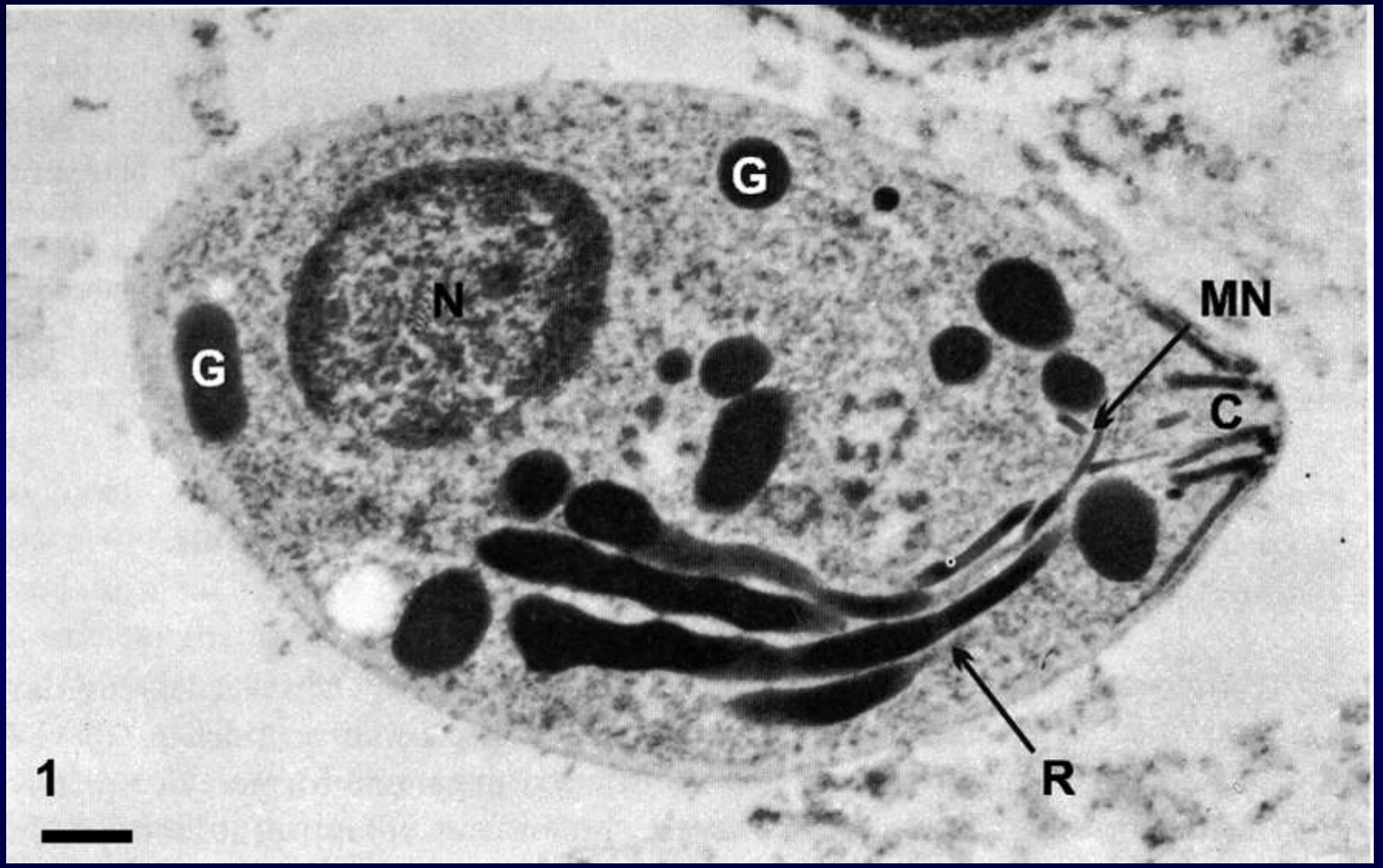

Transmission electron microscopy of a tachyzoites of *Toxoplasma gondii* submitted to the ethanolic phosphotungstic acid technique, which labels structures containing basic proteins. In addition to the nucleus (N), staining of the dense granules (G), Rhoptries (R), Micronemes (M) and the Conoid (C) is observed. Bar, 0.3µm. After De Souza and Souto-Padrón 1978.

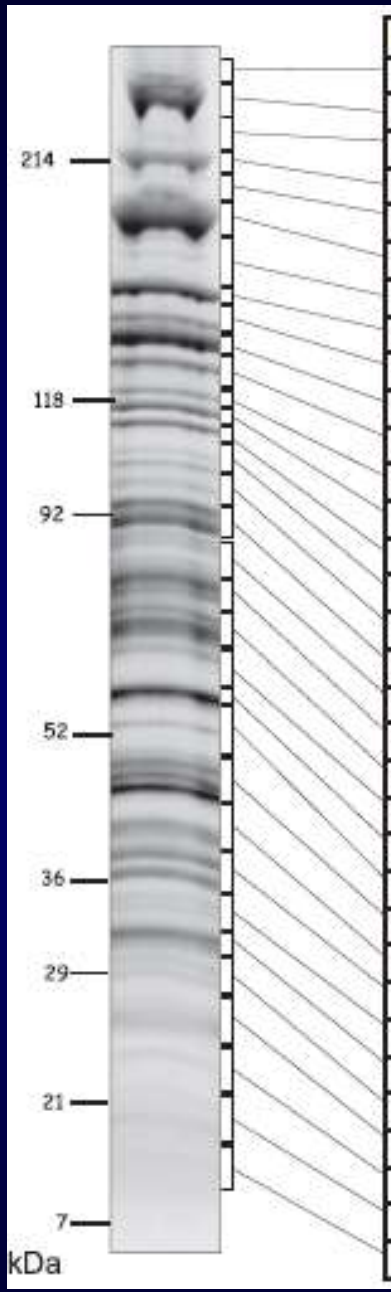

Known rhoptry proteins	Additional proteins
	5 hits
RON1, RON3, RON6/9, RON8	10 hits
RON3, RON8	5 hits
RON3,	8 hits, including porin
RON3	5 hits
RON3, RON3L1	2 hits
	3 hits, including EtMIC4
(RON2)	
RON2L2	
RON4/4L	1 hit
RON4/4L, ROP 14/14B/48	5 hits
RON2L1	8 hits
	1 hit
	3 hits
	8 hits
ROP30/25/32,	12 hits, including actin, HSP70
ROP10, ROP30/25/32	26 hits, including succinate dehydrogenase
ROP30/25/32,	16 hits, including fumarase, ATP synthase
(RON10)	
ROP2A/17.31	8 hits, including citrate synthase
	15 hits, including AMA,carbonic anhydrase
	5 hits, including AMA, quinone oxidoreductase
RON3	11 hits, including mitochondrial carrier protein
(SUB)	9 hits, including prohibitin, porin
	9 hits, including prohibitin, adenylate kinase
	18 hits, including EtSAG1,Peroxiredoxin
	9 hits, including peroxiredoxin, SOD
	9 hits, including SOD, thioredoxin peroxidase
	3 hits
	12 hits, including cytochrome oxidase
	3 hits

The rhoptry proteome of *Eimeria tenella* sporozoites (Oakes et al., 2013)

An example of one-dimensional gel fractionation of *Eimeria tenella* rhoptry proteins, with annotation showing the mapping of peptides corresponding to known rhoptry proteins, and other additional hits. This is the rhoptry preparation from 28 June 2003

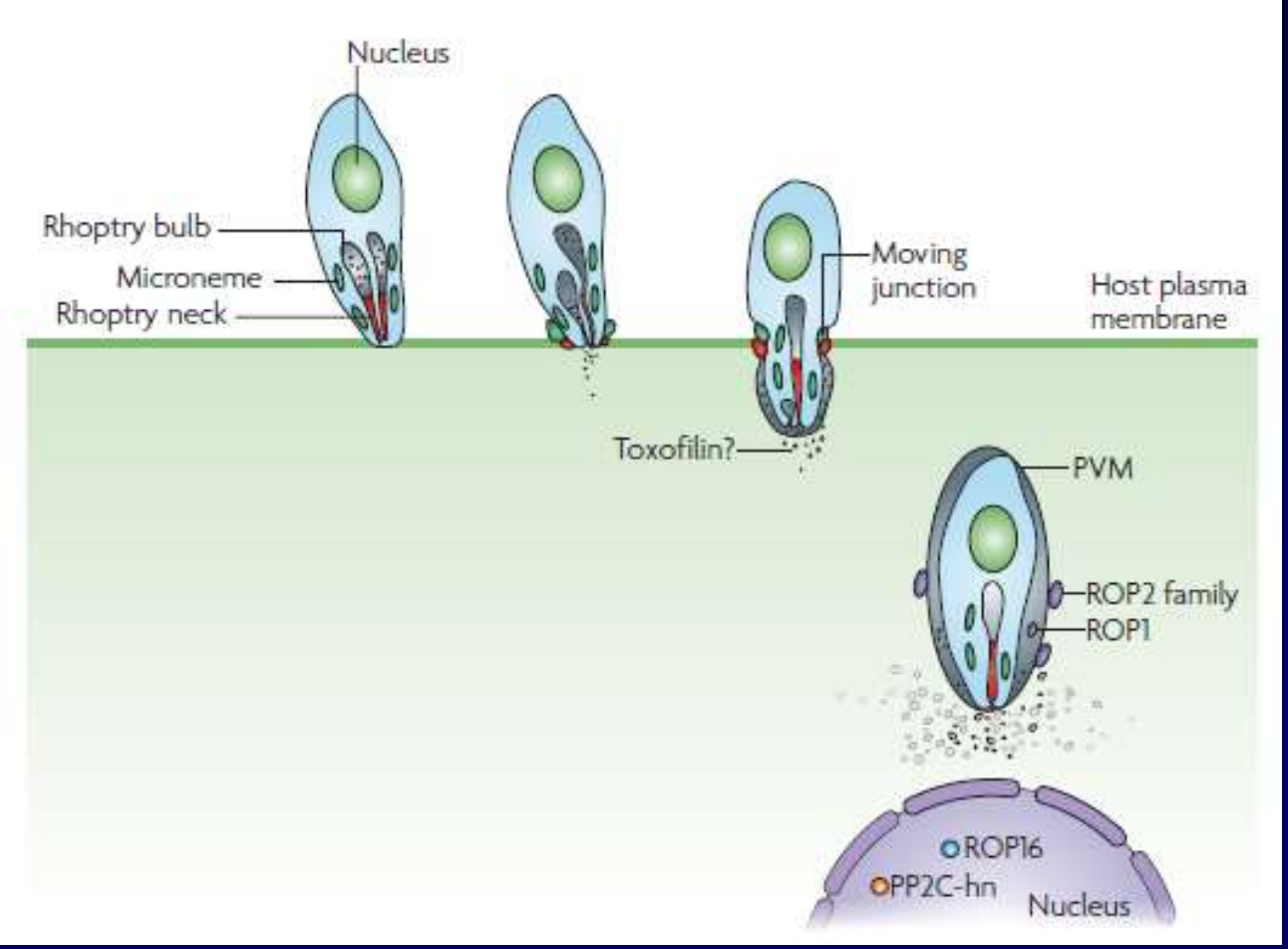

Kiss and spit:
the dual roles
of *Toxoplasma* rhoptries
(Boothroyd, Dubremetz, 2008)

Schematic model for rhoptry contribution to invasion. Rhoptry bulbs (grey) and rhoptry necks (red) release their contents during the invasion process in concert with simultaneous release by micronemes (green). RON2, RON4 and RON5 collaborate with micronemal AMA1 to create the moving junction, which migrates down the surface of the parasite, forming a ring of contact with the host plasma membrane. This effectively excludes many host plasma membrane integral proteins and results in the generation of a parasitophorous vacuole membrane (PVM), which envelopes the parasite. ROP2 family members are injected during invasion, perhaps in association with small vesicles, and ultimately end up on the host cytosolic side of the PVM. ROP1 is also observed in association with the injected vesicles, but most of this protein ends up inside the parasitophorous vacuole lumen. ROP16 and PP2C-hn (hn is the abbreviation for host nucleus) are not observed in the vesicles, but accumulate inside the host nucleus. Other soluble rhoptry proteins (for example, toxofilin) are also presumed to be injected, but in the absence of a concentrating mechanism they will be present at too low a concentration to be detectable (only a few rhoptries secrete their contents during invasion and any proteins that they release will be diluted by up to a million-fold or more in the host cytosol).

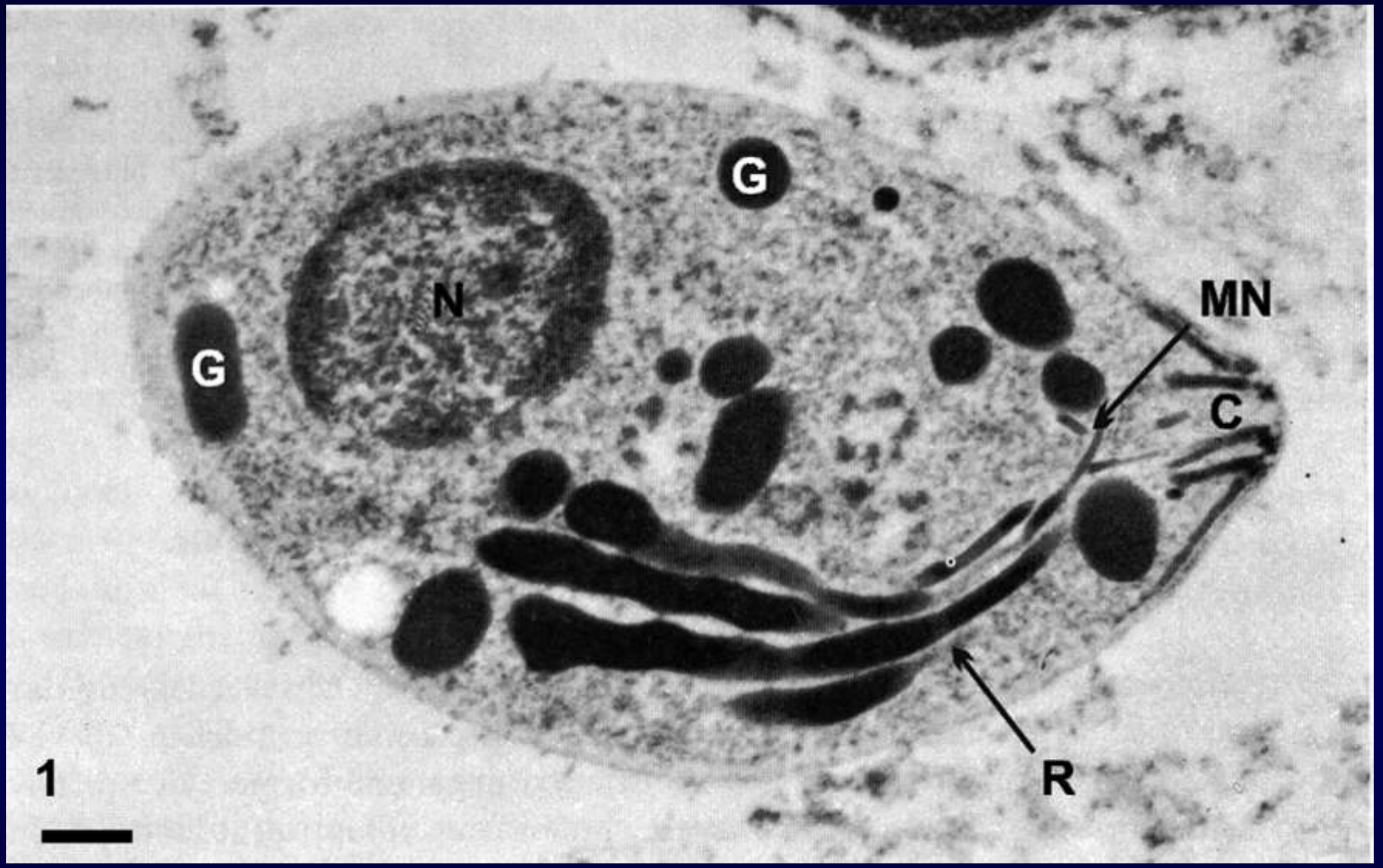

Transmission electron microscopy of a tachyzoites of *Toxoplasma gondii* submitted to the ethanolic phosphotungstic acid technique, which labels structures containing basic proteins. In addition to the nucleus (N), staining of the dense granules (G), Rhoptries (R), Micronemes (M) and the Conoid (C) is observed. Bar, 0.3µm. After De Souza and Souto-Padrón 1978.

Dense granules (bodies)

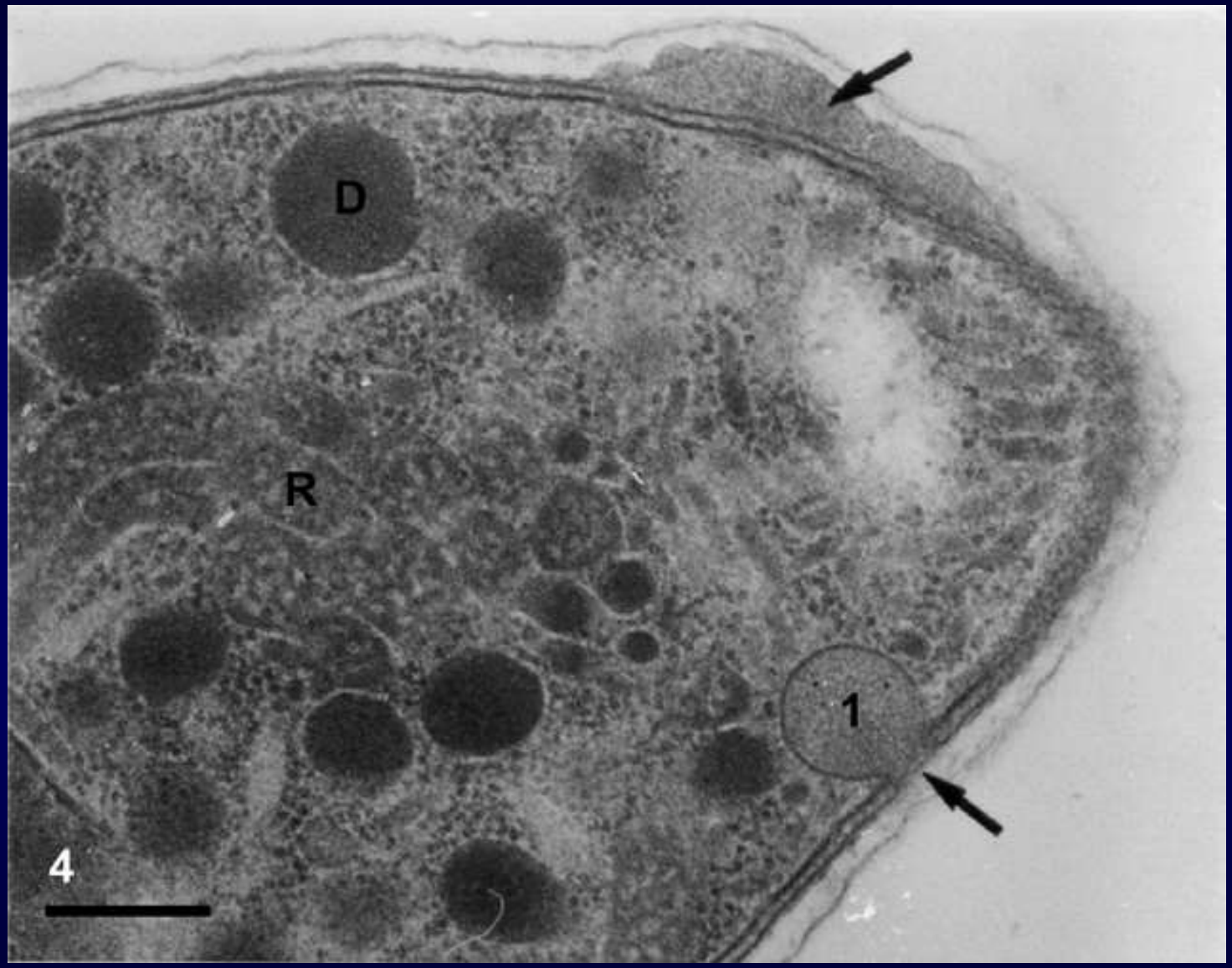

Secretion of the dense granule content (arrows) in the lateral side of the tachyzoite form of *Toxoplasma gondii*. D, dense granules; R, rhoptries. Bar, 0.35 μm. (de Souza, 2006)

Interactions between secreted GRA proteins and host cell proteins across the parasitophorous vacuolar membrane in the parasitism of *Toxoplasma gondii*

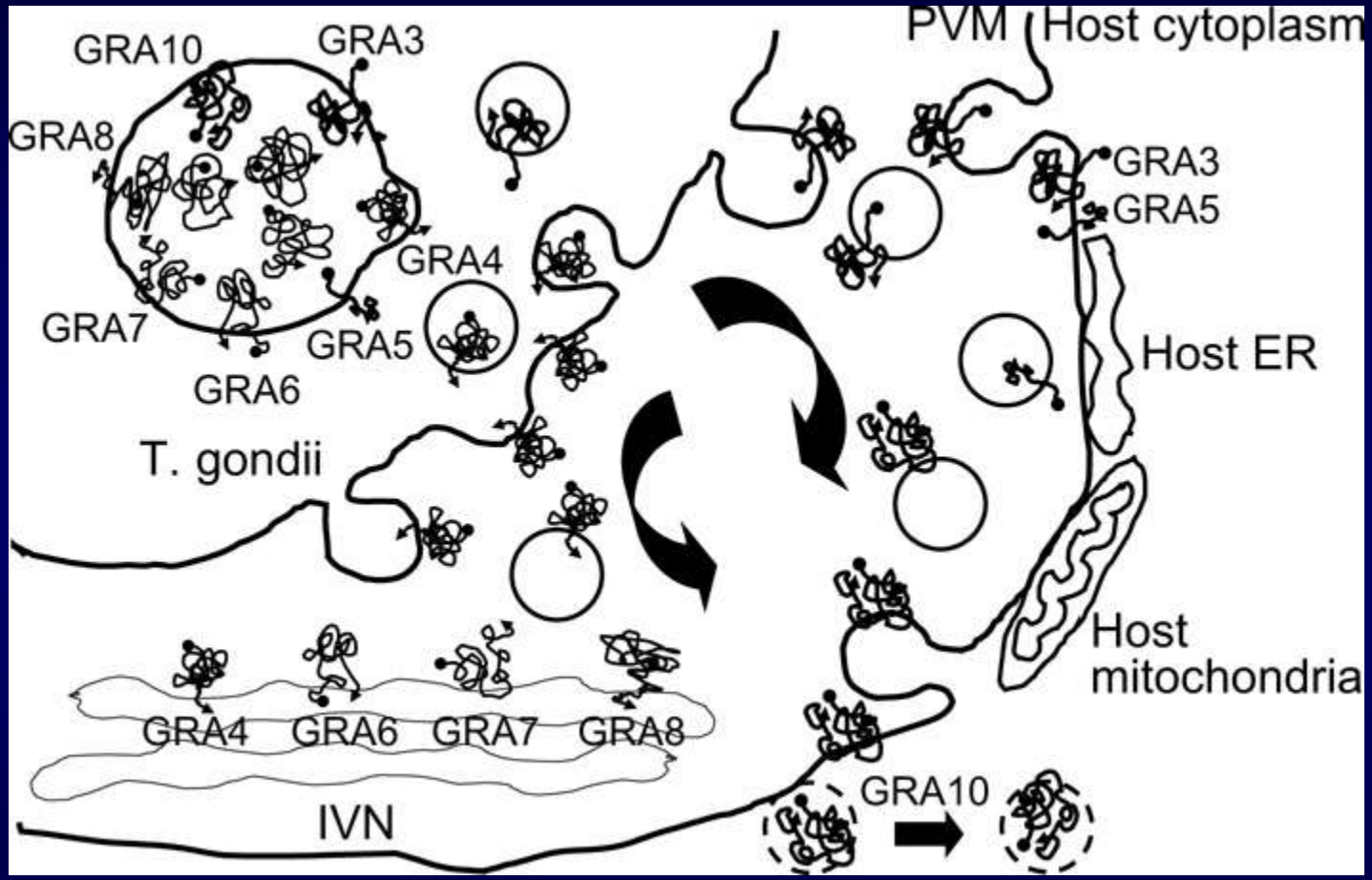

Secretion of GRA proteins with transmembrane domains within the amino acid sequences. GRA4, 6, 7 and 8 are trapped in the IVN within the PV, and participate in the interaction with host components across the PVM, whereas GRA3, 5 and 10 are secreted into the PVM for the direct interaction. GRA10 may be a candidate that is secreted over the PVM and interacts with host nuclear proteins.

(Hye-Jin et al., 2006)

Cell invasion: *Toxoplasma gondii* tachyzoites

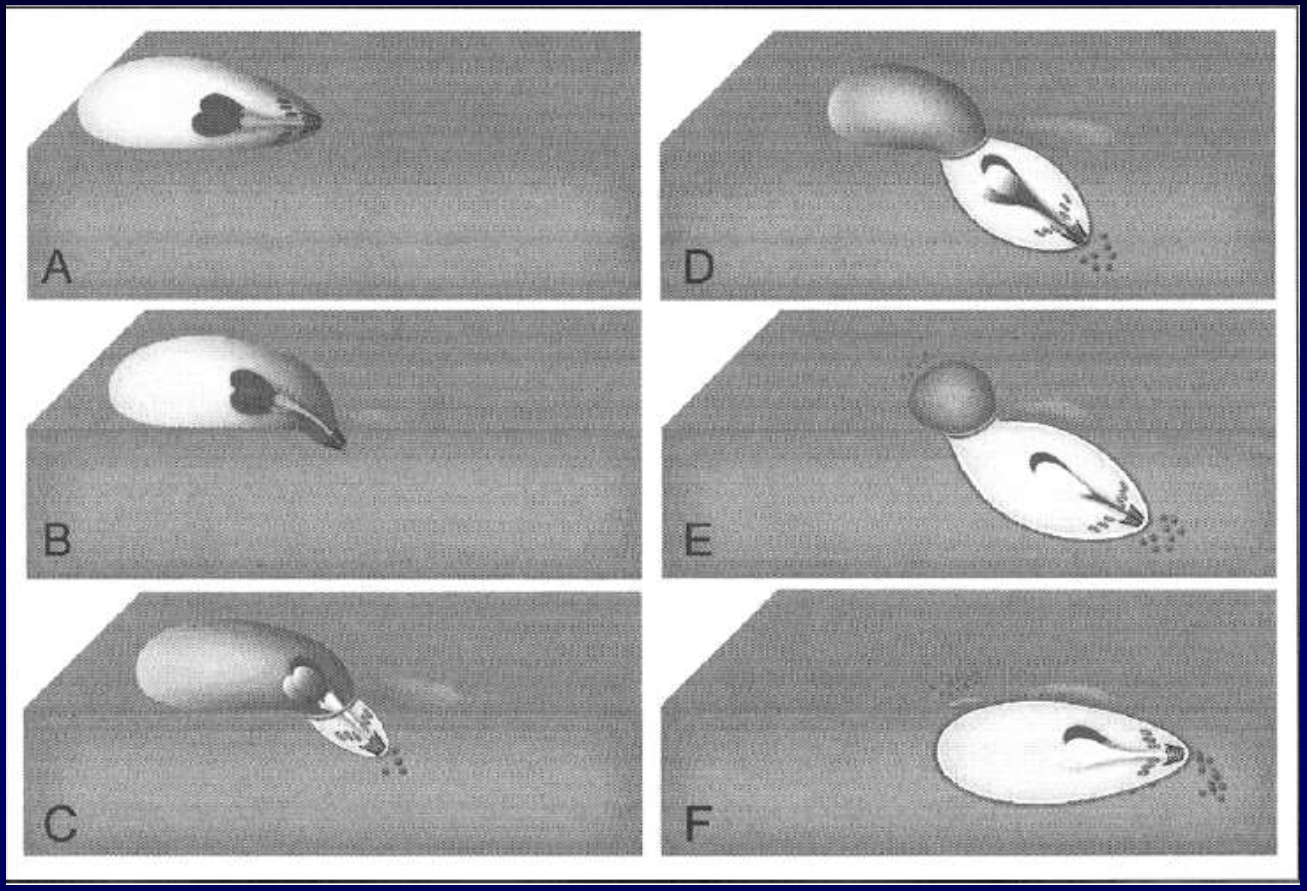

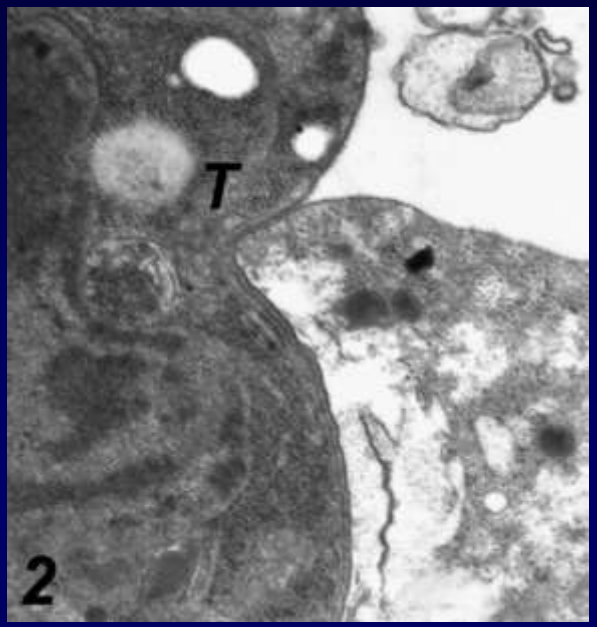

(Toulah et al., 2011)

Overview of host cell invasion by *T. gondii tachyzoltes.* A) A tachyzoite glides over the surface of a host cell, powered by its actin-myosin-based motor. The thimble-shaped conoid at the apical tip of the parasite repeatedly protrudes and retracts. Adhesins (green) are found both intracellularly, within small tubular micronemes, and on the parasite surface, concentrated towards the apical end. B) The conoid is extended when the parasite begins to invade, bringing the apical tip of the parasite into intimate contact with the host cell. Microneme secretion increases, delivering more proteins to the parasite surface. An invagination of the host cell membrane begins to develop. C) Active penetration of the host cell begins, driven by the same actin-myosin motor that drives gliding motility. Rhoptry neck proteins (light blue) are secreted and associate with the microneme protein TgAMAI to form the moving junction, through which the parasite enters the host cell. Most microneme proteins are capped, accumulati ng posteriorly; they are thought to be kept out of the parasitophorous vacuole by sieving action of the moving junction. Rhoptry bulb proteins (dark blue) begin to be secreted into the host cell. D,E) Microneme proteins continue to be capped towards the posterior end, where they are cleaved within their transmembrane domains. Rhoptry secretion continues, with rhoptry proteins contributing to the formation of the parasitophorous vacuole. The parasite squeezes through the moving junction, visibly constricting at the point of entry, into the deepening vacuole. F) Microneme proteins are shed from the posterior end of the parasite. Invasion is complete when the parasitophorous vacuole membrane pinches closed. A patch of protein originally derived from the rhoptry necks is found transiently at the site of entry, associated with the host plasma membrane. Note that dense granules and dense granule secretion^ are not illustrated in this diagram, for simplicity.

(Mital, Ward, 2008)

Прикрепительные аппараты грегарин и других паразитических альвеолят

Digyalum oweni

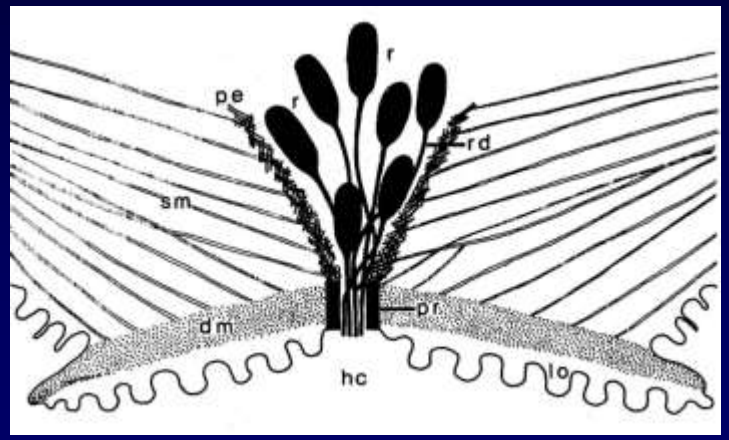

Pyxinia firmus

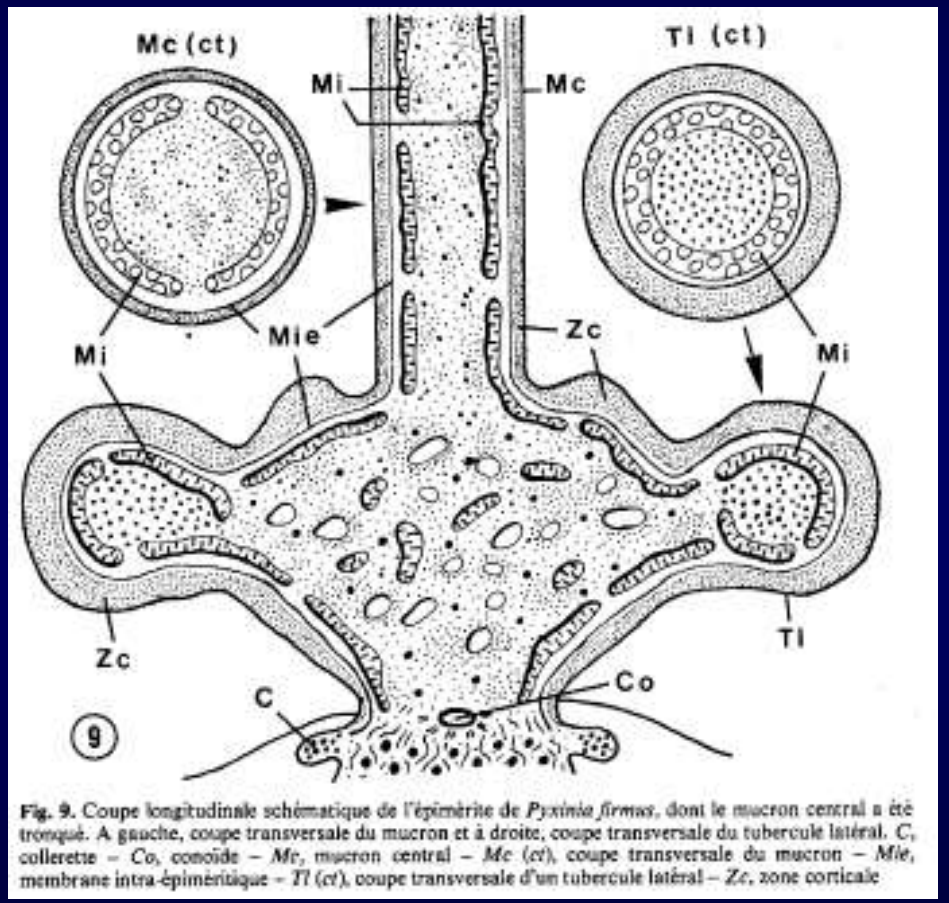

Fig. 9. Coupe longitudinale schématique de l'épimérite de *Pyxinia firmus*, dont le mucron central a été tronqué. A gauche, coupe transversale du mucron et à droite, coupe transversale du tubercule latéral. *C*, collerette – *Co*, conoïde – *Mr*, mucron central – *Mc* (*ct*), coupe transversale du mucron – *Mie*, membrane intra-épimérítique – *Tl* (*ct*), coupe transversale d'un tubercule latéral – *Zc*, zone corticale

Lecudina sp.

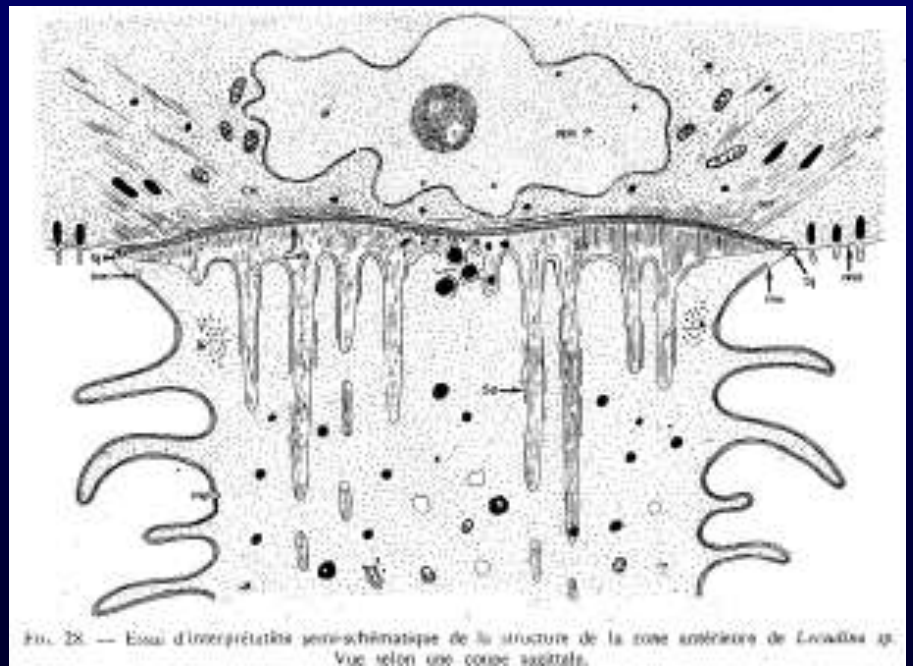

Fig. 28. — Essai d'interprétation semi-schématique de la structure de la zone antérieure de *Lecudina sp.* Vue selon une coupe sagittale.

(из разных источников)

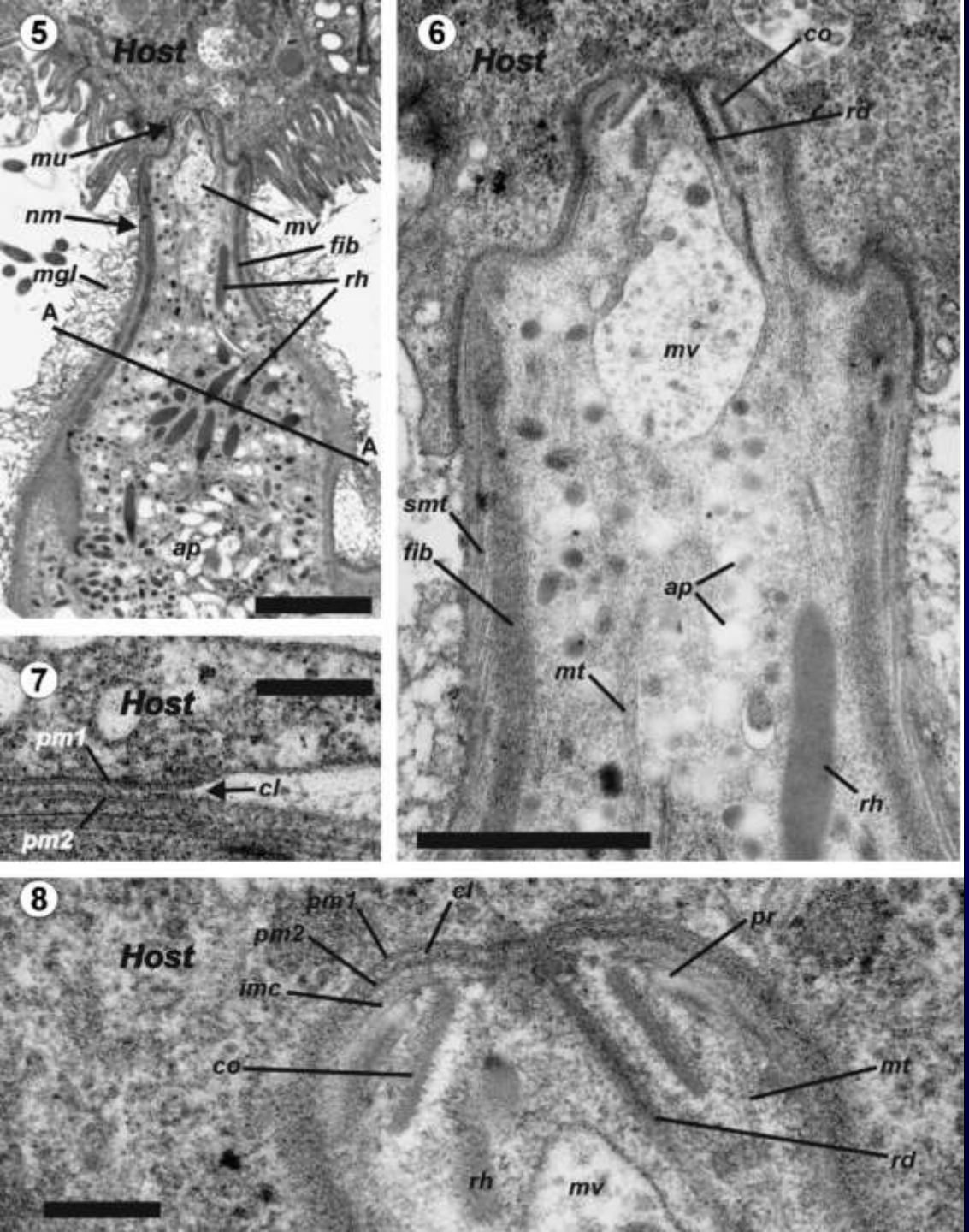

Fine structure and putative feeding mechanism of the archigregarine *Selenidium orientale* (Apicomplexa: Gregarinomorpha)

Fine structure of the forebody of *Selenidium orientale* trophozoite (TEM, longitudinal sections. 5, 6, 7, specimen No. 1; 8, specimen No. 2). 5, 6. Trophozoite forebody at different magnifications. 7. Peripheral area of a septated junction between parasite and host cell. 8. Mucron. Abbreviations: amylopectin granule (ap), modified glycocalyx of trophozoite anterior part (mgl), cortical fibrillar bundles (fib), clearance (cl) between host cell and gregarine plasma membranes (pm1 and pm2, respectively), conoid (co), host cell (Host), microtubules (mt), mucron (mu), mucronal vacuole (mv), neck of mucron (nm), polar ring (pr), rhoptry (rh), rhoptry duct (rd), inner membrane complex (imc), Line and letters A–A on 5: level of the section. Scale bars: 5 - 2 mkm, 6 - 1 mkm, 7, 8 - 0.2 mkm.

(Simdyanov & Kuvardina, 2007)

Fine structure and putative feeding mechanism of the archigregarine *Selenidium orientale* (Apicomplexa: Gregarinomorpha)

Putative feeding scheme of trophozoites of *Selenidium* gregarines. A. Local lysis of the host cell plasmalemma by rhoptry secretion (arrow). B. Myzocytosis event: swallowing of the host-cell cytoplasm through the temporary cytostome–cytopharyngeal complex (arrow) and formation of the nascent mucronal vacuole. C. Cytopharynx closure, the nascent mucronal vacuole is fully formed, the previous vacuole is divided into smaller ones which are transported via the microtubular network into the trophozoite, and the disrupted site of the host-cell plasmalemma is restored. Numbers (1–3) indicate the positions of vacuoles formed during preceding myzocytosis events (the current event is No. 4).

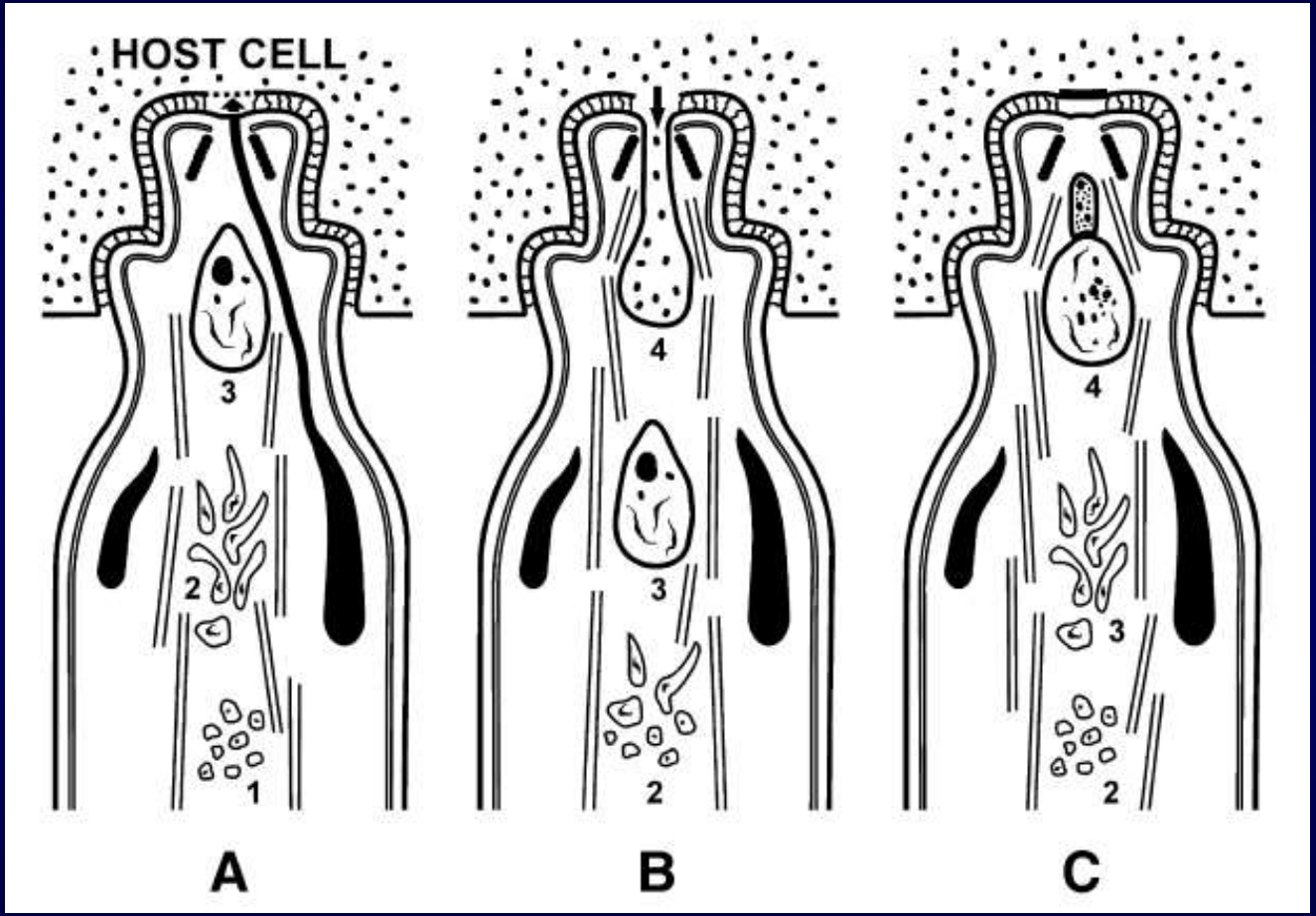

(Simdyanov & Kuvardina, 2007)

Food Uptake and the Fine Structure of the Dinophyte *Paulsenella sp.*, an Ectoparasite of Marine Diatoms

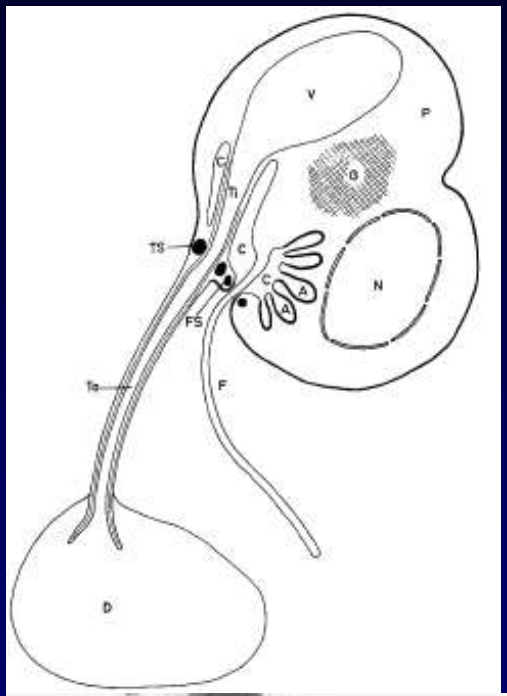

Feeding *Paulsenella* cell, schematically. A ampullae of the pusule open towards the common cavity (C) around the flagellar bases [only the longitudinal flagellum (F) is drawn] and the internal part *(Ti)* of the feeding tube, its exits are surrounded by the flagellar sphincters (FS). The outer part of the feeding tube *(To)* merges into the cytoplasm of the diatom cell (D) (frustule not drawn); at its entry into the cell body the feeding tube sphincter (TS). G Golgi apparatus, N nucleus, P cytoplasm and V food vacuole of the *Paulsenella* cell. Cell covering with amphiesmal structure: thick line; single membranes: thinner line; microtubules of the microtubular basket: very thin line.

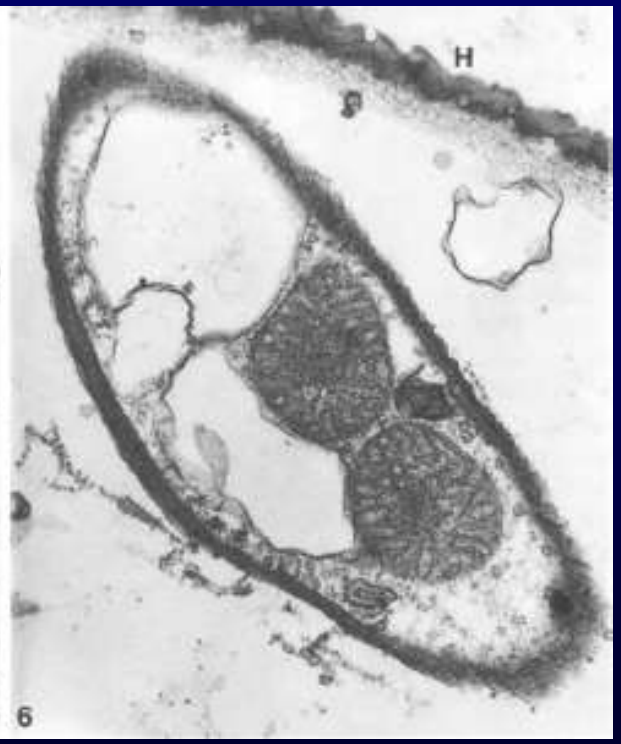

Fig. 5. Cell F, distal opening of the feeding tube (T) within the host cytoplasm, oblique-longitudinal, containing a host chloroplast cut tangentially. MTs in the feeding tube cytoplasm, x 34,000.

Fig. 6. Cell F, feeding tube with host mitochondria, oblique section. MTs in the feeding tube cytoplasm, x 31,000

(Schnepf & Deichgraber, 1985)

Intracellular parasite invasion strategies (Sibley, 2004): gliding motility

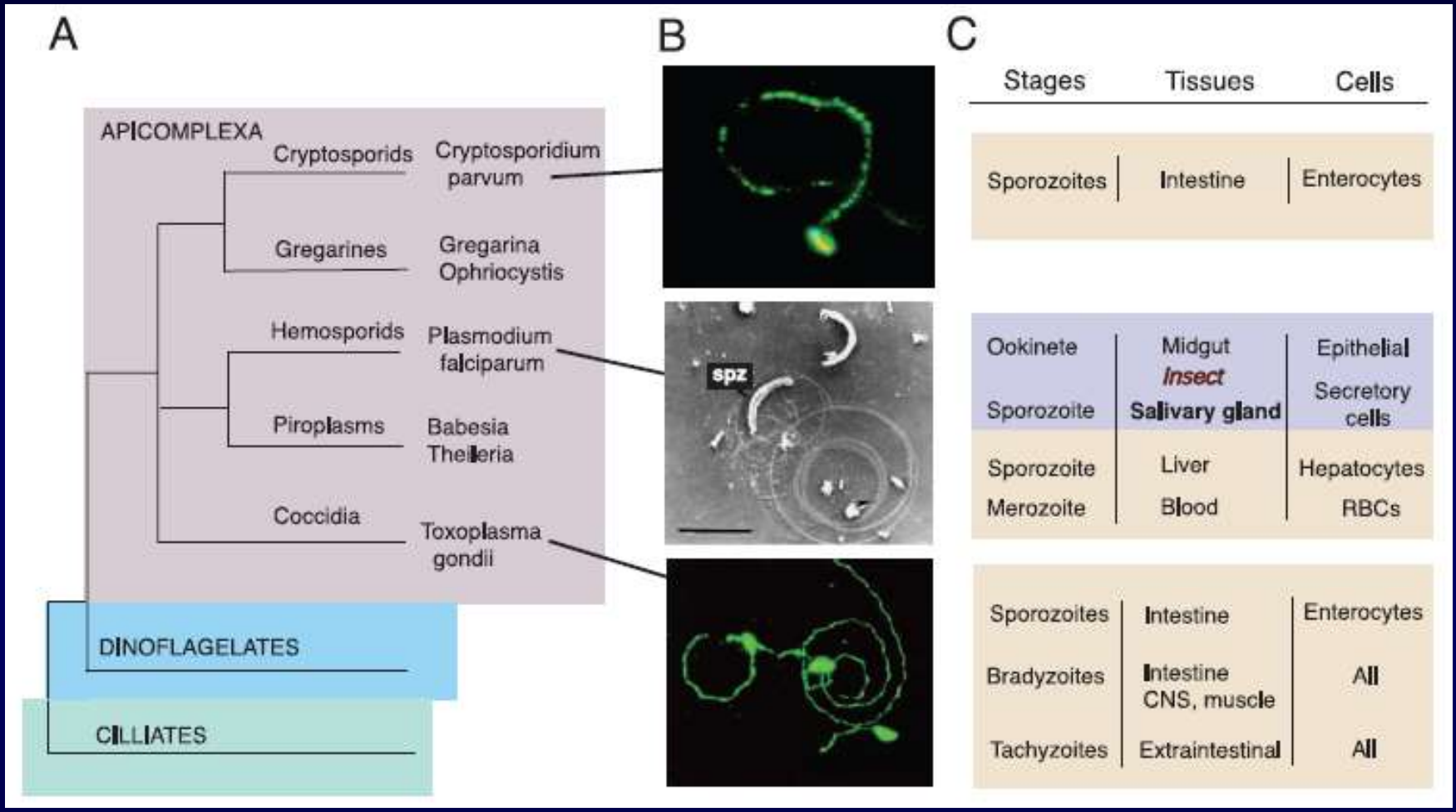

Gliding motility is a conserved feature of apicomplexans. (A) Phylogenetic relations are depicted on the basis of life histories and small subunit RNA phylogeny. (B) Gliding motility by apicomplexans deposits characteristic trails on the substrate. Cryptosporidium trail image revealed by staining with monoclonal antibody 3E3 against a 25-kD surface protein and fluorescently conjugated secondary antibodies. (C) Summary of motile life-cycle stages, tissues involved in migration, and cells invaded by apicomplexan human pathogens.

(Sibley, 2004)

Gliding motility powers invasion and egress in Apicomplexa (Frénal et al., 2017)

The importance of secretory organelles and the cytoskeleton in the motility and invasion of zoites

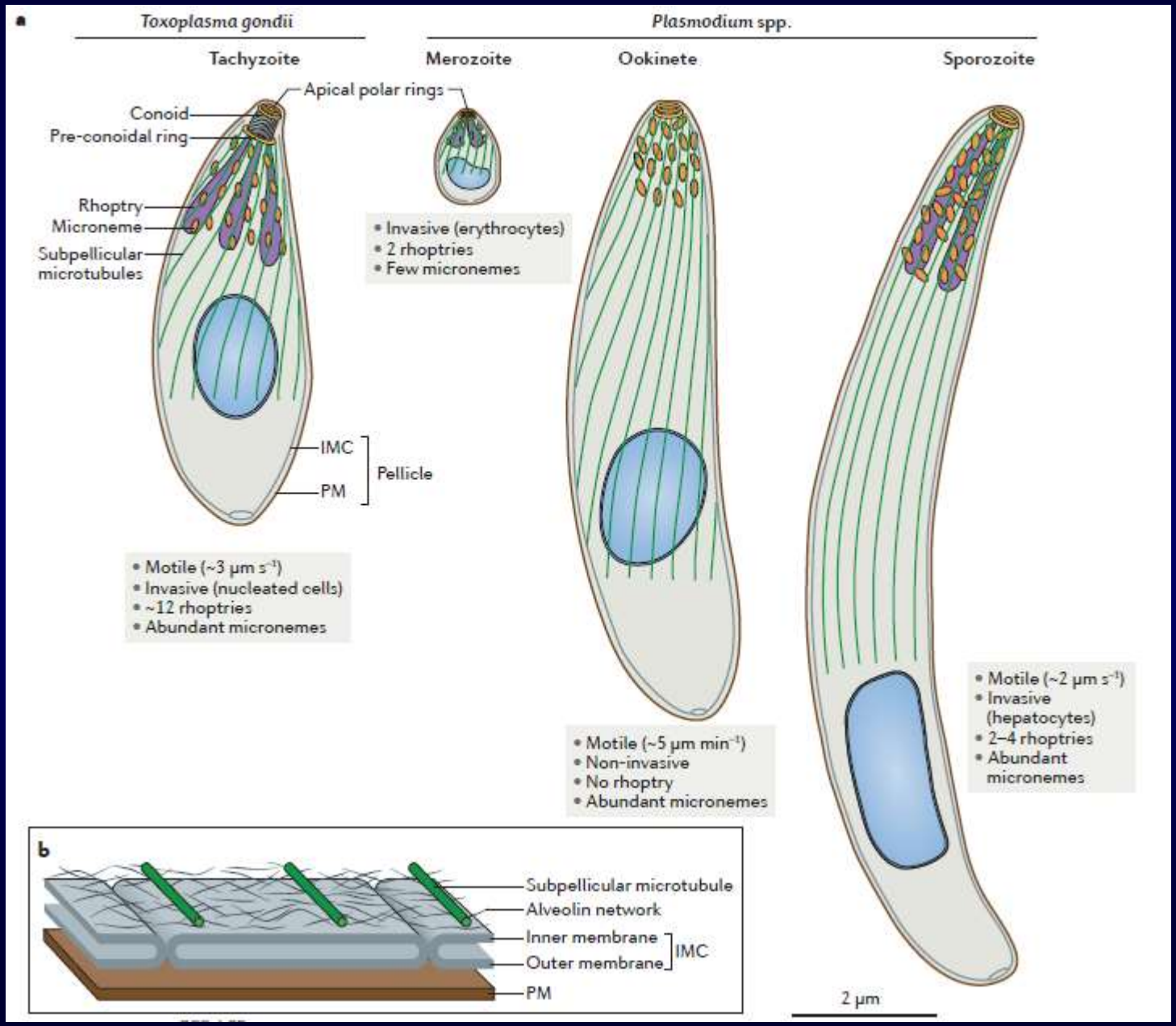

Intracellular parasite invasion strategies (Sibley, 2004)

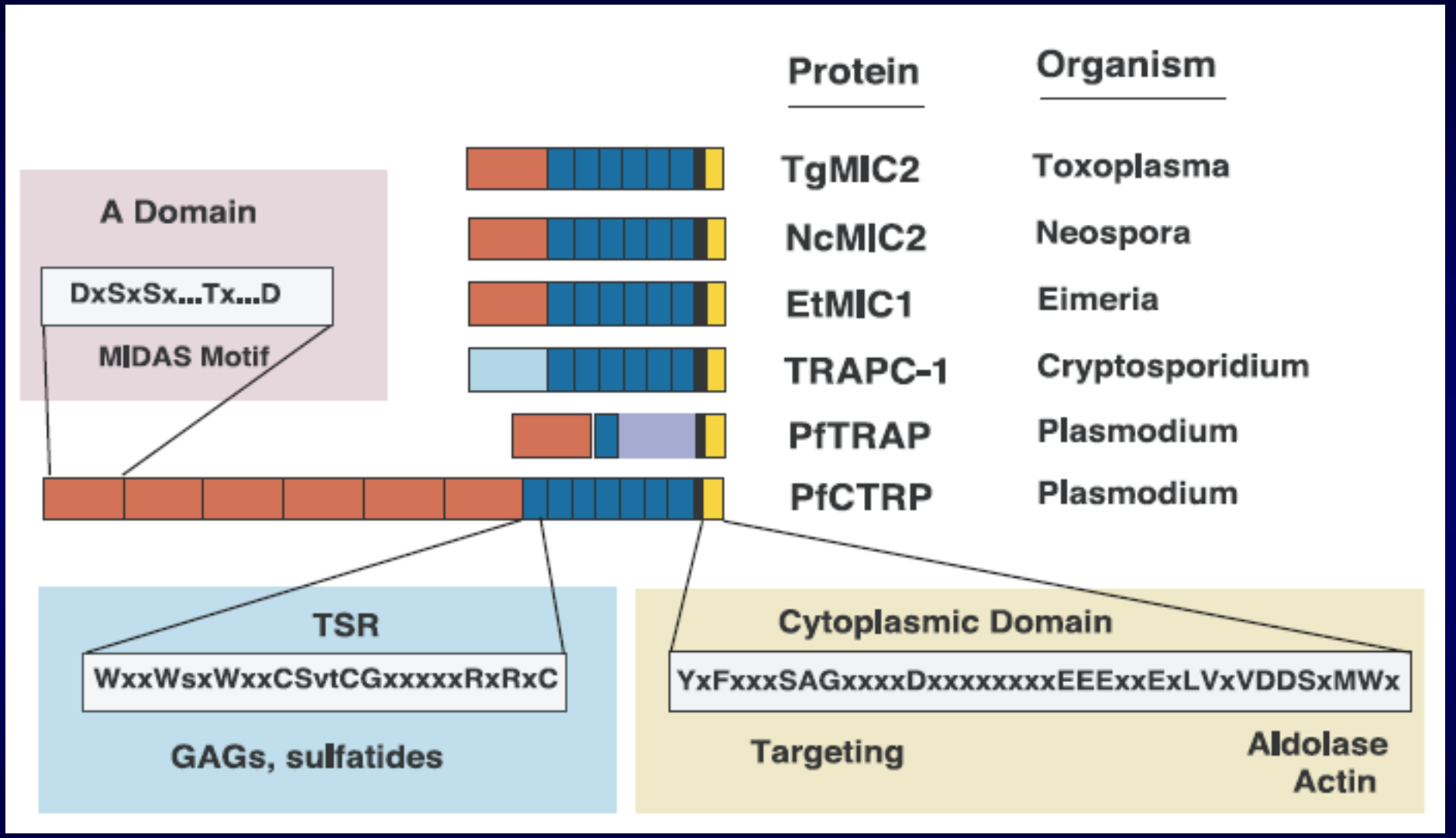

TRAP family homologs are expressed by a variety of apicomplexan parasites. TRAP homologs have one or more integrin A domains containing a conserved MIDAS motif followed by one or more TSRs. The C-terminal cytoplasmic domain contains sorting motifs defined in MIC2 and a region that links to the actin cytoskeleton via bridging with aldolase. Consensus residues are shown in capitals; x indicates any amino acid (Sibley, 2004).

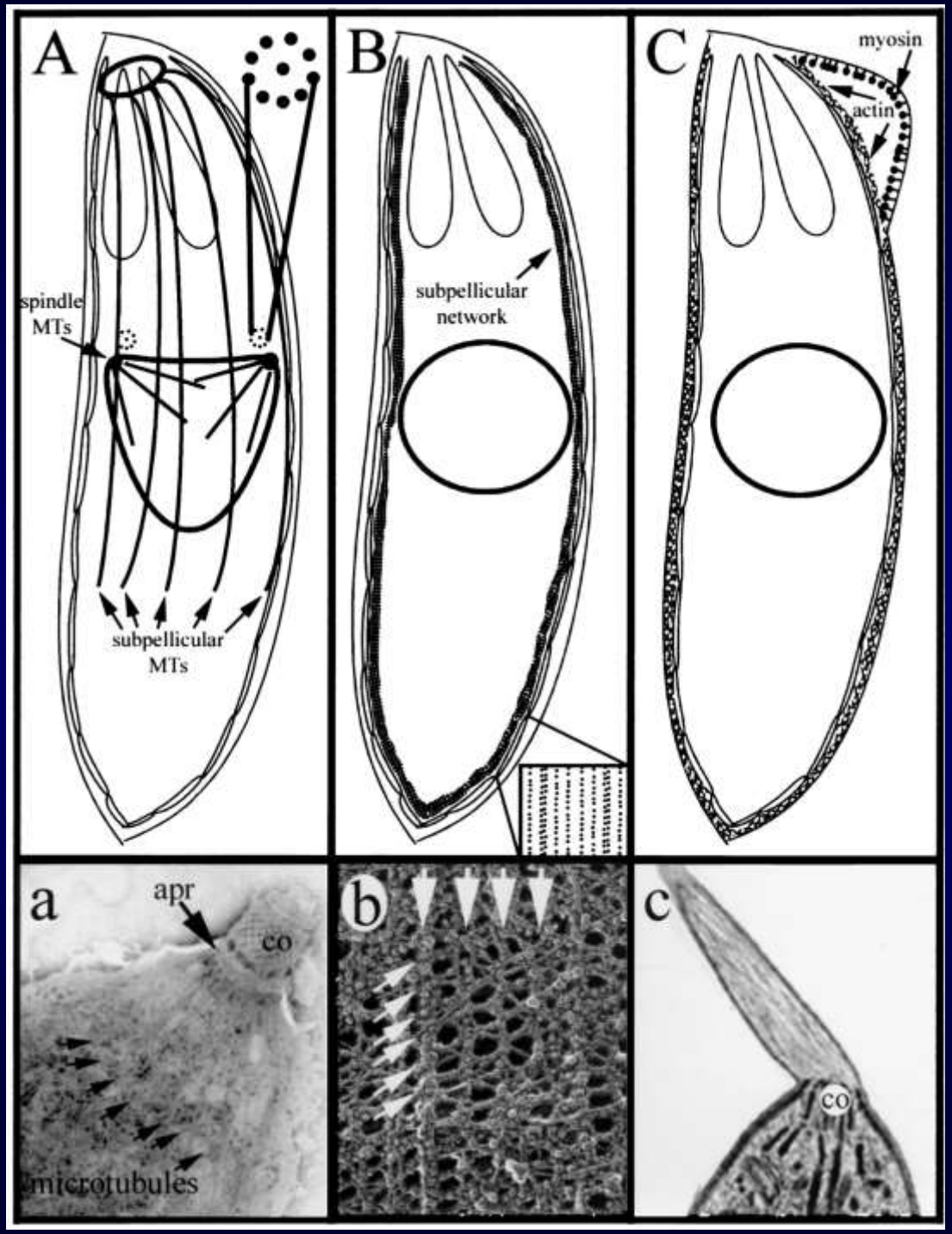

Cytoskeletal elements in the Apicomplexa.

•(A) The subpellicular microtubules radiate out of the apical polar ring and run down the cytosolic face of the IMC. The spindle microtubules are nucleated from spindle pole plaques within the nuclear membrane. Centrioles (consisting of nine singlet microtubules surrounding a central singlet microtubule) are adjacent to the spindle pole plaques. (a) Isolated, negatively strained conoid (co), apical polar ring (apr), and subpellicular microtubules from *T. gondii* (113). (B) A network of intermediate filaments, the subpellicular network, underlies the length of the IMC. The lower right inset illustrates the pattern of IMPs (intramembranous particles) revealed by freeze fracture of the IMC. These particles may represent the transmembrane domains of receptors that link the subpellicular network to the cytoplasmic face of the inner membrane complex. (b) Glycerol- and detergent-extracted, freeze-dried replicas of *Toxoplasma* tachyzoites illustrate the regular array of the subpellicular network filaments. (Image of the *Toxoplasma* network kindly provided by J. Heuser.) (C) Actin is localized between the plasma membrane and the IMC. When the plasma membrane is separated from the IMC, actin remains associated with the IMC and myosin is associated with the plasma membrane. (c) Actin filaments protrude beyond the conoid (co) of *Toxoplasma* tachyzoites treated with jasplakinolide, a drug that induces actin polymerization (Morrissette, Sibley, 2002).

Скольжение: взаимодействие с субстратом посредством «моторного» комплекса белков?

Схема строения пелликулы *Toxoplasma* и связанного с ней белкового «моторного» комплекса

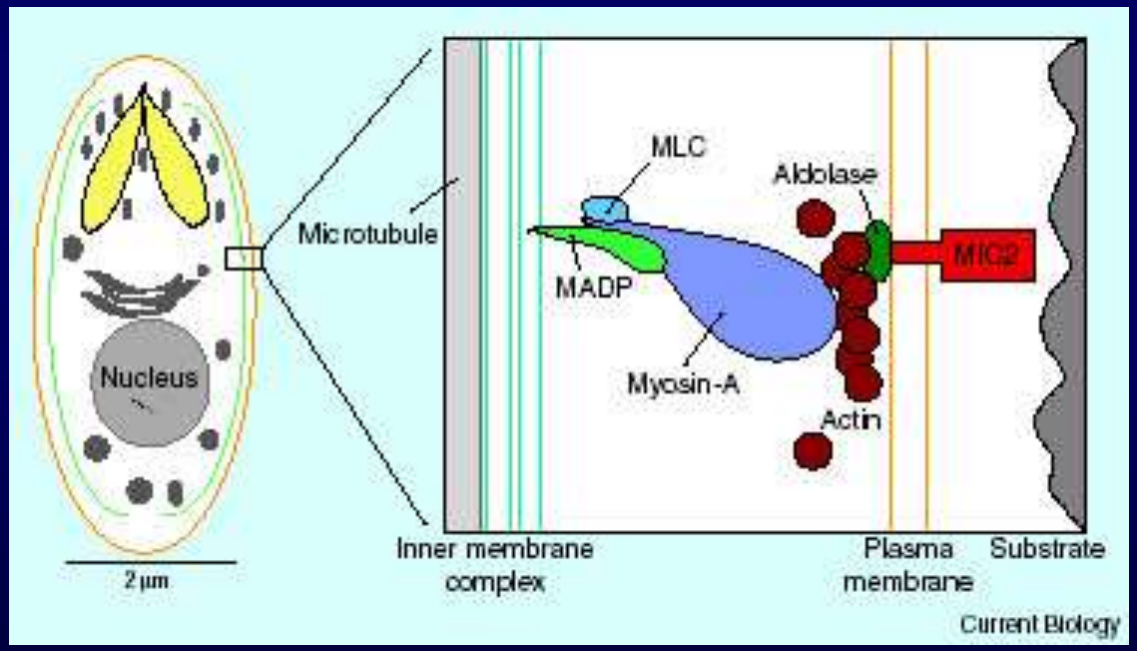

(Heintzelman, 2003)

Схема движения спорозоита *Toxoplasma*

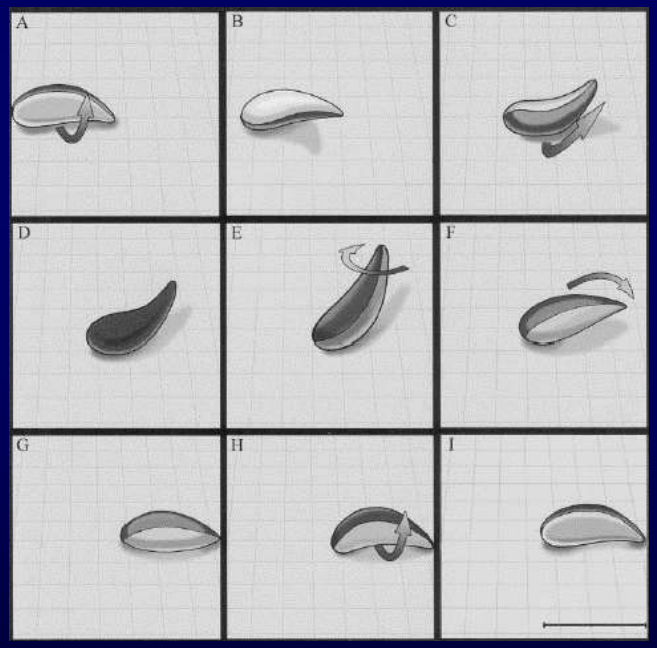

(Hakansson et al, 1999)

Gliding motility powers invasion and egress in Apicomplexa (Frénal et al., 2017)

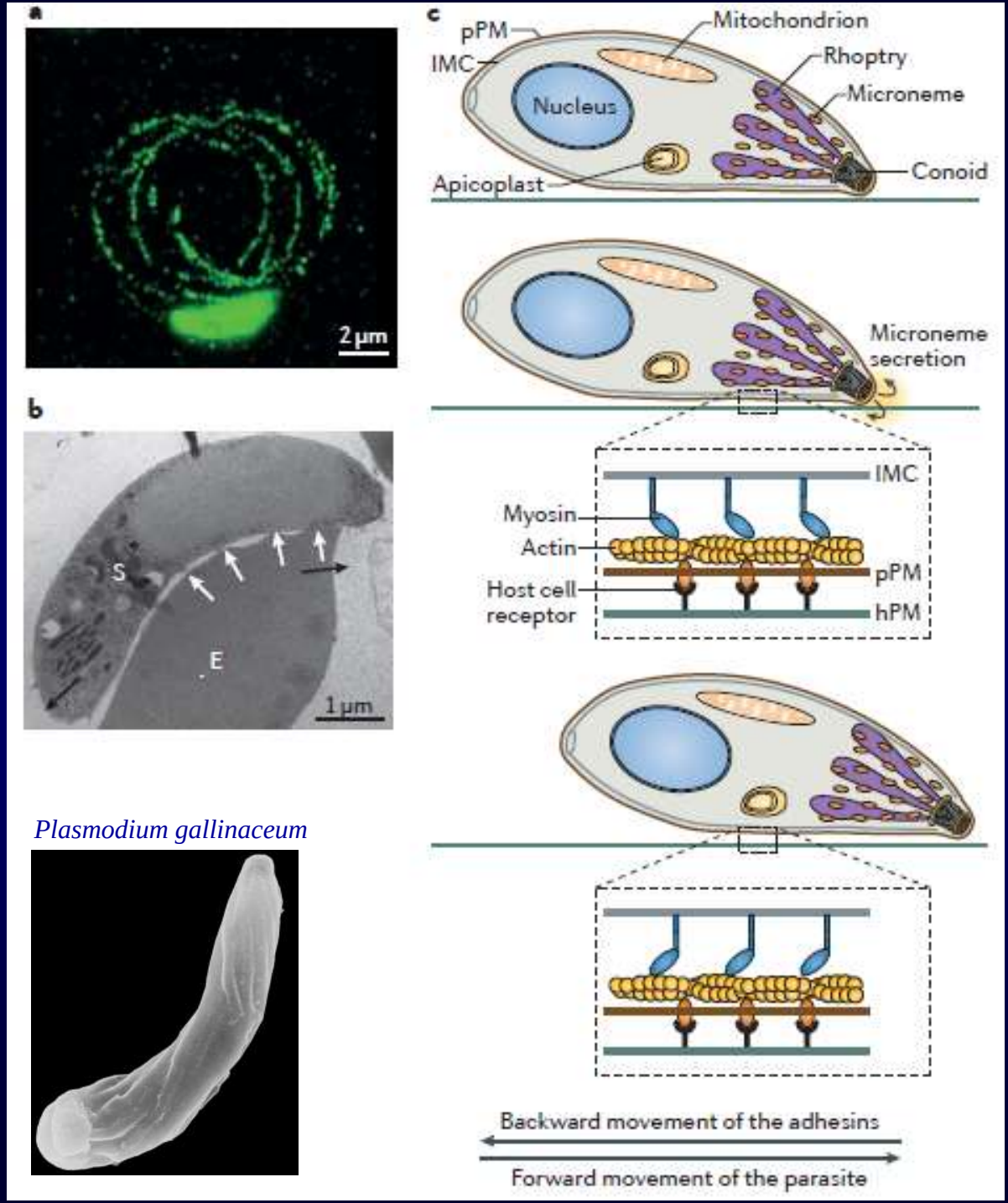

Plasmodium gallinaceum

Gliding motility in Apicomplexa. a. The motility of *Toxoplasma* spp. tachyzoites can be visualized by the trails (shown in green) deposited on a coated surface, which demonstrate circular gliding. The circular motion on a 2D surface is translated into a helical movement in tissues or in a 3D matrigel, and this helical movement can be described as a clockwise corkscrew trajectory that is linked to the left-handed twisted microtubules of the zoite cytoskeleton99–101. **b.** An *Eimeria nieschulzi* sporozoite (S) gliding along a rat erythrocyte (E) *in vitro*. Several sites of interaction are visible (indicated by the white arrows). The black arrows indicate the forward gliding of the sporozoite and the stretching of the erythrocyte. **c.** A generalized model of gliding motility in Apicomplexa. The exocytosis of secretory microneme organelles (orange) occurs at the apical pole of the parasite. During this process, transmembrane adhesive proteins that are embedded into the microneme membrane become inserted into the parasite plasma membrane (pPM), where they interact with extracellular receptors on the host cell (shown in black). Gliding motility results from the rearward translocation of these adhesin–receptor complexes, which is powered by the myosin motors (blue) along actin filaments (yellow) in the space between the inner membrane complex (IMC) and the pPM. hPM, host cell plasma membrane.

Gliding motility powers invasion and egress in Apicomplexa (Frénal et al., 2017)

Gliding motility is initiated at the apical pole and depends on the glideosome complex

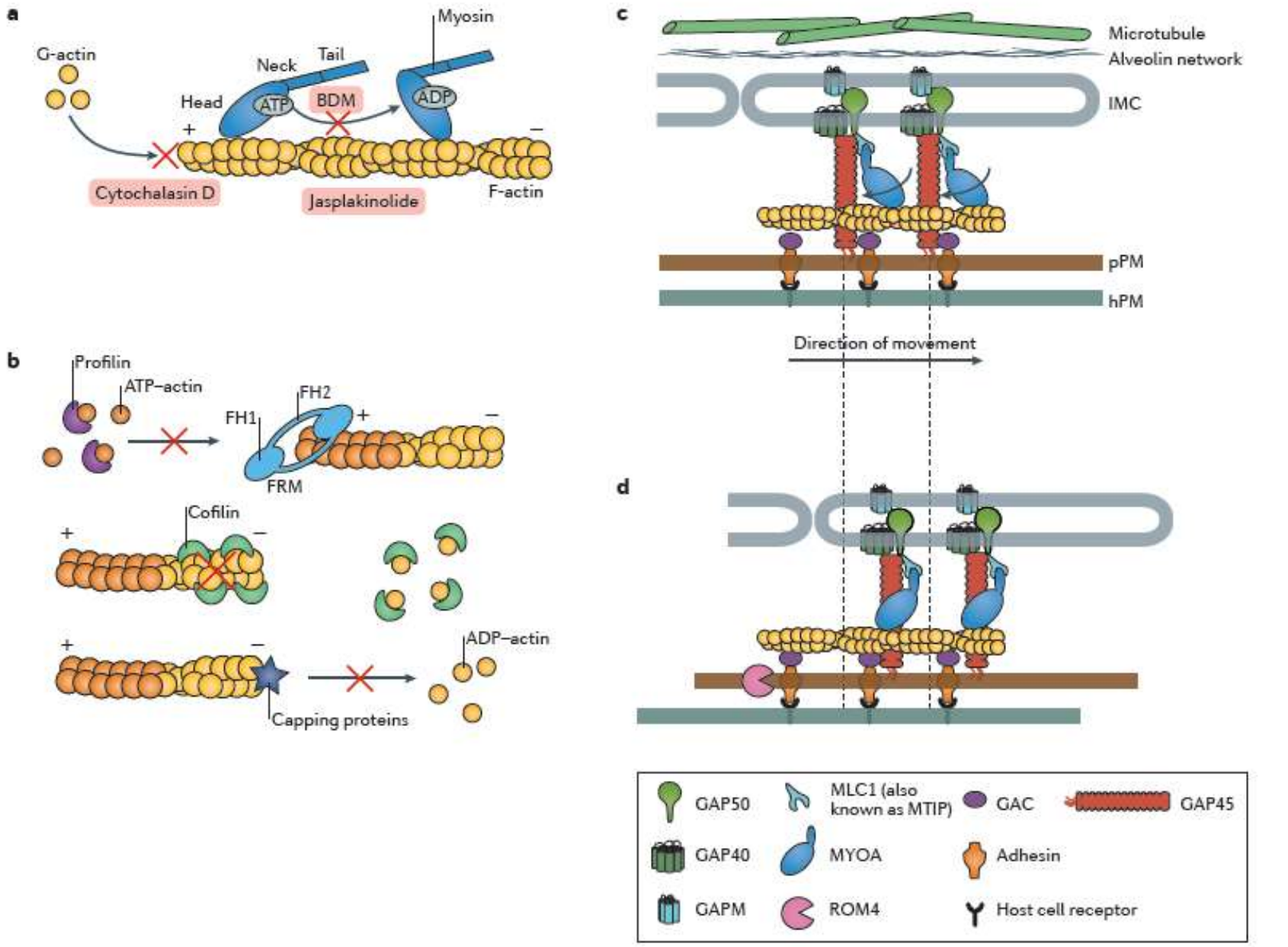

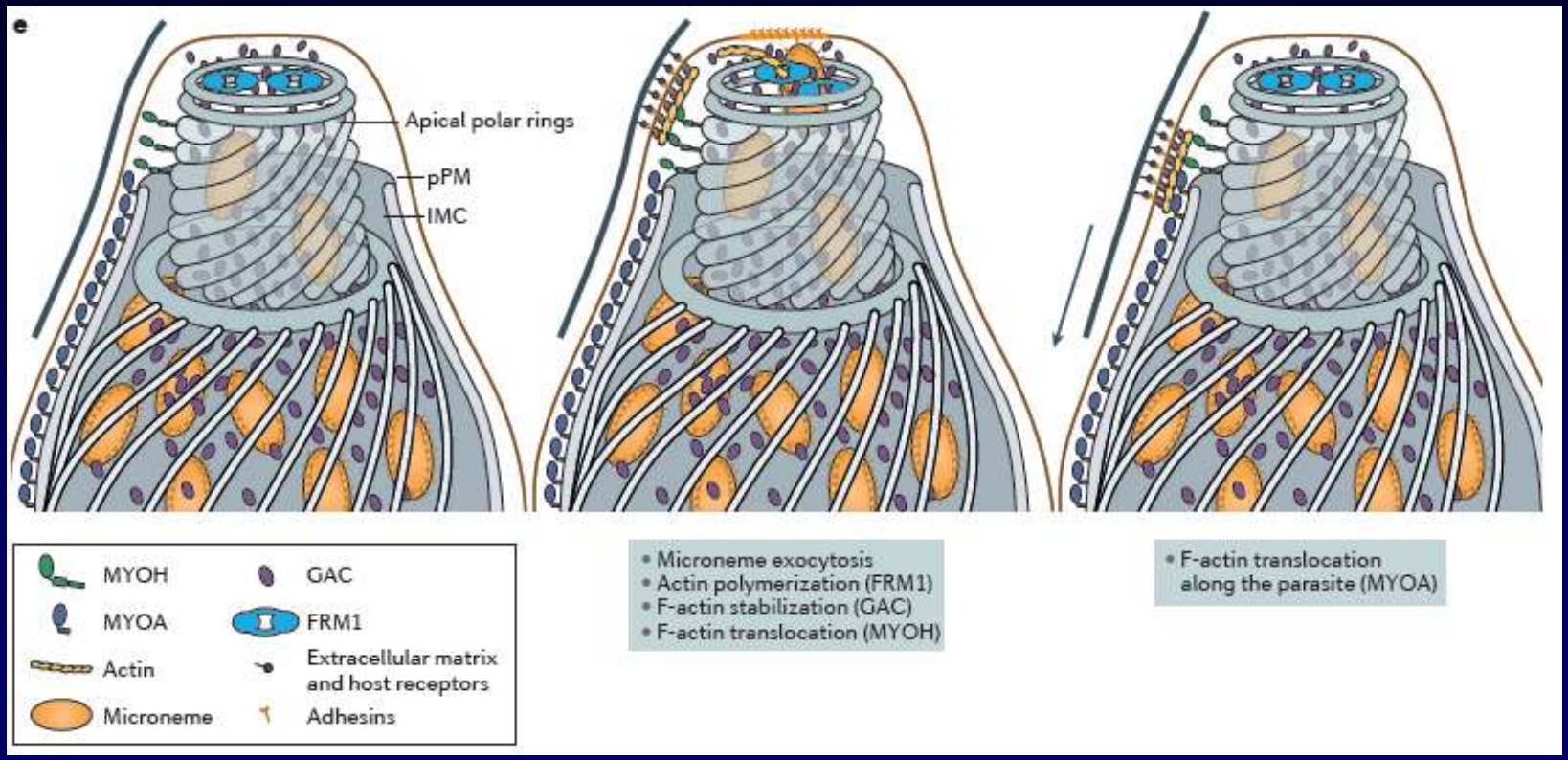

a. The action of the drugs that have been used to identify the involvement of actin and myosin in motility and invasion. Cytochalasin D binds to the barbed end (+) of actin, inhibiting polymerization, and jasplakinolide can bind to and stabilize actin filaments (F-actin). These toxins inhibit the motility of *Toxoplasma gondii* tachyzoites and consequently their invasion. 2,3-butanedione monoxime (BDM), which is known to block myosin heavy chain II ATPase activity, also inhibits parasite invasion. **b.** Formins (FRMs) are the only known actin nucleators and actin-polymerizing factors in apicomplexans. The FRM homology 2 (FH2) domain remains associated with the barbed end during actin polymerization. Profilin binds to ATP–actin monomers and promotes the polymerization of F-actin by delivering globular actin (G-actin) to the nascent filament or by augmenting FRM activity. In *Toxoplasma gondii*, profilin does not augment FRM activity but contributes to maintaining the pool of G-actin and not actin depolymerization (red cross). Cofilin (also known as actin-depolymerizing factor (ADF)) also contributes to the sequestration of G-actin. Conversely, capping proteins prevent the depolymerization of F-actin by binding to its pointed end (–). **c.** The core motility complex is composed of the myosin A (MYOA) motor and its myosin light chain (myosin light chain 1 (MLC1) in *Toxoplasma gondii*; MYOA tail domain-interacting protein (MTIP) in *Plasmodium* spp.) linked to the inner membrane complex (IMC) proteins gliding-associated protein 40 (GAP40) and GAP50 through an interaction with GAP45. In addition, GAP45 maintains the spacing of the parasite plasma membrane (pPM) and the IMC. Glideosome-associated connector (GAC) bridges F-actin and adhesins. The glideosome is also linked to the underlying cytoskeleton, probably through members of the GAPs with multiple-membrane spans (GAPM) family, thus enabling the generation of traction forces. **d.** The conformational change of the myosin head domain on the F-actin following ATP hydrolysis drives the forward movement of the parasite. Surface-expressed rhomboid-like protease 4 (ROM4) cleaves the transmembrane domain of adhesins to disengage their interaction with host receptors. **e.** A schematic showing a magnified view of the apical pole of a *T. gondii* tachyzoite; motility is initiated at this site. Following calcium signalling, microneme exocytosis occurs at the apex of the parasite. Adhesins secreted by micronemes are inserted into the pPM and interact with host cell receptors or the extracellular matrix. At the tip, FRM1 polymerizes F-actin that is stabilized by GAC. GAC also interacts with the cytoplasmic tails of the adhesins and, together with F-actin and the adhesin–receptor complexes, is translocated backwards by the action of myosin heavy chains MYOH (at the level of the conoid) and MYOA (along the IMC). hPM, host cell plasma membrane. Parts **a**–**d** are adapted with permission from Frénal, Soldati-Favre, 2013. Part **e** is adapted with permission from Jacot et al., 2016.

Gliding motility powers invasion and egress in Apicomplexa (Frénal et al., 2017)

Motility drivers egress and invasion

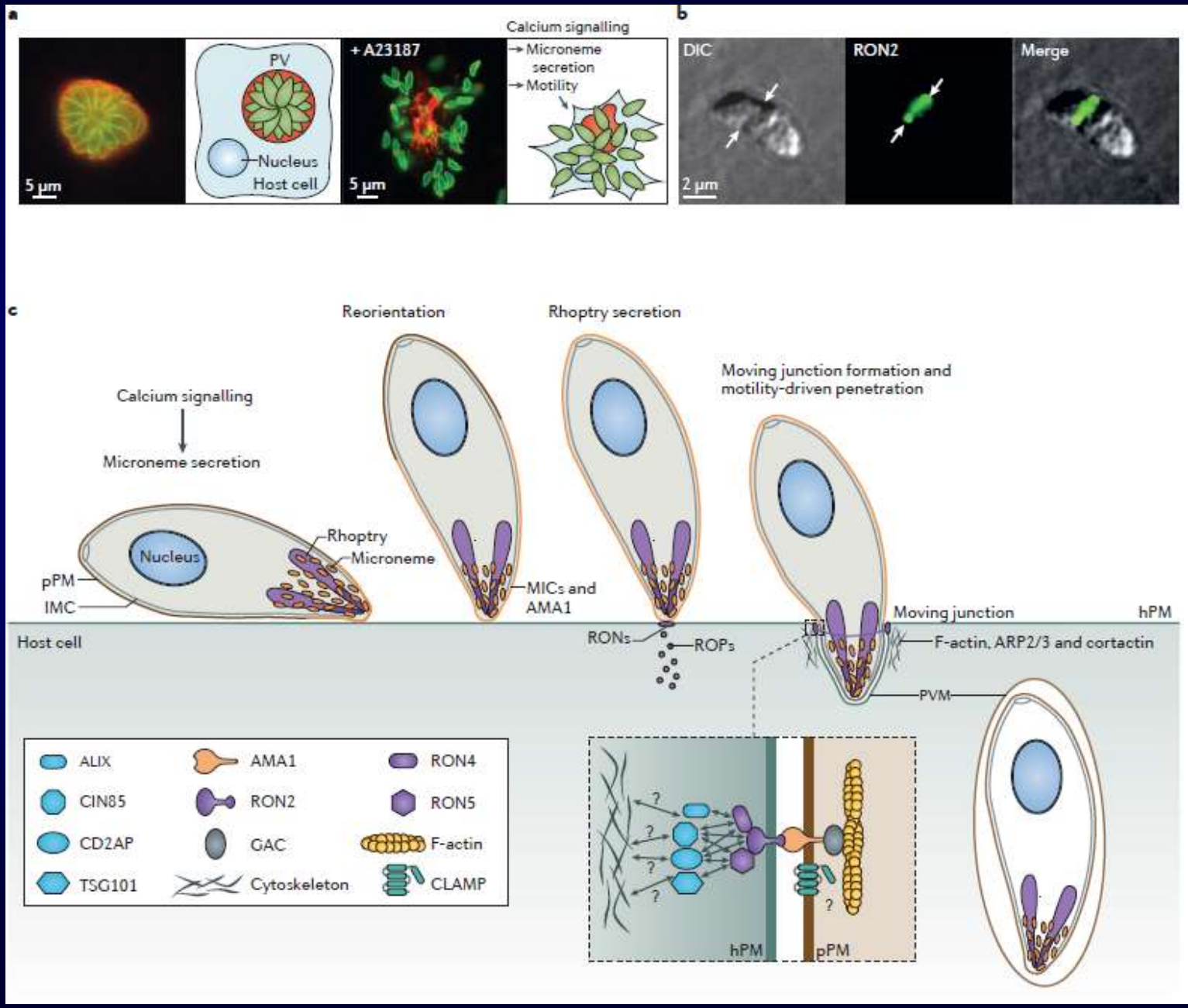

Gliding motility powers invasion and egress in Apicomplexa (Frénal et al., 2017)

Motility drivers egress and invasion

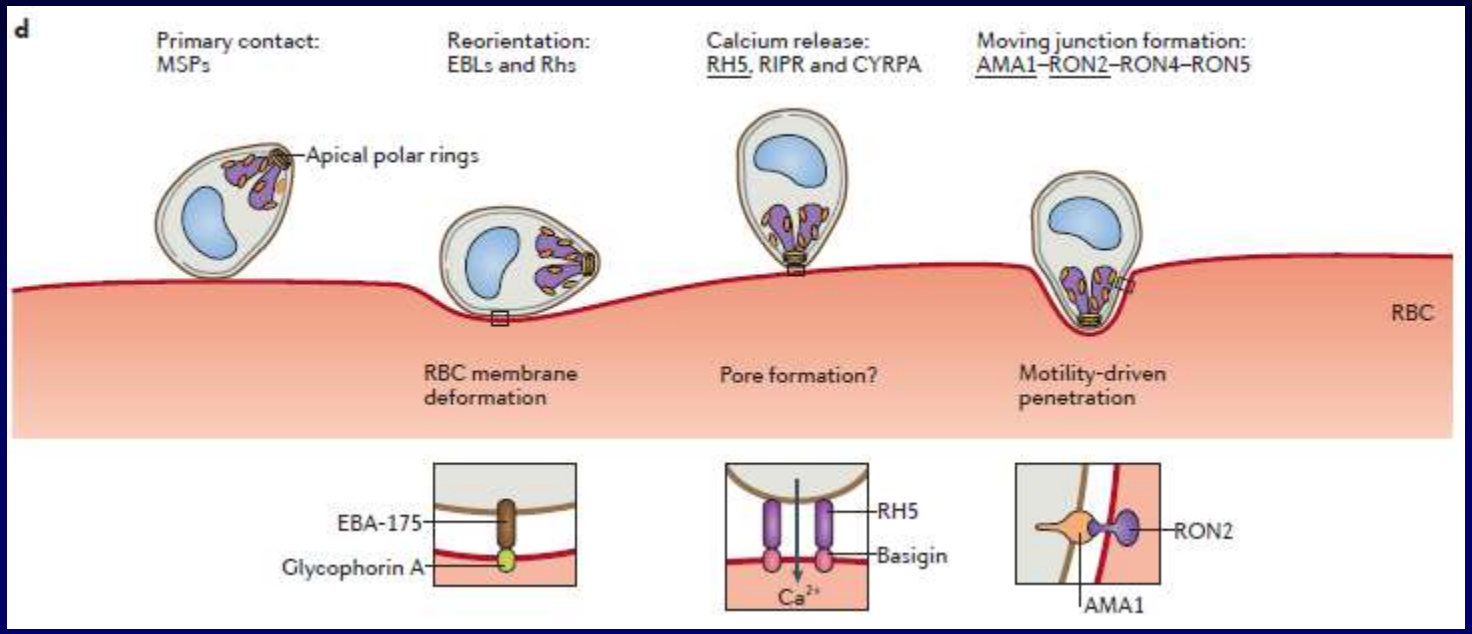

Motility drives egress and invasion. a | The two panels on the left show an immunofluorescence image and a schematic representation of intracellular tachyzoites residing in a parasitophorous vacuole (PV). The two images on the right show an immunofluorescence image and a schematic representation of parasites freshly egressed from the PV and host cell after induction by the calcium ionophore A23187. The PV is stained using a dense granule marker (dense granule protein 3; red) whereas anti-SAG1 antibodies were used to detect the pellicle of the parasites (green). **b** | Immunofluorescence images of an invading *Toxoplasma gondii* tachyzoite; the moving junction, labelled with anti-rhoptry neck protein 2 (anti-RON2) antibodies, is visible as a ring (green). The white arrows indicate the constriction of the moving junction. **c** | The invasion process of extracellular *T. gondii* tachyzoites, beginning with host cell adhesion, followed by the secretion of the content of micronemes (microneme proteins (MICs) and apical membrane antigen 1 (AMA1)), and the subsequent reorientation of the parasite, which places its apical pole in juxtaposition with the host cell plasma membrane (hPM). Subsequently, the secretion of RONs enables the formation of the moving junction between RON2–RON4–RON5 and AMA1, thus supporting the motility-driven progression of the parasite into the target cell. The magnified view (inset) highlights the interaction between the glideosome and the moving junction, and the interactions between the moving junction and host proteins (ALG2-interacting protein X (ALIX), CBL-interacting protein of 85 kDa (CIN85), CD2-associated protein (CD2AP) and tumour susceptibility gene 101 protein (TSG101)). Claudin-like apicomplexan microneme protein (CLAMP) also follows the moving junction during invasion, but its role is unknown169. After invasion, the parasite is enclosed in the parasitophorous vacuole membrane (PVM). **d** | After the egress of *Plasmodium* spp. merozoites, invasion starts with weak interactions between merozoite surface proteins (MSPs) and the surface of the red blood cell (RBC). Parasite reorientation occurs following tight interactions of erythrocyte-binding antigens (EBAs) and reticulocyte binding-like homologues (RHs) with host cell receptors. The binding of EBA-175 to glycophorin A mediates marked deformability of the RBC membrane, which is required for invasion117. At the tip of the merozoite, the binding of RH5 to basigin triggers calcium release170 and the formation of the moving junction that supports the motility-dependent host cell invasion of the parasite. The underlined proteins are transmembrane proteins inserted in the plasma membrane. ARP2/3, actin-related protein 2/3; CYRPA, cysteine-rich protective antigen; DIC, differential interference contrast; F-actin, filamentous actin; GAC, glideosome-associated connector; pPM, parasite plasma membrane; RIPR, RH5-interacting protein; ROP, rhoptry proteins. Part **c** is adapted with permission from REF. 168, EDP Sciences. Part **d** is adapted from REF. 171; in this study, time-lapse imaging was used in combination with different methods of preventing merozoite–RBC interactions to provide the precise sequence of receptor– ligand interactions that occurs during the invasion process.

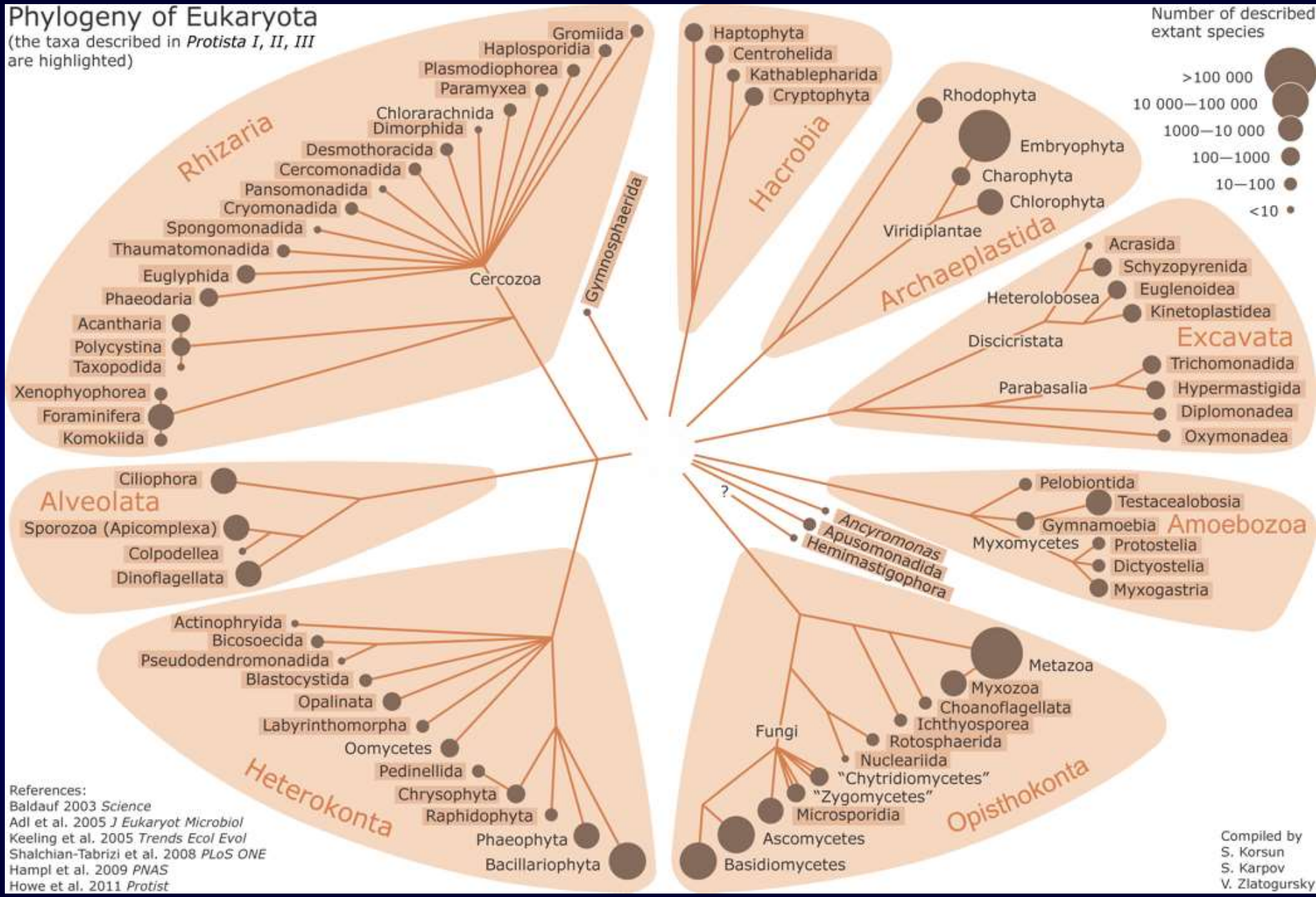

References:
Baldauf 2003 *Science*
Adl et al. 2005 *J Eukaryot Microbiol*
Keeling et al. 2005 *Trends Ecol Evol*
Shalchian-Tabrizi et al. 2008 *PLoS ONE*
Hampl et al. 2009 *PNAS*
Howe et al. 2011 *Protist*

Compiled by
S. Korsun
S. Karpov
V. Zlatogursky

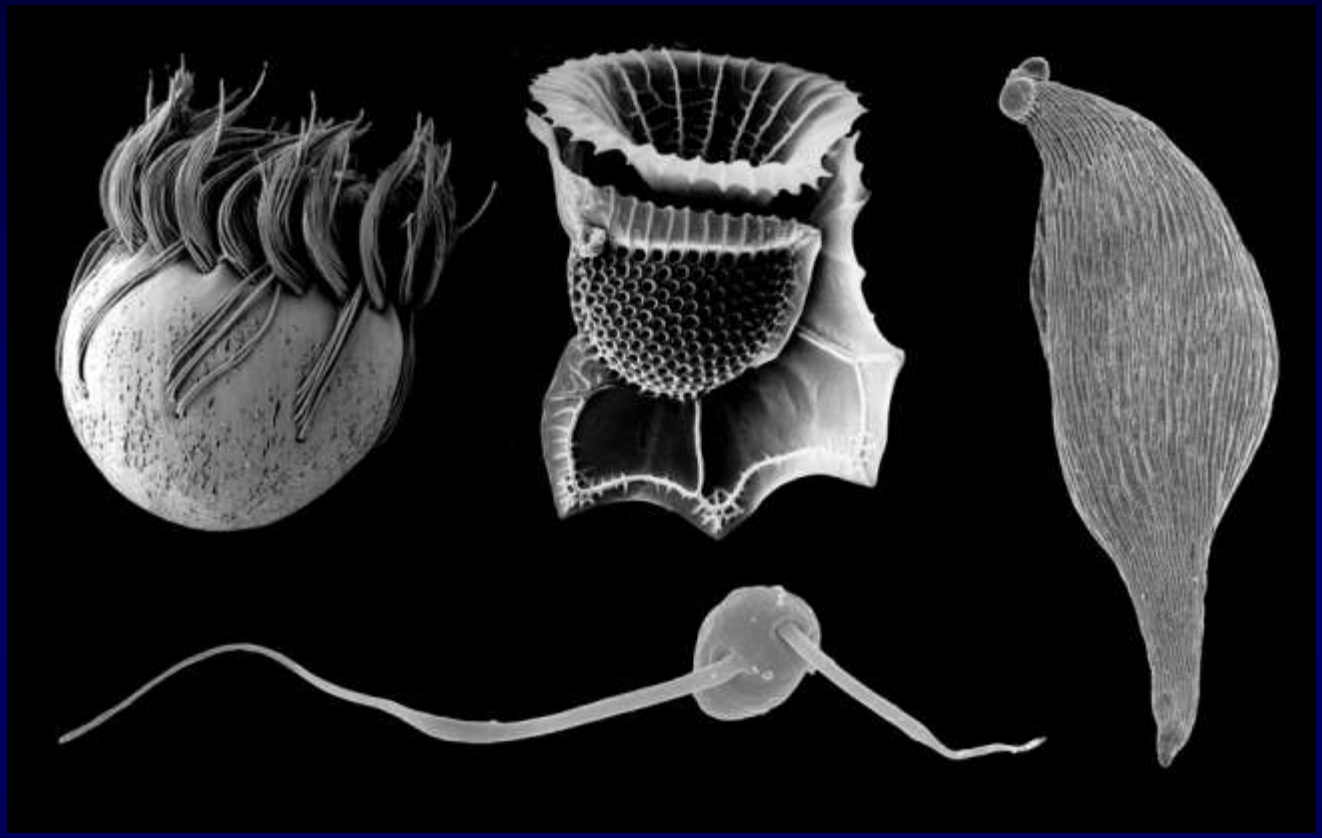

Scanning electron micrographs of representative alveolates. The three major groups of alveolates are ciliates [(a) *Halteria*], dinoflagellates [(b) *Ornithocercus*] and apicomplexans [(c) *Monocystis*]. Colpodellids [(d) *Colpodella*] are a group of flagellates inferred to have retained a large suite of ancestral character states. (Images are not to scale). (Leander, Keeling, 2003).

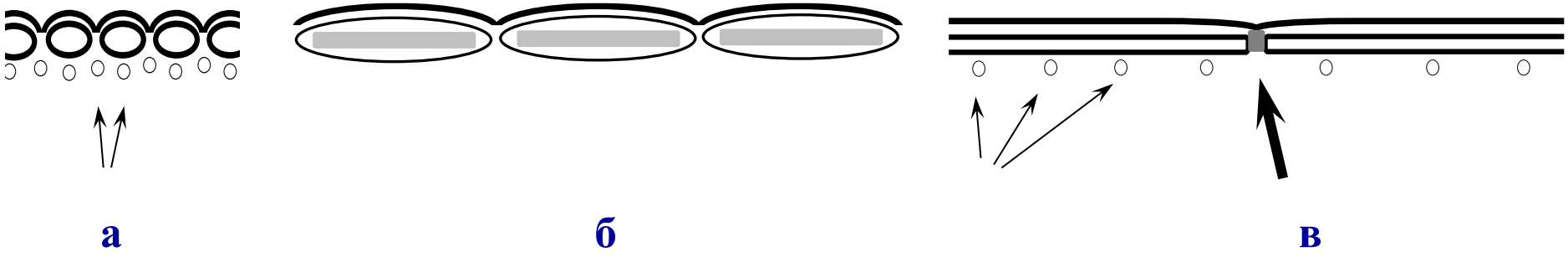

Структура покровов Alveolata (схематизированно):

***а* – инфузории; *б* – динофлагелляты, Colpodellida; *в* – споровики; маленькие стрелки указывают субпелликулярные микротрубочки, большая стрелка указывает микропору (Тихоненков и др., 2016)**

Hypothetical framework for inferring character states in ancestral alveolates.

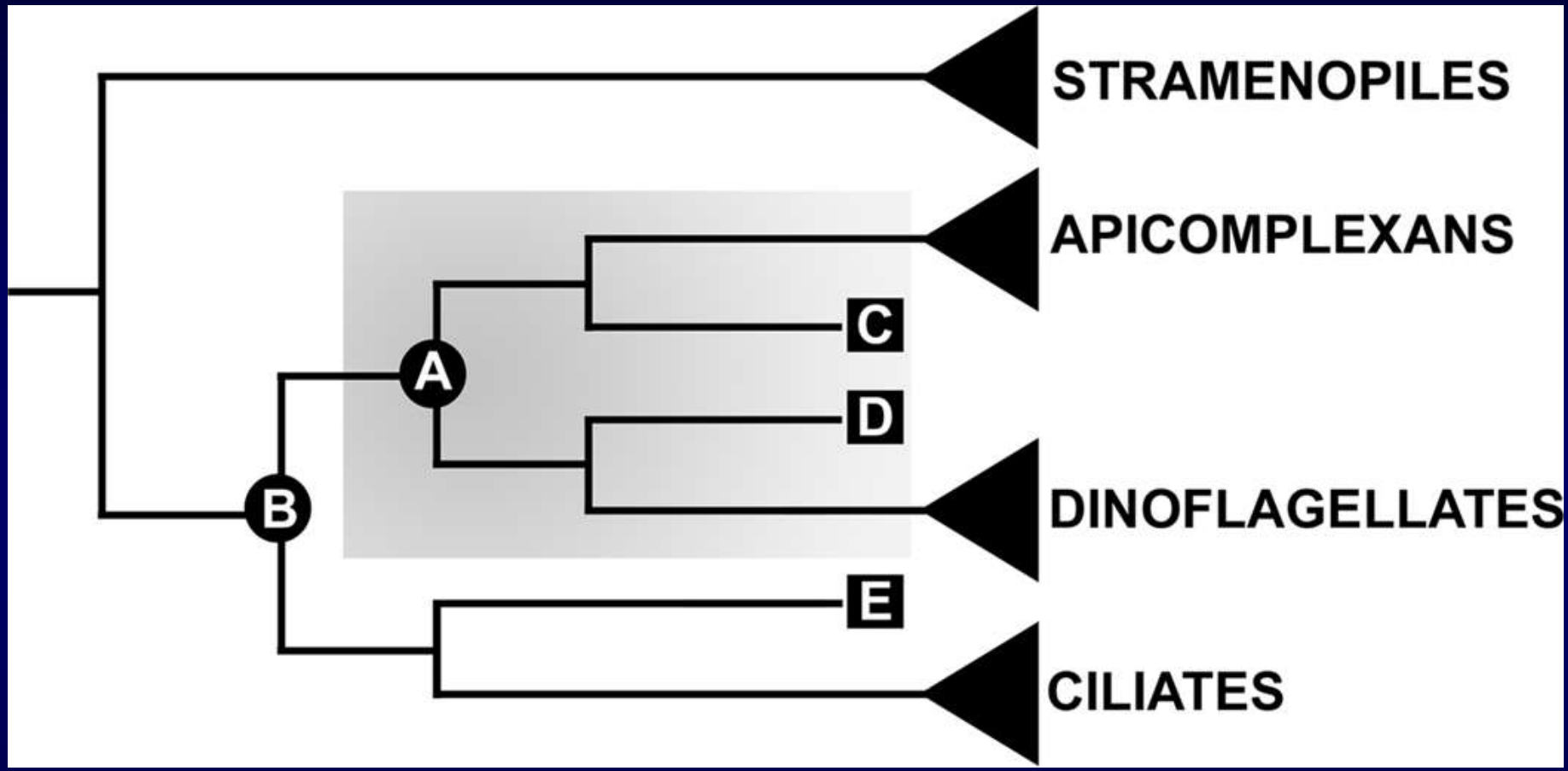

The three main groups of alveolates (apicomplexans, dinoflagellates, and ciliates) have very different modes of life and are extraordinarily divergent morphologically (as indicated by triangles), yet they are united by the presence of a distinct system of inner membranes (alveoli), micropores, and molecular sequence characters (Fast et al. 2002). Many extant alveolates that do not fit neatly within these three groups (lineages C, D, and E) may shed considerable light on two key questions: (1) What were the character states present in the most recent common ancestor of dinoflagellates and apicomplexans (extinct ancestor A) and (2) what were the character states present in the most recent common ancestor of all alveolates (extinct ancestor B)? If the earliest diverging extant sister lineage to apicomplexans (C) is strikingly similar on a state-by-state basis to the earliest diverging extant sister lineage to dinoflagellates (D), then unprecedented inferences can be made about the character states of ancestor A as indicated by the shaded box. Likewise, a comparative analysis of the earliest diverging extant sister lineage to ciliates (lineage E) with lineages C and D should provide important insights into the character states present in the extinct common ancestor of all alveolates (ancestor B). A better understanding of the biology and phylogenetic positions of these key taxa (lineages C, D, and E) will eventually lead to a more confident and accurate explanation for the origins of plastids and intracellular parasitism within alveolates (Kuvardina et al., 2002).

Hypothetical tree of Apicomplexa.

Three principal parasitic groups are coloured and their life cycle indicated, as well as Cryptosporidium that likely emerged from within gregarines. Numbers on branches and thickness indicates diversity (i.e. named species).

Jan Šlapeta, 2011

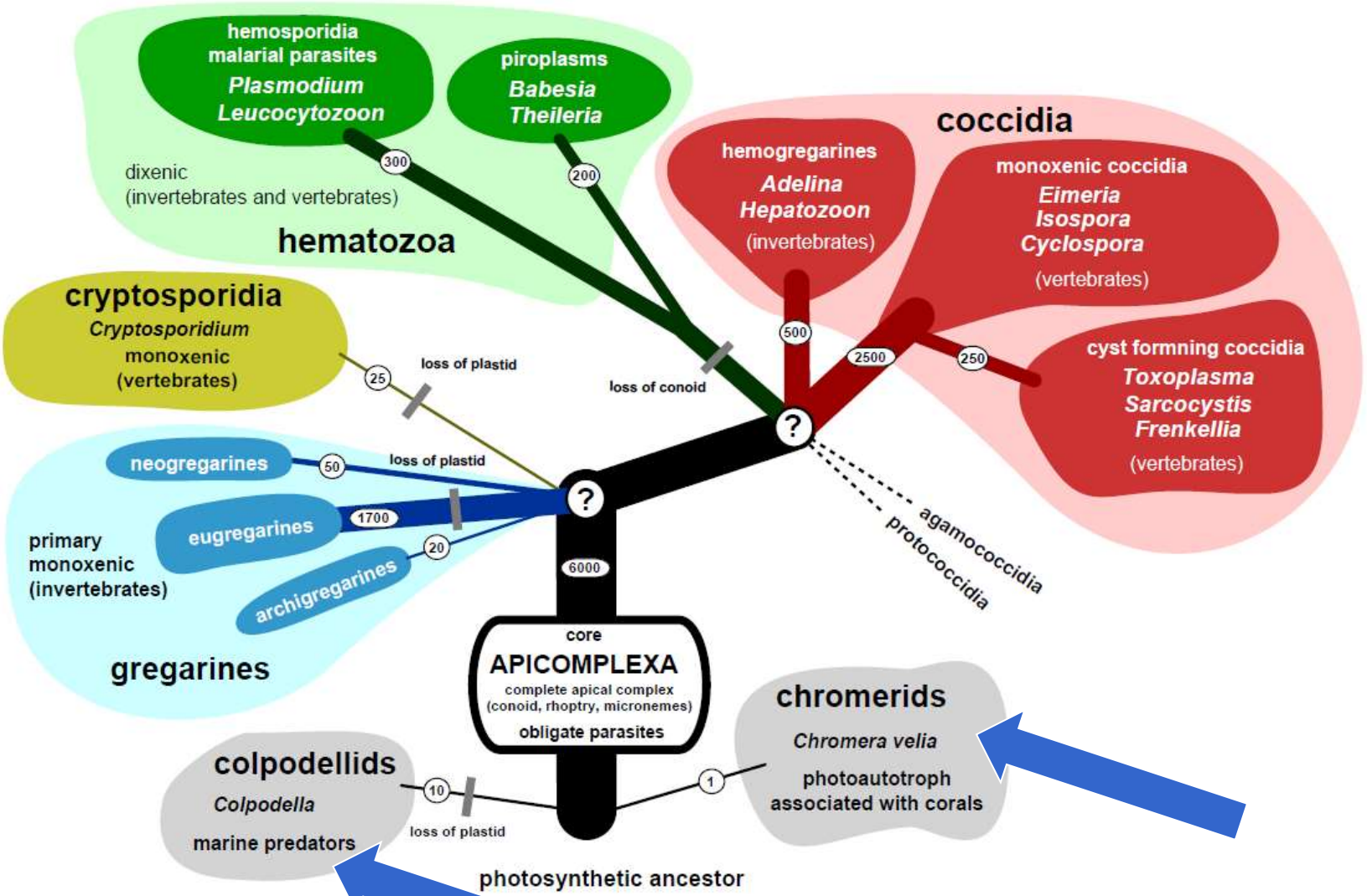

Chrompodellids (Janouškovec et al., 2015)

Жизненный цикл *Colpodella (Spiromonas) angusta*.

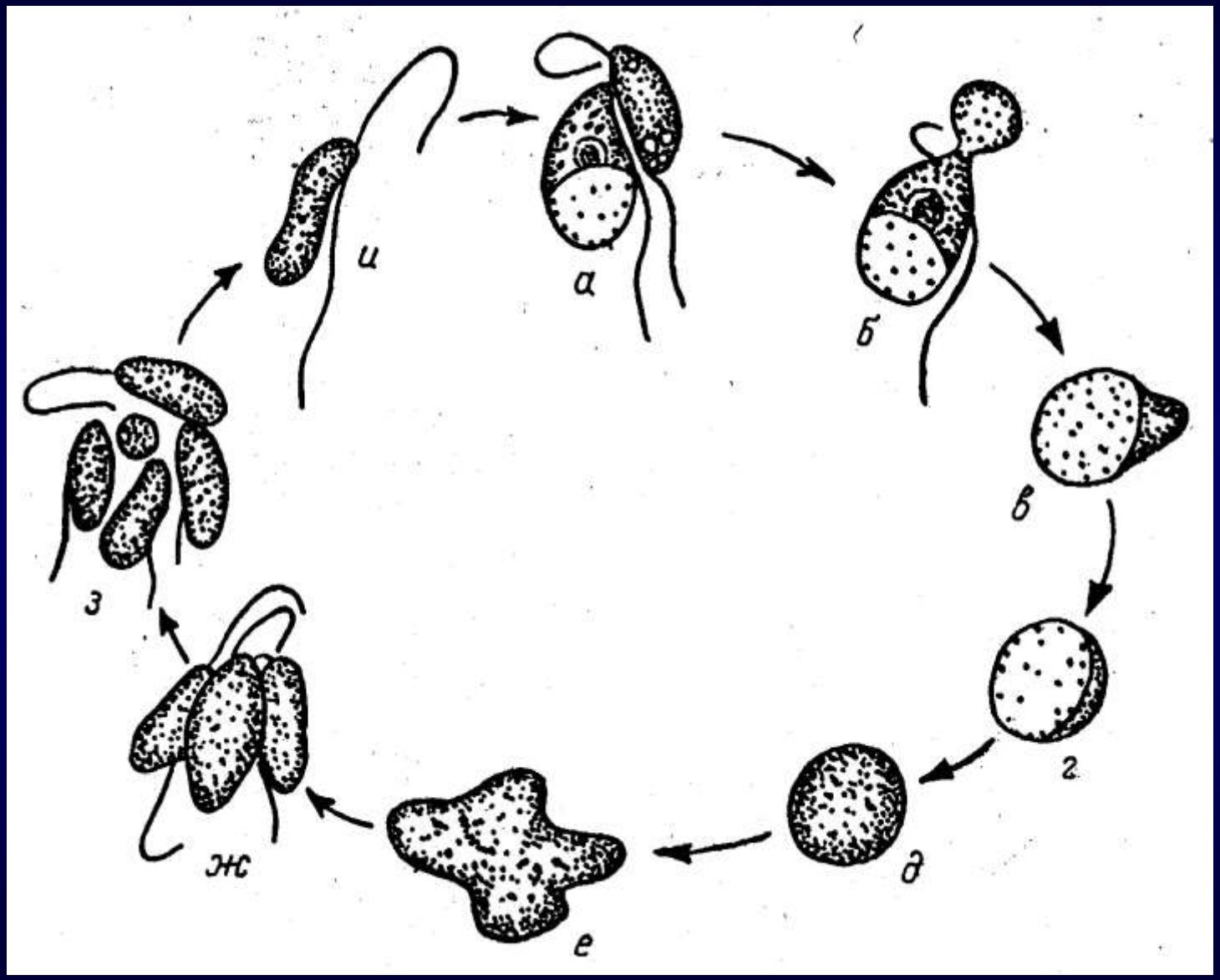

а, б – поедание жертвы; в-д – образование цисты; е-з – деление цисты на четыре особи; и – молодая особь (Крылов, Мыльников, 1986).

Схема строения *Colpodella* (*Spiromonas*) *angusta*.

Class Colpodellea (Kussakin Drozdov, 1998)

Order Colpodellida Cavalier-Smith, 1993 (=Spiromonadida Krylov, Mylnikov, 1986)

Fam. Colpodellidae Simpson, Patterson, 1996

Genus *Colpodella*

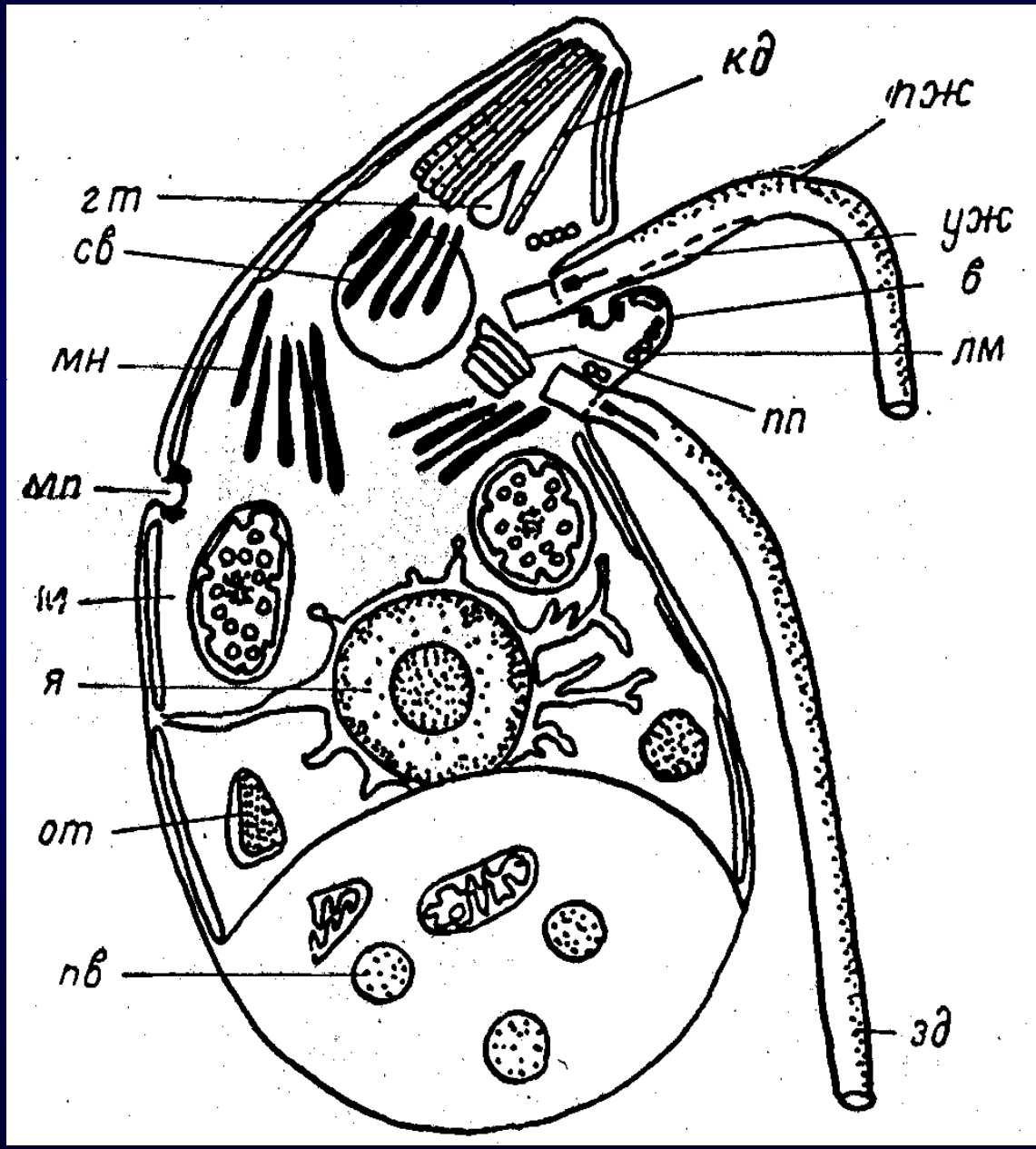

в –валик между жгутиками, гт – грушевидное тело, зд – задний жгутик, кд – коноид, лм – лента микротрубочек, м – митохондрия, мн – микронемы, мп – микропоры, от – осмиофильные тела, пв – пищеварительная вакуоль, пж – передний жгутик, пп – полосатая пластинка, св – сократительная вакуоль, уж – утолщение жгутика, я – ядро (Крылов, Мыльников, 1986).

The Morphology of Predatory Flagellate *Colpodella pseudoedax* Mylnikov et Mylnikov, 2007 (Colpodellida, Alveolata)

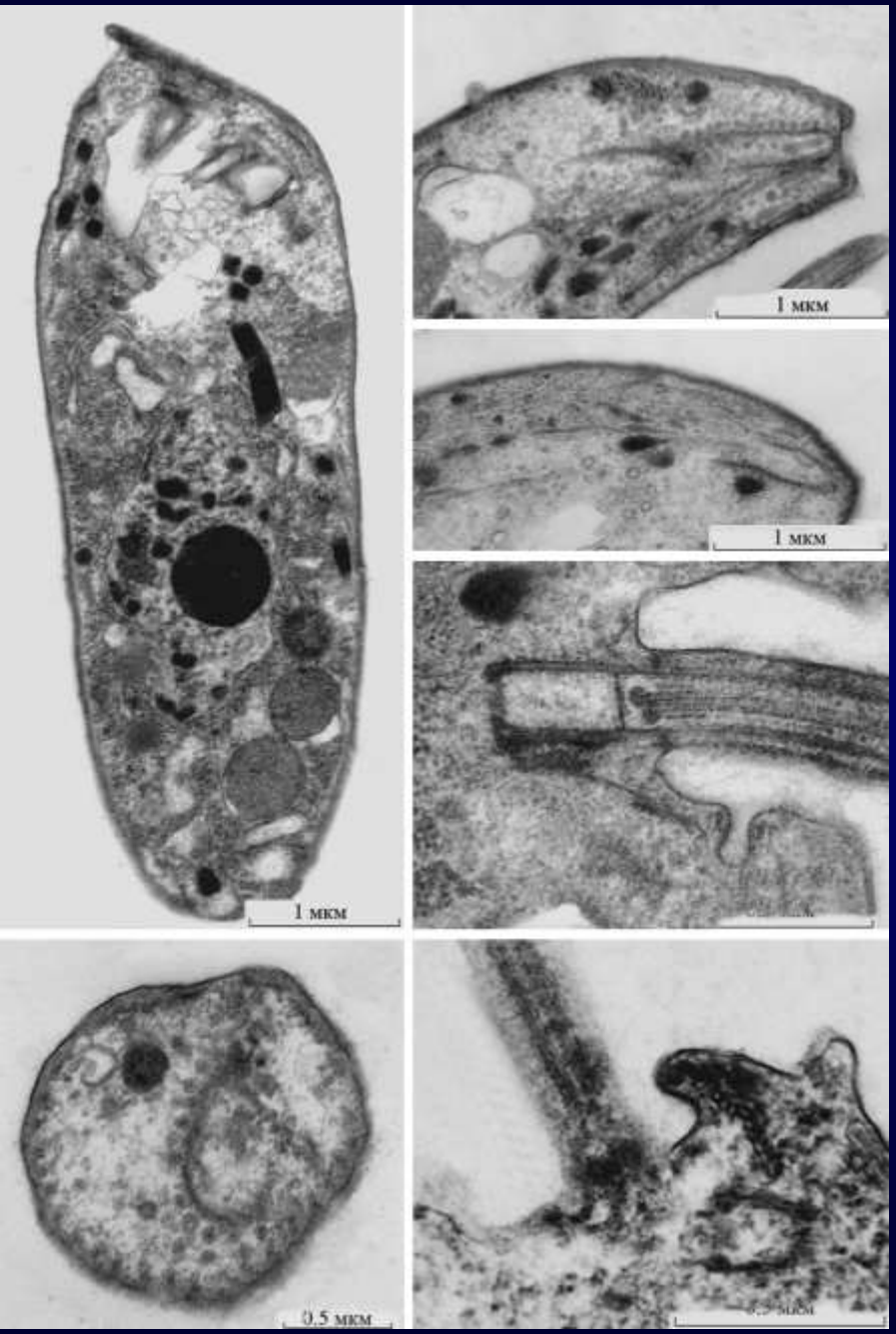

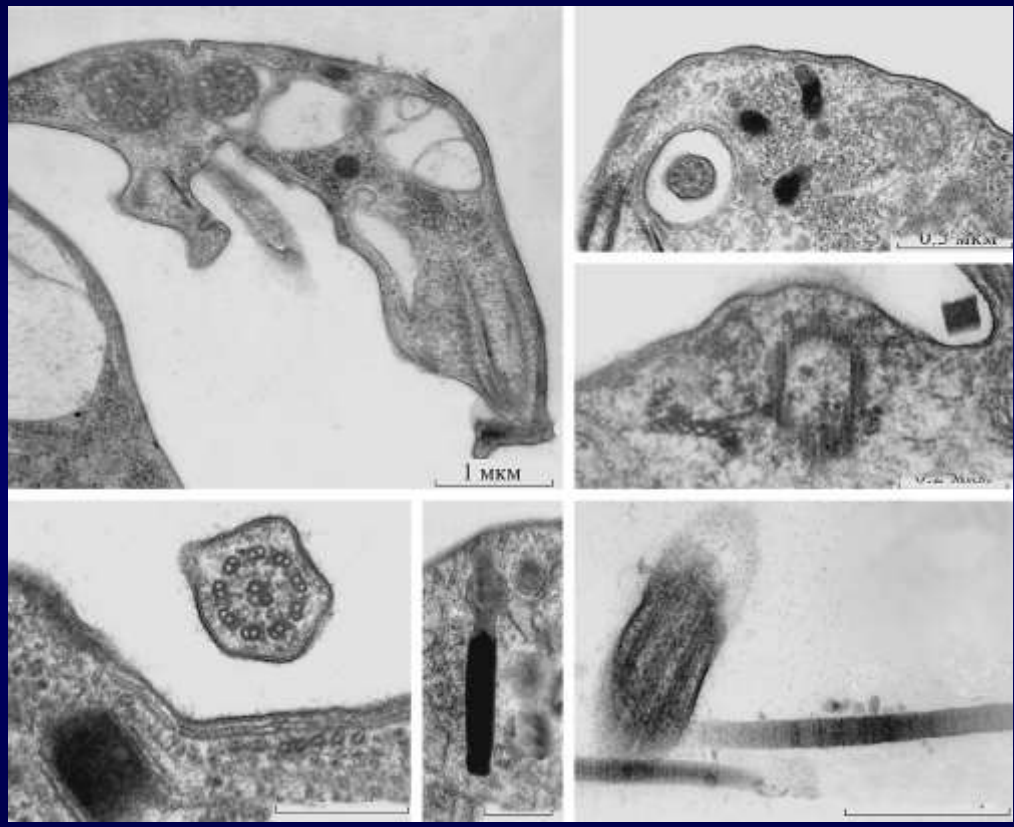

Morphology of *Colpodella pseudoedax* cell: (a) longitudinal section of the cell, (b, c, e) rostrum, (d) flagellum, (f) microtubular bands, (g) anterior end of the cell, (h) flagellar pocket, (i, j) microtubular bands' passage, (k, m) trichocyst; f.p is the flagellar pocket, fl is the flagellum, r.f is the rear flagellum, k is the kinetosome, cd is the conoid, mt. b is the microtubular band, m is the mitochondria, mn is the microneme, mp is the micropore, p is the pellicle, vs are the vesicles, r is the rostrum, rp is the ropty, c.v is the contractile vacuole, s.mt is the subpellicular microtubules, fld is the fold, tc is the trichocyst, c is the cylinder, nu is the nucleus (Myl'nikova, Myl'nikov, 2009).

General morphology of *Colpodella edax*.

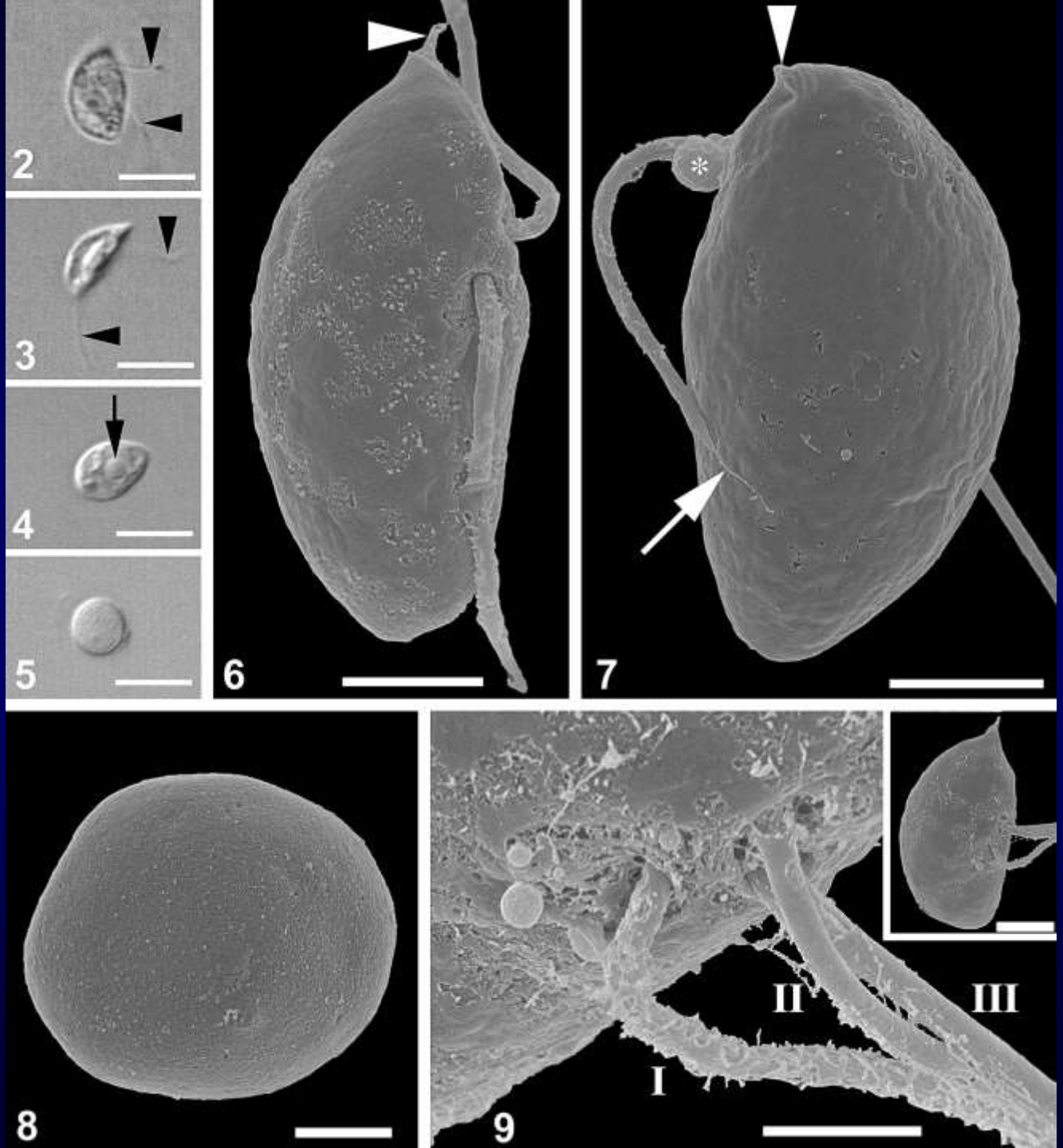

2–4. Light micrographs of zoospores showing cell shape, two flagella (arrowheads) and a centrally positioned nucleus (arrow) (Bar = 10 mm). **5**. Light micrograph of a resting cyst (Bar = 10 mm). **6**. Scanning electron micrograph (SEM) showing the apical rostrum (arrowhead) and the lateral insertion of two flagella on the right-hand side of a cell (Bar = 1.5 mm). **7**. SEM of the left-hand side of a cell showing the apical rostrum (arrowhead). In many cells, an amorphous protuberance (asterisk) was present near the flagellar insertions, and the anterior flagellum tapered to a fine thread (arrow) (Bar = 1.5 mm). **8**. SEM of a resting cyst showing scattered minute pores (arrows) (Bar = 1.5 mm). **9**. High magnification SEM showing the insertion of three flagella (Roman numerals) found in an otherwise normal looking cell (inset, Bar = 1.5 mm) (Bar =1 mm) (Leander et al., 2003).

Gamma-corrected ML tree (2lnL 5 14324) inferred from an alignment of 35 SSU rDNA sequences and 1442 sites, with stramenopiles as the outgroup, showing the phylogenetic position of *Colpodella*, *Perkinsus*, and *Parvilucifera* within alveolates (Kuvardina et al., 2002).

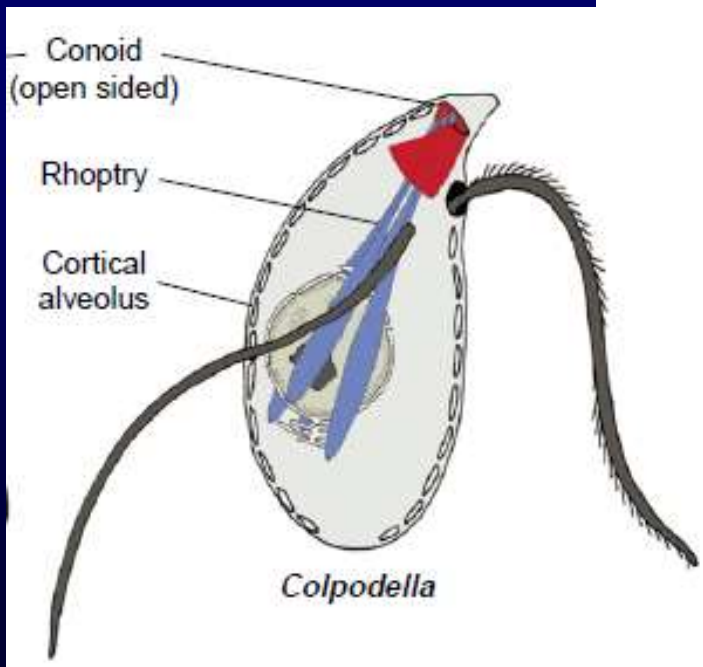

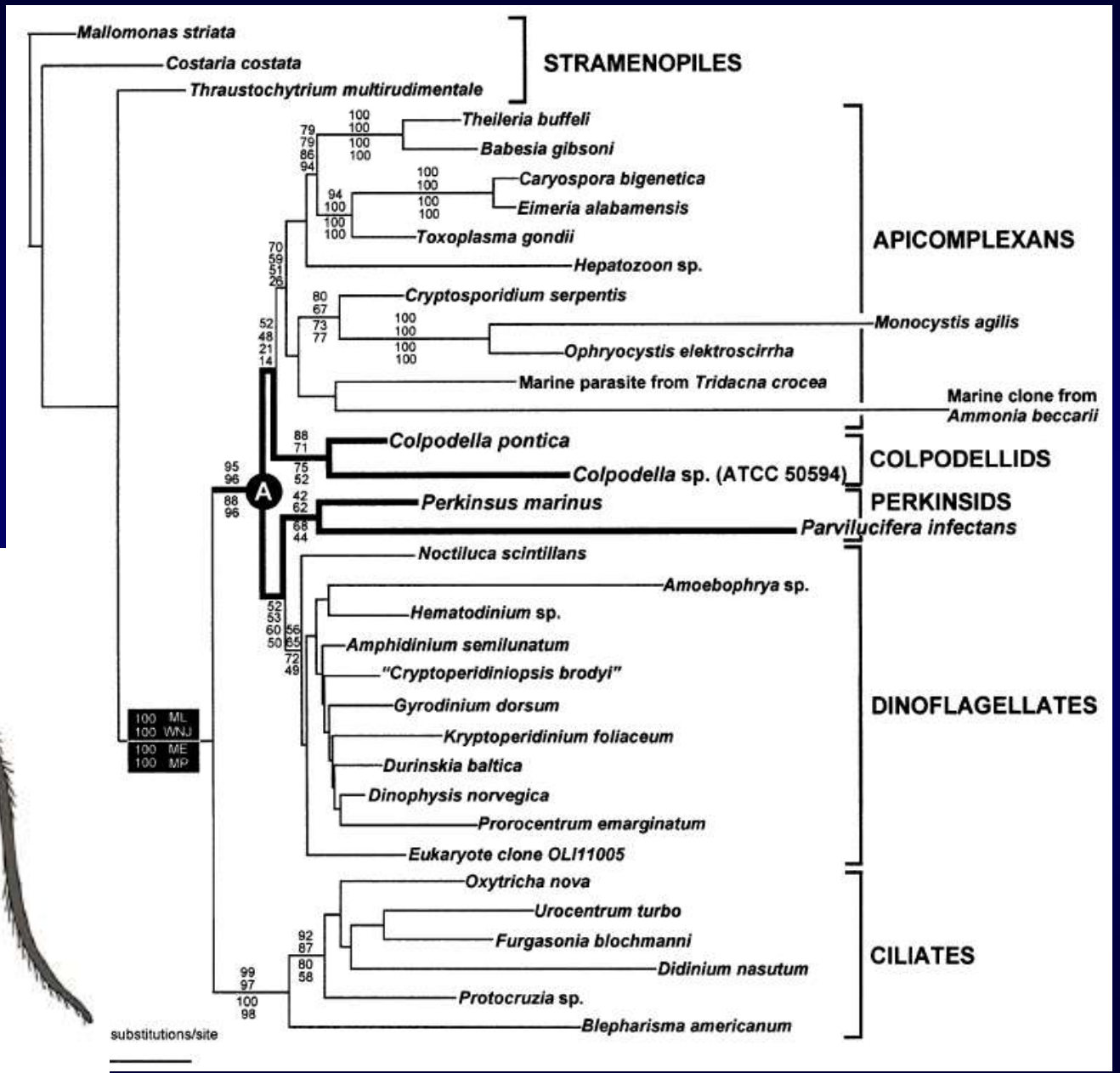

Perkinsea (Alveolata: Perkinsozoa)

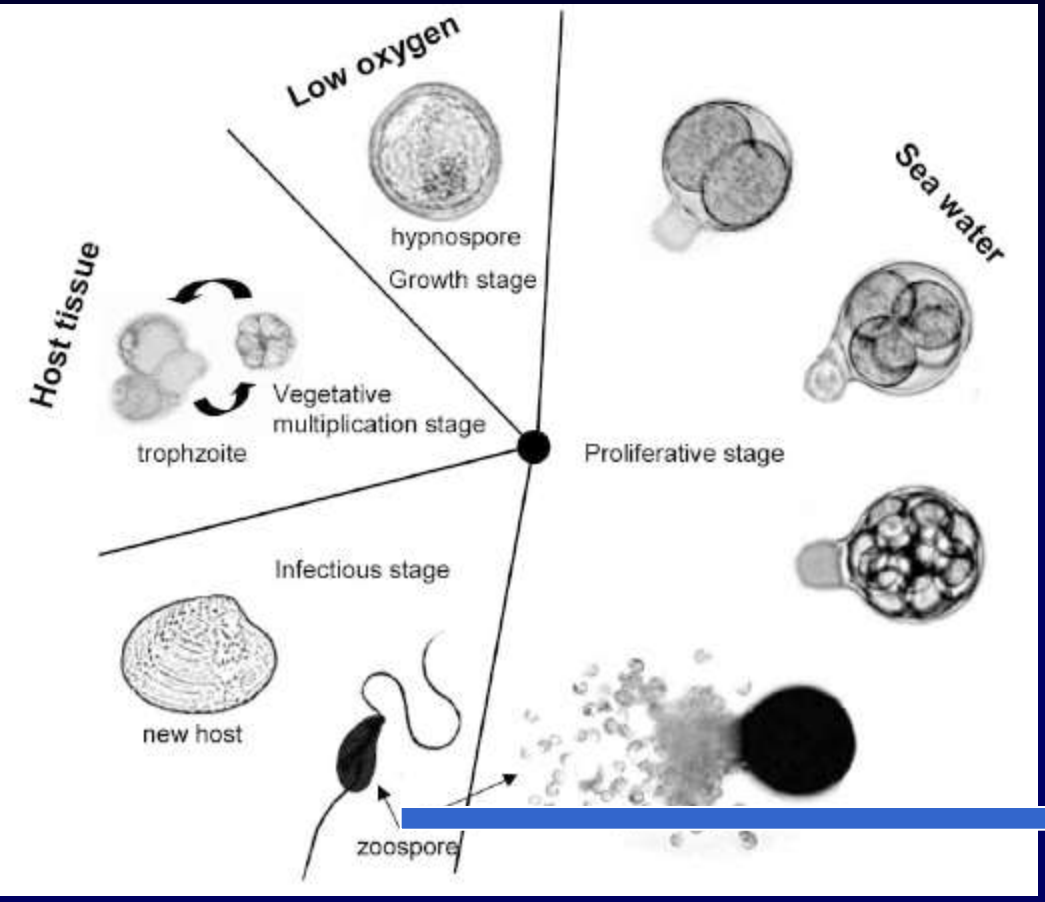

Life cycle of *Perkinsus olseni* parasitizing in the Manila clam *Ruditapes philippinarum*, (Modified from Auzoux-Bordenave et al. 1995, Choi et al., 2005) (From Choi & Park, 2010).

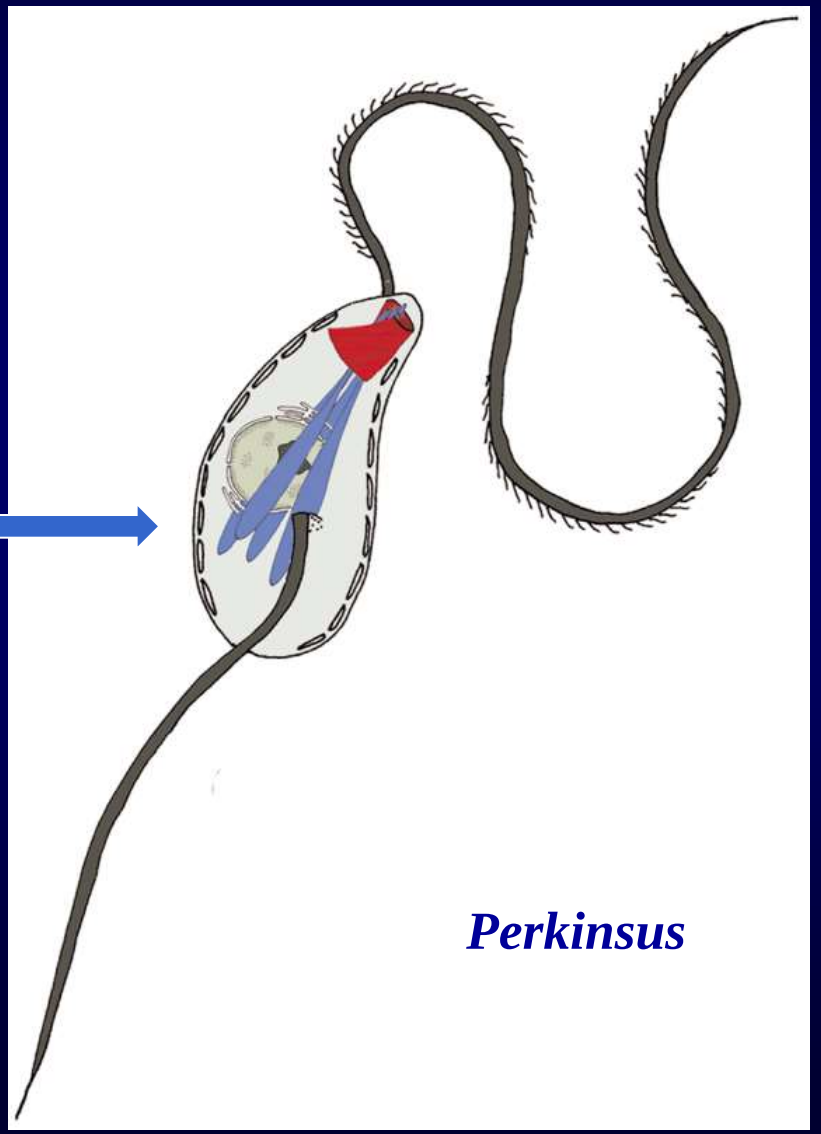

(Leander, Keeling, 2003)

Current phylogenetic framework for alveolates

Independent phylogenetic analyses of different molecular sequences show that ciliates diverged before the radiation of apicomplexans and dinoflagellates [14,15,30]. The earliest stages of alveolate evolution can be approached by addressing two key questions: (1) what character states were present in the most recent common ancestors of apicomplexans and dinoflagellates (Fig. I, node a); and (2) what were the character states present in the most recent common ancestors of all alveolates (Fig. I, lineage b)? If the earliest diverging sister lineages of apicomplexans (Fig. I, lineage c) and dinoflagellates (Fig. I, lineage d) turn out to be almost identical on a character state-by-state basis, then an extraordinarily confident inference could be made about the biological features of their common ancestor (Fig. I, node a), as indicated by the blue lines (Fig. I, Fig. I). Molecular phylogenies suggest that colpodellids and perkinsids, which are extraordinarily similar morphologically, represent lineages c and d, respectively (Fig. I). Both lineages possess an open-sided conoid (shown to the right) that is intermediate in form to the closed conoid of apicomplexans. The conoid homologue in dinoflagellates is unclear. Little is also known about the earliest diverging sister lineage to ciliates (Fig. I, lineage e) and the most recent common ancestor of all alveolates (Fig. I, node b). However, if lineage e and the inferred ancestor of apicomplexans and dinoflagellates (node a) turn out to share many character states (e.g. if Colponema represents lineage e), then a confident inference can be made about morphostasis in lineage e and the biological features of ancestor b (Fig. I). The gray shaded areas in Fig. I indicate strong degrees of morphostasis (Leander, Keeling, 2003).

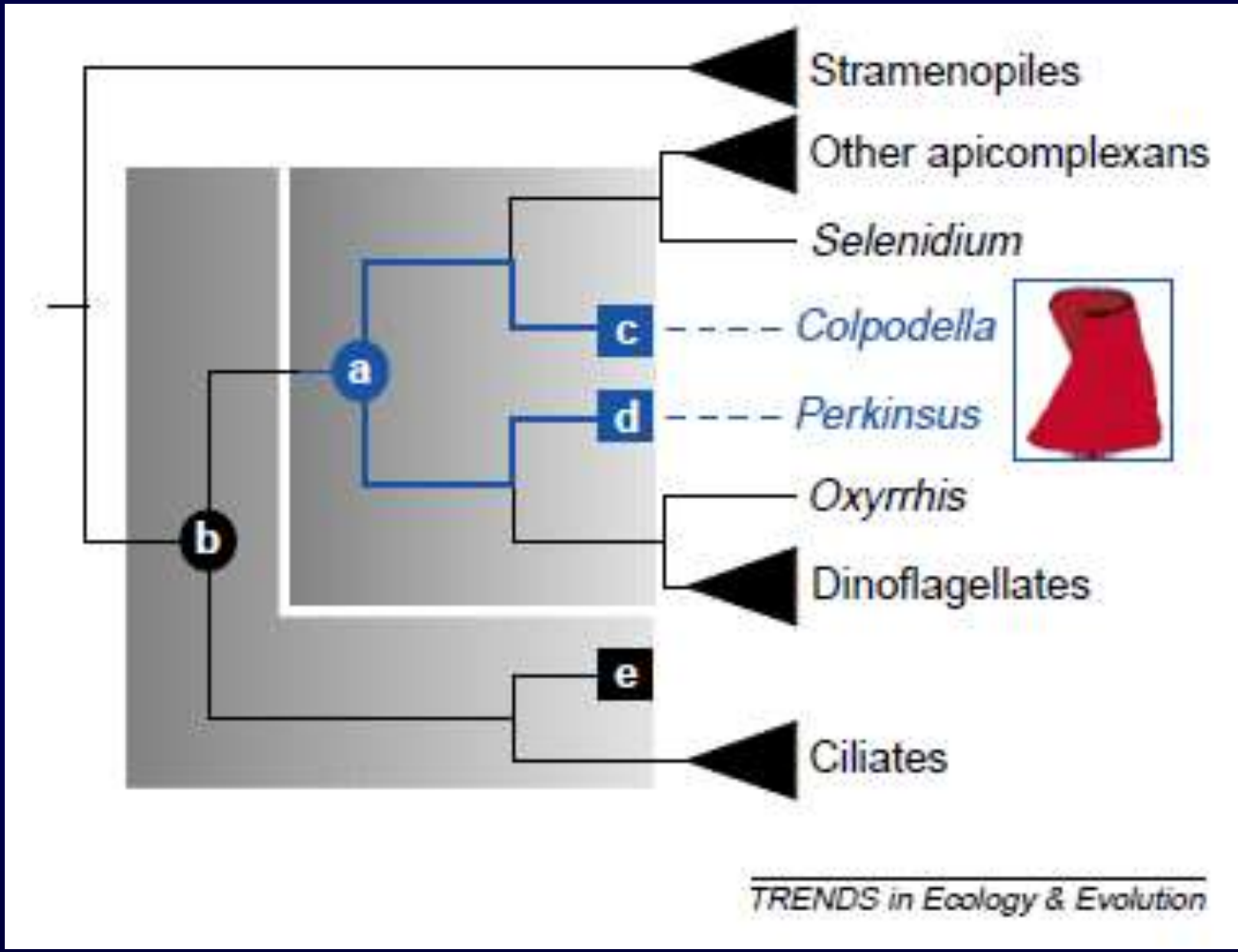

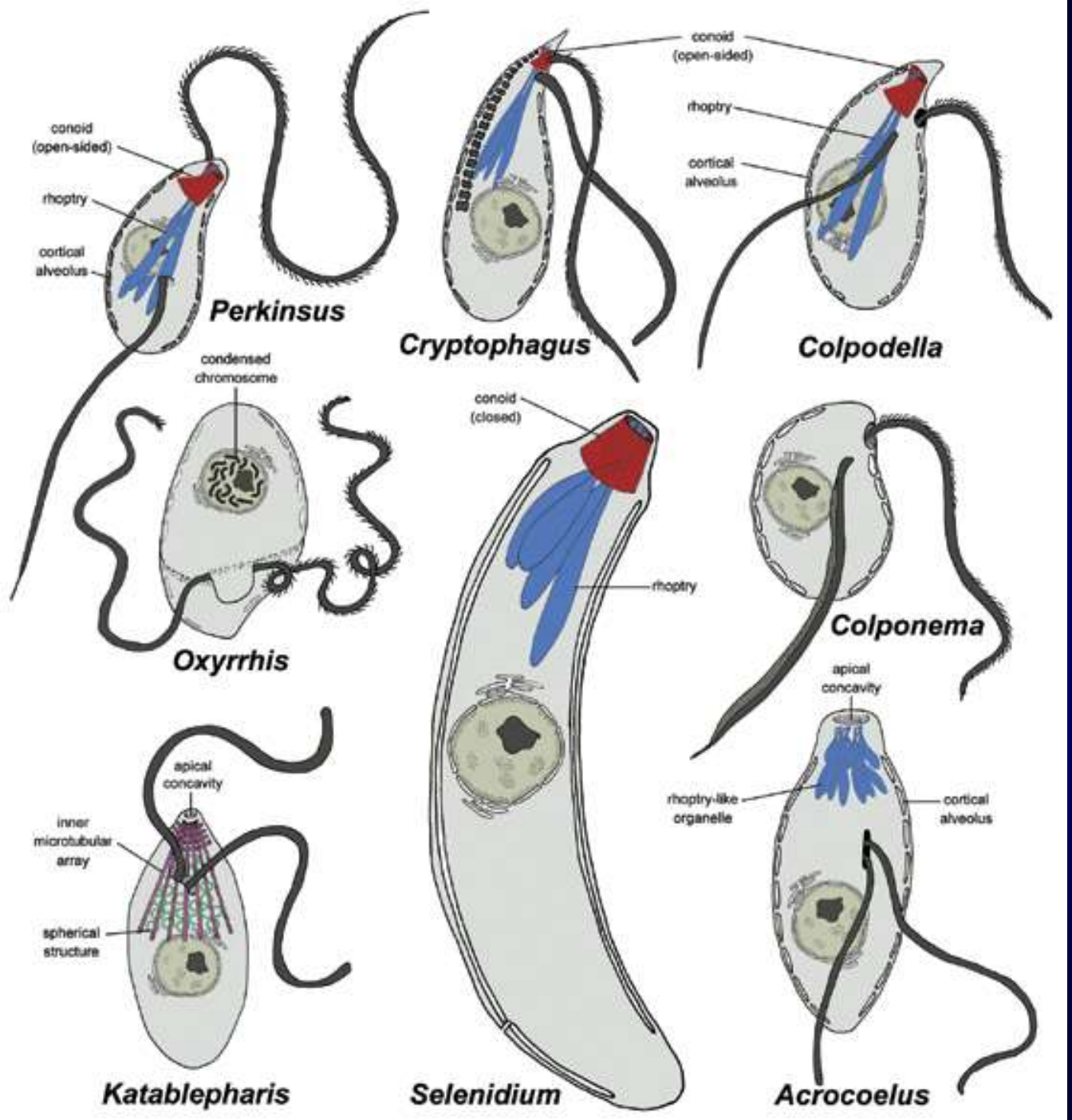

…the nearly identical ultrastructural characteristics of *Colpodella*, *Perkinsus*, and *Parvilucifera* species…. suggest that this morphology is the ancestral condition for all of Alveolata" (Siddal et al., 2001).

Major cytological features of eight lineages having strong degrees of morphostasis when compared with ciliates, dinoflagellates and most apicomplexans. Each organism is unicellular as indicated by the central nucleus and large nucleolus, and all but *Katablepharis* have the diagnostic feature of alveolates, cortical alveoli. The apical complex of the biflagellated zoospores in *Perkinsus*, *Parvilucifera* (not shown), *Cryptophagus*, and *Colpodella* comprise an open-sided conoid and rhoptries. The apical complex of 'true' apicomplexans, such as in the sporozoite and trophozoite of the archigregarine *Selenidium*, comprises a completely closed conoid and rhoptries. *Oxyrrhis* lacks an apical complex, has thin, permanently condensed chromosomes and is the nearest free-living sister lineage to dinoflagellates. *Katablepharis* is an enigmatic biflagellate with a putative apical complex-like apparatus associated with an apical concavity. The inner microtubular array is indicative of a longitudinally extended conoid, and the associated spherical structures are reminiscent of rhoptries in their cytological position near the cell apex and beneath the microtubular array. *Colponema* lacks obvious structures related to an apical complex, yet it is clearly a predatory alveolate that closely resembles *Colpodella* in general morphology and behavior. *Acrocoelus* is a biflagellated intestinal parasite of marine worms that lacks a conoid but possesses rhoptry-like organelles associated with an apical concavity. Several enigmatic organisms with alveolate-like features have not been shown for the sake of brevity, such as *Pirsonia* and *Phagodinium*. (Images are not to scale) (Leander, Keeling, 2003).

Chrompodellids are a large sister group of apicomplexans with a complex distribution of photosynthesis

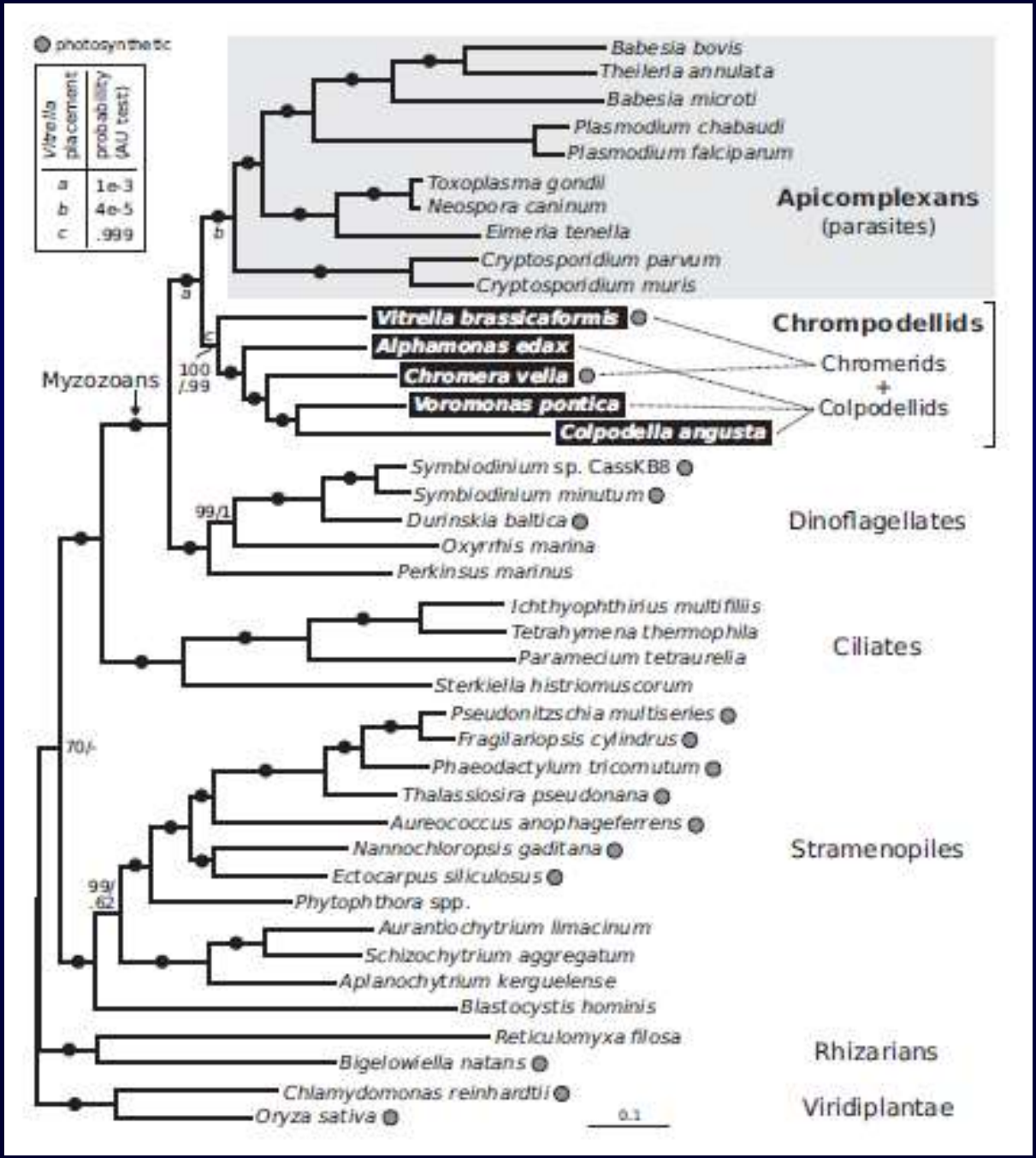

Maximum likelihood and Bayesian analyses inferred from the concatenation of 85 proteins (23,111 amino acids) resolve the relationships among apicomplexans and their relatives and demonstrate that the photosynthetic chromerids and predatory colpodellids are paraphyletic. Best RAxML tree (LG+GAMMA model) is shown with nonparametric bootstraps/Phylobayes posterior probabilities at branches. Full black circles indicate 100/1.0 support. Two alternative placements for *Vitrella* (at positions marked a and b) were rejected by approximately unbiased (AU) test at P = 0.005 (box) (Janouskovec et al., 2015).

Chromera velia as an example of the possible flagellar origins of the apical complex

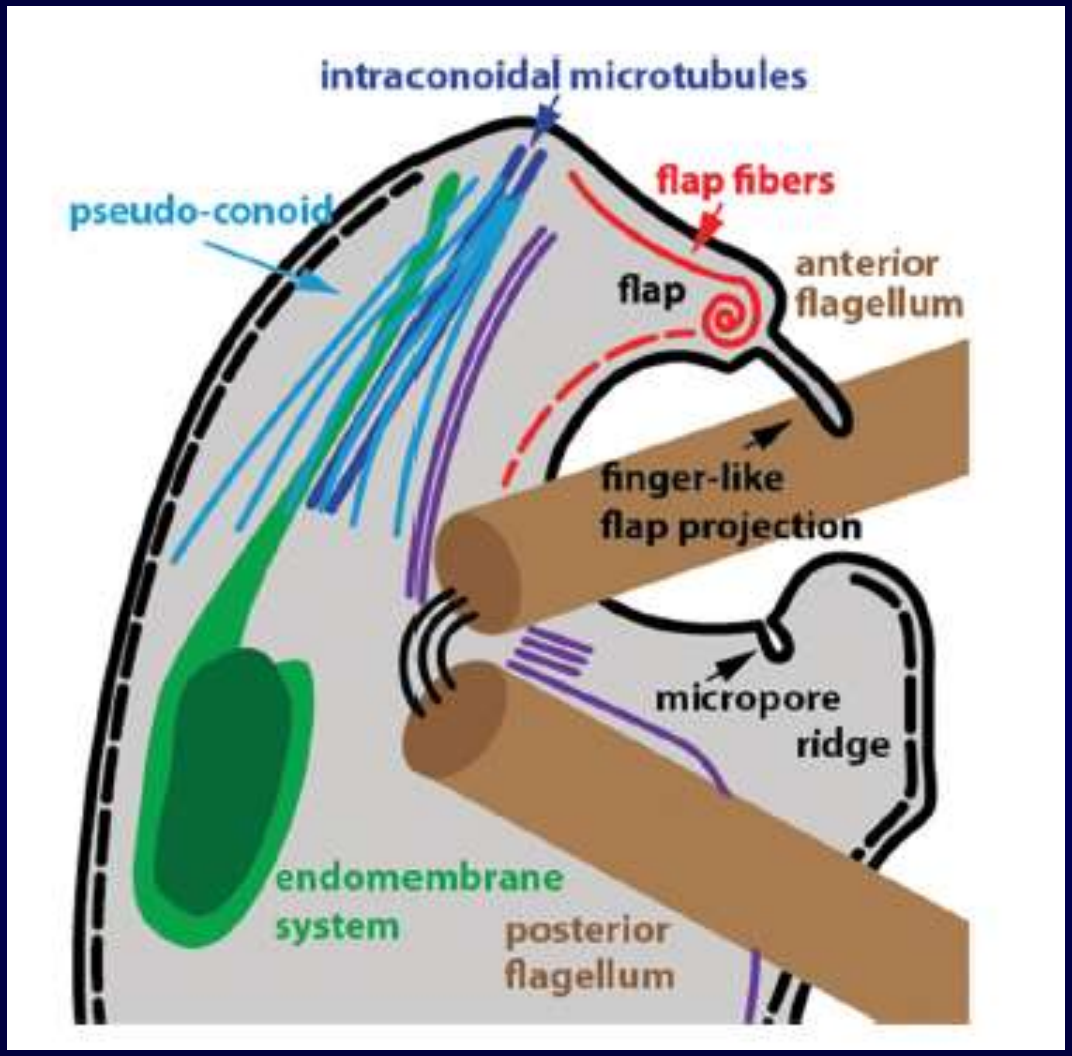

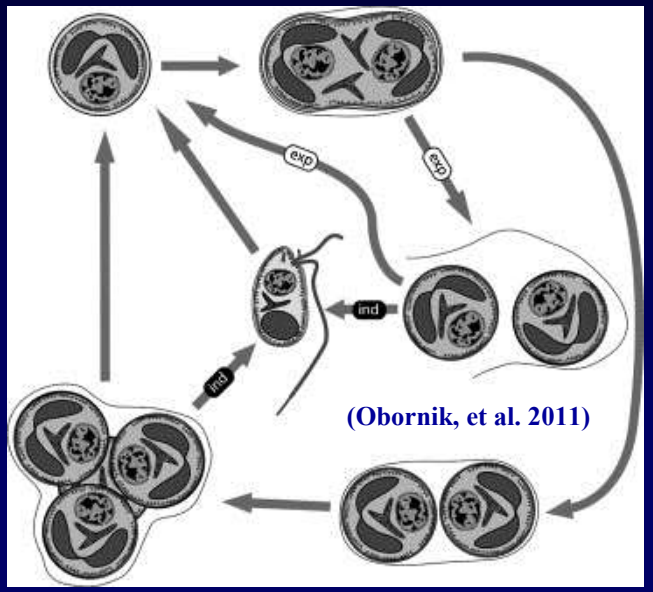

Cartoon representation of the apical complex and flagella of *C. velia*. Representations of the microtubules of the pseudoconoid (light blue) and flagellar rootlets (purple) are indicative of relative positions only and not the numbers of individual microtubules. The alveoli (inner membrane complex) are represented by a dotted black line beneath the plasma membrane (thick black line). The laminar connector joining the two basal bodies is shown as three thin black lines (Portman et al., 2014).

Character evolution of the apical complex among myzozoans (Okamoto, Kelling, 2014).

Color of the tree branches indicate trophic strategy of the linages; orange: photysynthetic, blue: predatory; grey: parasitic. Character evolution is indicated with triangles; green: acquisition of a character, yellow: transition of a character, white: loss of a character.

The flagellar contribution to the apical complex: a new tool for the eukaryotic Swiss Army knife? (Portman, Šlapeta, 2014)

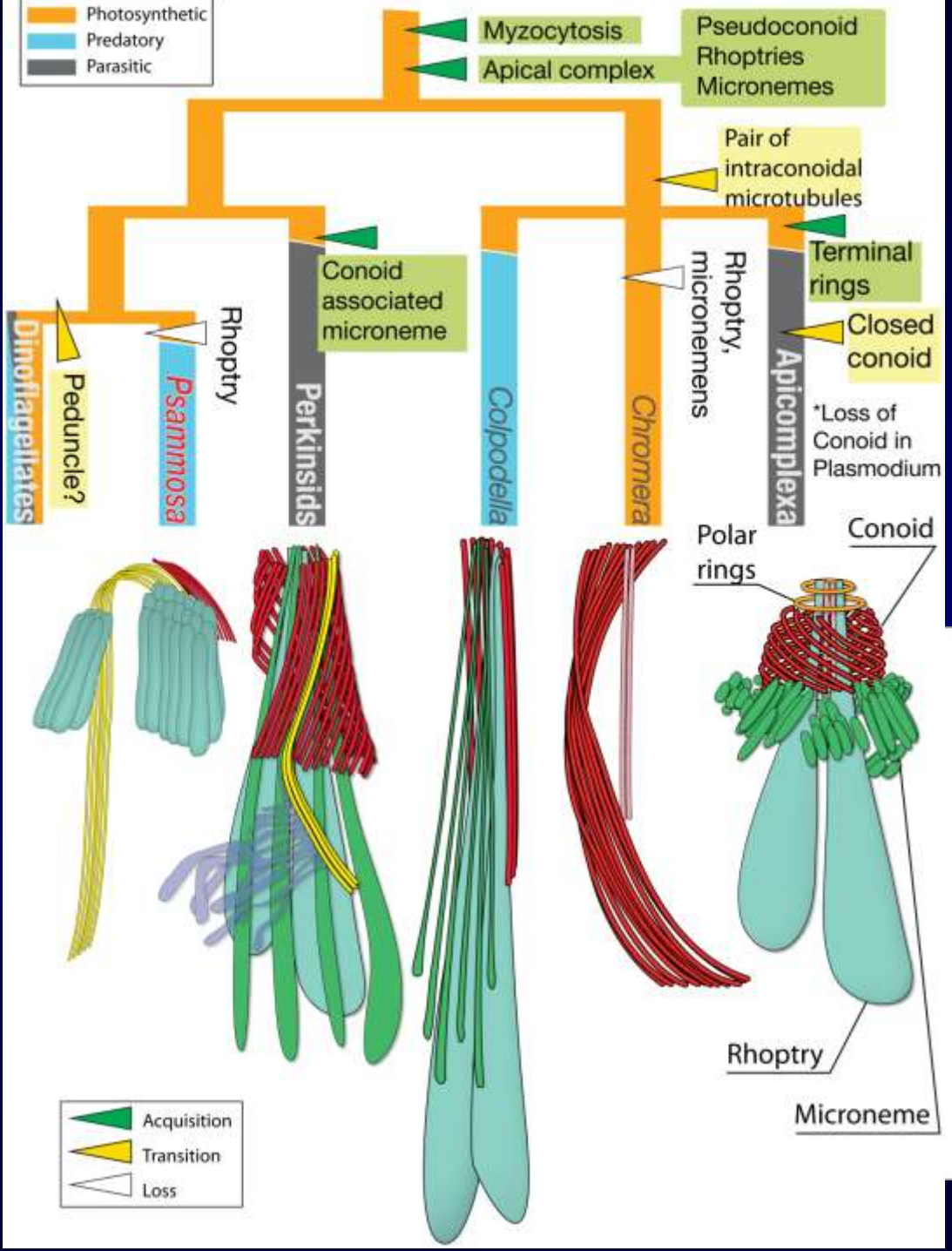

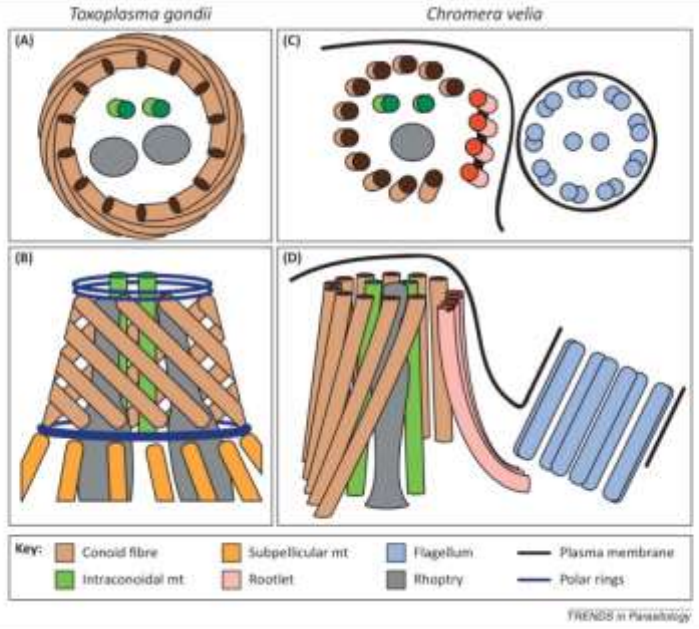

Cartoon representation of the apical complex of *Toxoplasma gondii* and *Chromera velia*.

Factors mediating plastid dependency and the origins of parasitism in apicomplexans and their close relatives

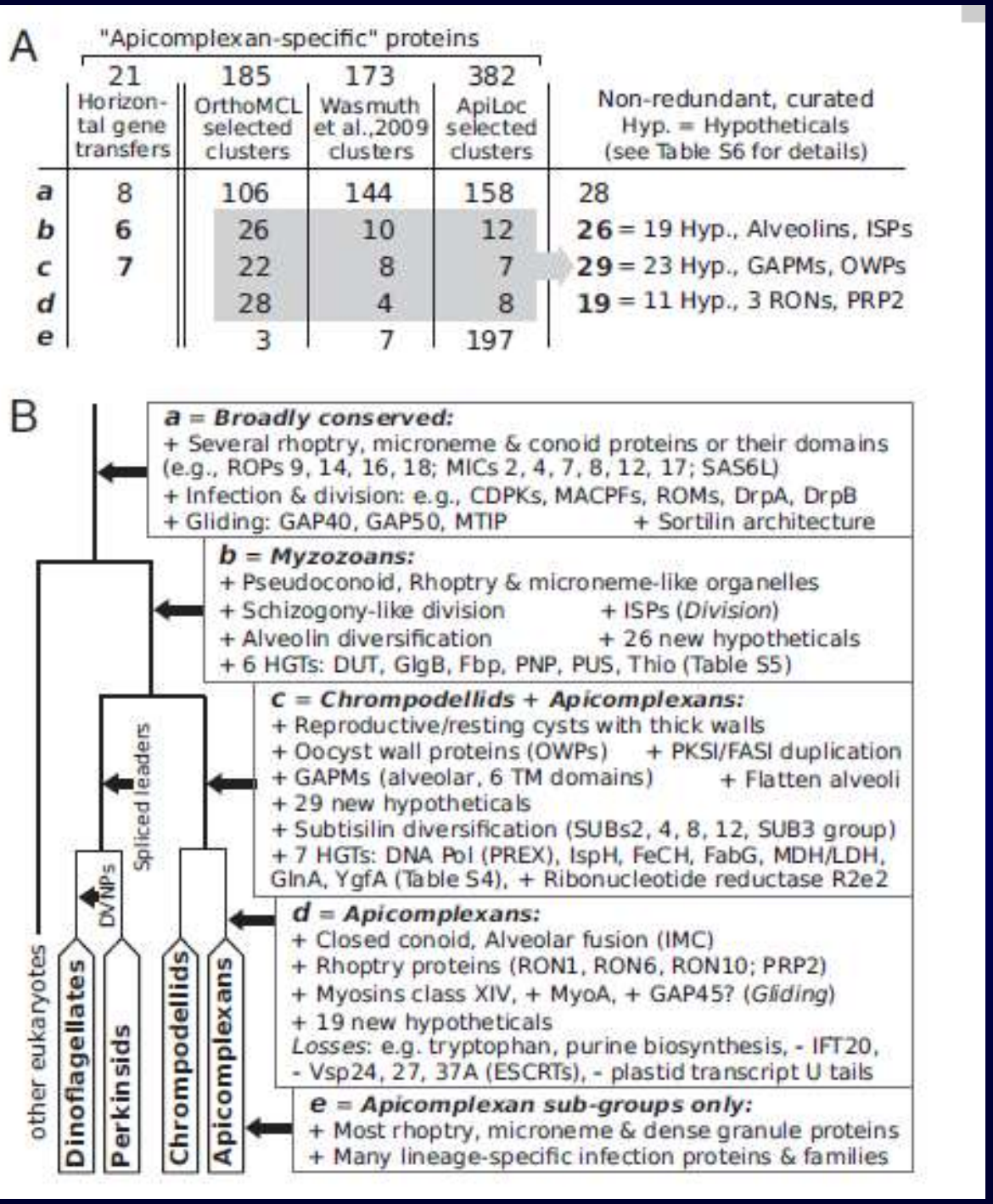

Alveolins – структурные белки внутреннего мембранного комплекса (IMC) пелликулы.
HGTs – horizontal gene transfers.
ISPs - IMC-subcompartment-proteins.
Sortilin protein – ответственен за транспорт веществ из ап.Гольджи в лизосомы..
GAPMs - Apicomplexan Glideosome-associated Proteins of the IMC.
Subtilisins (SUBs) – proteases.
The spliced leader (SL) is a gene that generates a functional ncRNA.
DVNPs – Dinoflagellate viral nucleoproteins.

(Janouškovec et al., 2015)

Multiprotein phylogeny of apicomplexans and related taxa

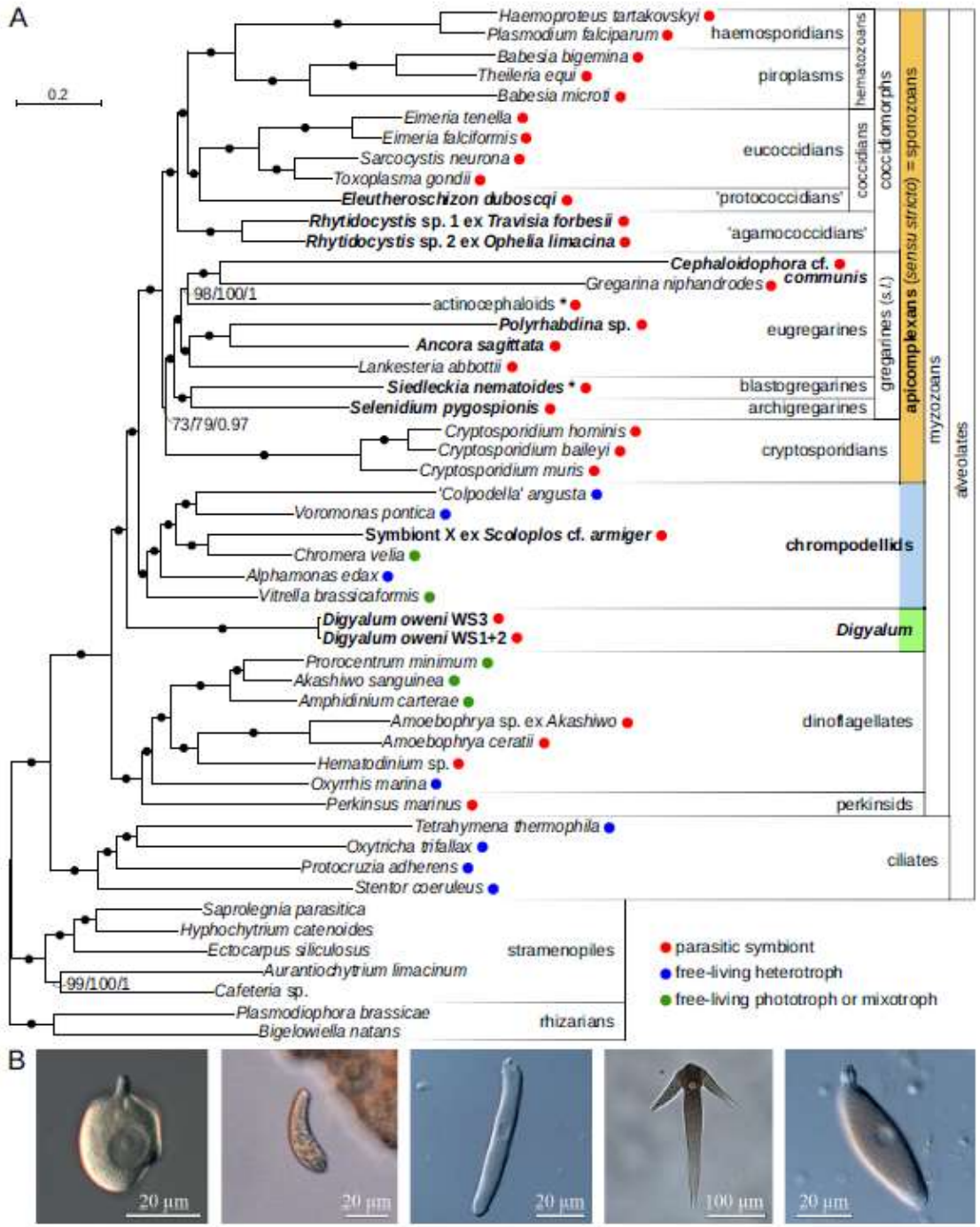

(A) Maximum likelihood tree (IQ-TREE) of apicomplexans and their relatives based on 296 concatenated protein markers. Species newly sequenced in this study are in bold. Values at branches correspond to UFBoot2 supports (1000 replicates, LG+G4+F+C60+PMSF model), non-parametric bootstraps (100 replicates, LG+G4+F+C60+PMSF model), and Bayesian posterior probabilities (PhyloBayes, consensus of 10 independent runs, CAT+GTR+G4 model). Black dots indicate 100/100/1 support. Actinocephaloids and *Siedleckia nematoides* are hybrid taxa (* symbol) composed from sequences of three parasites and two distant sequence variants, respectively. Values in parentheses behind species names show % of missing data in the phylogenetic matrix. Sequence sources and the phylogenetic matrix are found in Supplementary file 2 and Figure 1—source data 1, respectively. Single quotation marks indicate potentially problematic taxonomic assignments (formal group names are in Figure 1—figure supplement 1). (B) Light micrographs of some species studied, left to right: *Digyalum oweni*, *Symbiont X*, *Selenidium pygospionis*, *Ancora sagittata*, *Polyrhabdina* sp., with the anterior end facing up (Janoušhkovec et al. 2019).

От свободноживущих жгутиконосцев до паразитических споровиков

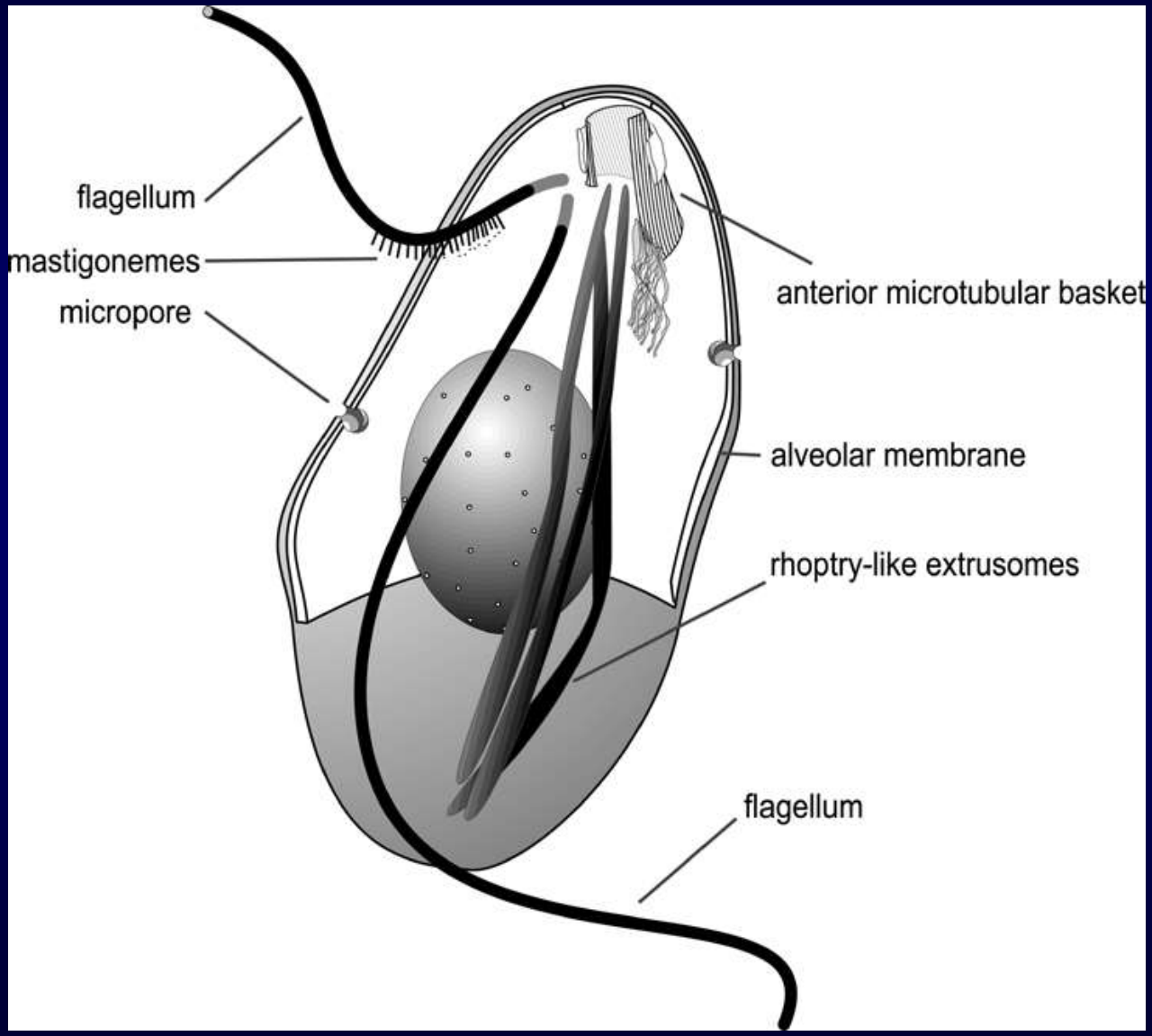

- Митохондрии с трубчатыми кристами?
- Наличие пластиды
- Микронемы?
- Трихоцисты?
- Вентральная бороздка (канавка) сродни борозде Excavata?

Illustration of the morphology of *Colpodella*, *Perkinsus*, and *Parvilucifera* which is indicated to be the plesiomorphic condition for the Alveolata. Thickened branches indicate implied retention of the *Colpodella*/*Perkinsus* morphology.

(Siddal et al., 2001)

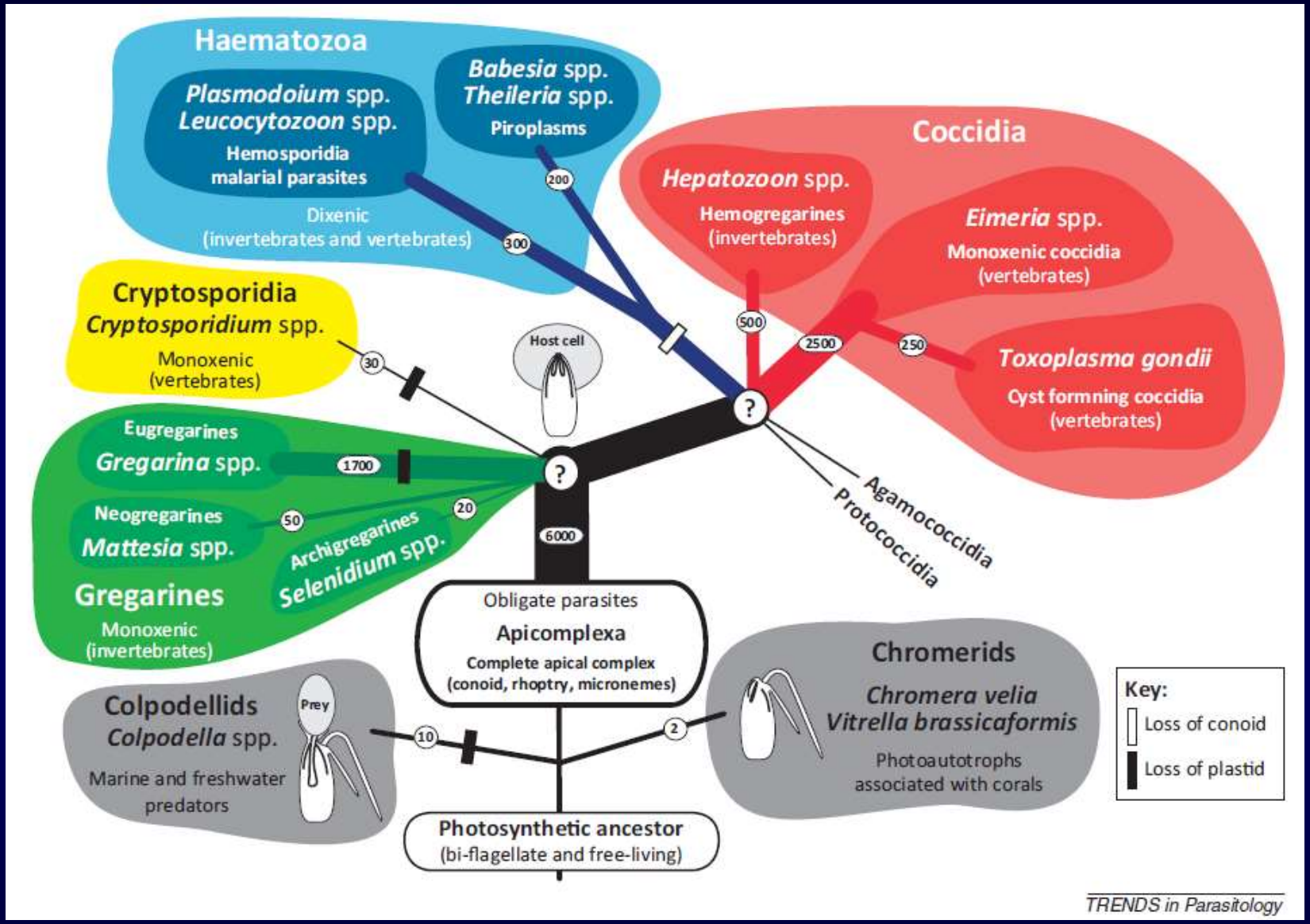

Apicomplexa and their closest sisters: colpodellids and chromerids. Schematic representations depicting the relationship and diversity (thickness of branches) of the dominant groups based on formally identified species (approximate number on branches). Question marks indicate uncertainty in branching order. Apicomplexan, colpodellid, and chromerid outlines document the presence or absence of flagella and the feeding strategy of the group. Host organisms for Apicomplexa are indicated in brackets (Portman, Šlapeta, 2014).